BOND BEHAVIOUR OF CFRP TO CONCRETE SUBSTRATE UNDER DYNAMIC STRAIN RATES

by

Jonathan Harman

B.Sc.E. (Civil Engineering) University of New Brunswick, Fredericton, 2017

A Thesis Submitted in Partial Fulfillment
of the Requirements for the Degree of

Master of Science in Engineering

in the Graduate Academic Unit of Civil Engineering

Supervisor: Alan Lloyd, PhD, PEng, Department of Civil Engineering

Examining Board: Peter Bischoff, PhD, PEng, Department of Civil Engineering
Samira Rizaee, PhD, PEng, Department of Civil Engineering
Clodualdo Aranas, PhD, PEng, Department of Mechanical Engineering

This thesis is accepted by the
Dean of Graduate Studies

THE UNIVERSITY OF NEW BRUNSWICK

April, 2023

ABSTRACT

This thesis explores the high strain rate bond behaviour of carbon fibre reinforced polymer (CFRP) sheets externally bonded to concrete. The experiments covered herein detail the bond behaviour when the bond between the CFRP sheet to concrete is subjected to dynamic loading, which is compared against previous studies on the bond behaviour under static loading. The ultimate strains and forces experienced by the CFRP sheets are compared against specimens tested under static strain rates, and Dynamic Increase Factors (DIFs) are then calculated. The bond stresses are calculated using the strain measurements obtained from the Digital Image Correlation (DIC) software and are compared against the static values found in previous research, showing a reduction in bond stress with an increase in strain rate. The failure mode of the CFRP bond is also explored and compared to past research.

ACKNOWLEDGEMENTS

I would like to extend my thanks to the following people:

- My supervisor: Dr. Alan Lloyd for his guidance throughout my studies. He has provided invaluable insight, and encouragement to continue my pursuit of higher education. I truly appreciate all the help he has provided me.
- The UNB Civil Engineering administrative staff: Alisha Hanselpacker, Angie Stewart, and MaryBeth Nicholson, for the assistance they have provided me throughout my degree.
- The UNB Civil Engineering laboratory technicians: Andrew Sutherland, Greg Grear, and Chris Forbes, for all the hard work they did in helping and guiding me through the construction and experimentation conducted in the laboratory.
- My parents, David and Cindy, for the motivation and love they have always shown me.
- The pets I have had and cherished throughout my degree, their unconditional love was always able to put a smile on my face.
- And most importantly my wife, Emily. For always being there for me, supporting and helping me through the difficult times, and for both pushing me when I needed it as well as reminding me to take breaks when I felt overwhelmed. I could not have completed this without her.

TABLE OF CONTENTS

LIST OF TABLES

LIST OF FIGURES

LIST OF SYMBOLS

CFRP	=	Carbon fibre reinforced polymer
DIC	=	Digital image correlation
DIF	=	Dynamic increase factor
DIF_{Le}	=	Dynamic increase factor, effective bonded length
DIF_{Load}	=	Dynamic increase factor, load
DIF_{ε}	=	Dynamic increase factor, strain
f'_c	=	Specified compressive strength of concrete (MPa)
f'_{co}	=	10 MPa
f_y	=	Specified yield strength of reinforcing bars (MPa)
E_f	=	Modulus of Elasticity, CFRP sheet (MPa)
FRP	=	Fibre reinforced polymer
L_e	=	Effective bonded length
$L_{e,dynamic}$	=	Effective bonded length, dynamic specimens
$L_{e,static}$	=	Effective bonded length, static specimens
L160	=	160 mm bonded length group
L240	=	240 mm bonded length group
L350	=	350 mm bonded length group
RC	=	Reinforced concrete
SHP	=	Split Hopkinson bar
t_f	=	Thickness, CFRP composite (mm)
VARTM	=	Vacuum Assisted Resin Transfer Molding
x_i	=	Location *i* along CFRP sheet (mm)
α_{fy}	=	Factor produced from the yield stress of a reinforcing bar used to calculate the DIF for reinforcing bars subjected to tensile loading
α_{fu}	=	Factor produced from the ultimate stress of a reinforcing bar used to calculate the DIF for reinforcing bars subjected to tensile loading
δ	=	Stress factor used to calculate the DIF of concrete subjected to tensile loading
ε	=	Strain (%, or, mm/mm)
ε_i	=	Strain at location *i* (%)
$\dot{\varepsilon}$	=	Strain rate (s^{-1})
ε_{max}	=	Maximum strain (%)
τ_{avg}	=	Average bond stress (MPa)
τ_{max}	=	Maximum bond stress (MPa)

1. INTRODUCTION

1.1 General

Reinforced concrete (RC) and prestressed concrete structures can be subjected to deterioration and corroding steel reinforcement, partially due to salts placed on roads to remove ice. This deterioration has caused the strength of critical members to decrease, requiring retrofit. Bridges are also seeing higher traffic volumes and higher loads than ever before, which adds to the deterioration. This has led to existing structures requiring retrofit in the form of additional reinforcing to increase strength (Meier, 1996). Research into the blast and impact resistance of fibre reinforced polymer (FRP) concrete is limited and retrofitting against these types of loads has become more necessary in recent years due, in part, to terrorist activities, among other typical impacts from motor vehicles (Pham et al., 2016). Several techniques exist for retrofit of RC structures including externally applied steel plates, concrete jacketing, and, more recently, externally applied FRPs.

RC bridges all around the world face the problem of corroding reinforcing steel. A variety of factors such as member type, and the environment a member is exposed to leads some members and structures to experience more extensive corrosion than others. As stated, de-icing salts can cause this corrosion; however, deterioration is also caused by inadequate design, poor quality of construction, and continued neglect. The concrete cover provided protects the steel from corrosion, though this protection may be inadequate as either the concrete carbonizes, or chloride ions reach the steel from the outside. In order to achieve the original strength of a member prior to the reinforcing steel corroding, a variety of FRP composites may be applied to strengthen the member (Kamaitis, 2002).

The three most commonly used FRP composite materials are: glass, carbon, and aramid. Each of these externally bonded FRP materials differ in their response to loads (Correia, 2013). This project, however, will focus solely on carbon FRP (CFRP) composite sheets.

CFRP sheets are able to increase the stiffness and strength of RC structures, but their use may also result in more brittle failures (Pesic et al., 2003). The brittle failure is in part due to the CFRP material being linear elastic up to failure, with little to no plastic response (Ceroni, 2010). While CFRP material exhibits a brittle failure, the material often does not reach its ultimate stress due to the most common method of failure for the various types of externally bonded FRP, delamination. Delamination is when the FRP prematurely peels off due to a failure in the bond between the FRP and the substrate material, which is also a brittle failure (Bizindavyi et al., 1999).

Despite problems with delamination and its brittle behaviour, CFRP has many benefits over other reinforcing materials. The main advantages of CFRP are the high strength to weight ratio, its ease of installation on retrofit projects, and its elastic properties up until failure. This final point, however, can also work against the material, as CFRP is very brittle with no ductility capacity (Campbell, 2010).

Glued-on strain gauges are typically used to measure the strains that are experienced by CFRP in experimental testing. Strain gauges, however, have proven to be unreliable and can be inaccurate. These inaccuracies are partly due to only measuring very localized strains, which are then averaged when the strain across a field is required (Zhu, et al., 2014). Some materials may be better suited using strain gauges, though since CFRP has a very non-uniform surface due to both the material and the adhesive, there could be local fluctuations in the strain data collected with these traditional strain gauges. This contrasts

with the use of digital image correlation (DIC) in this research, which is intended to measure the strains over an entire field. DIC not only has the potential to be more accurate, but also much easier to use than an array of traditional strain gauges (Zhu, et al., 2014).

Dynamic and impact loading can be the result of many different scenarios, including vehicle impact, ship impact on bridge piers, terrorist attacks, or debris being blown onto a structure, among others. There have been studies over the years that have investigated specific cases of impact loads, which generally utilizes a drop-weight test or Split-Hopkinson Pressure (SHP) bar to determine the dynamic properties of specimens (Pham et al., 2016).

Investigating the dynamic properties of FRP is an important step in understanding the full material response. It has been shown in many materials including concrete and steel that as the strain rate increases, the material response changes. This has generally been shown to be an increase in strength, ultimate strain, and stiffness as strain rate increases, though the response of FRP under a wide range of strain rates from static through a variety of dynamic strain rates is still unknown.

1.2 Aim and Objectives

The aim of this study is to understand the dynamic response of the bond behaviour between a CFRP sheet and concrete substrate. This was done with the application of an impact load in a CFRP-to-concrete double lap pull-out shear test while measuring the strains using DIC as opposed to the more traditional strain gauges. The work carried out in this thesis forms the second part of a more extensive research program investigating the bond behaviour of FRP strengthened members under static, dynamic and impact loading.

The objectives of this study include:

- Understanding the dynamic behaviour of CFRP sheets bonded to reinforced concrete prisms;
- Performing experiments under dynamic loading conditions and comparing the results with those found by other researchers. This includes comparisons to the first part of this research program that studied the static response;
- Using DIC analysis software to find and measure strain readings across the surface of the CFRP sheets. These measurements will be used to calculate bond properties, which will be compared against those found under static loading.

1.3 Scope of Study

The scope of this experimental investigation into the interfacial bond between CFRP sheets and concrete substrate under dynamic loading conditions includes the following:

1. Previous experimental studies on CFRP bonded to concrete substrate under both static and dynamic conditions are reviewed. This included compiling the results found from these tests and the static results from the first part of this research program;
2. Design and construction of the testing apparatus in dynamic loading.
3. Testing of CFRP sheets bonded to concrete specimens in double lap pull-out shear tests under dynamic loading conditions. These tests were separated into three groups with the differentiating variable being the bonded length of the CFRP sheet;
4. Evaluation of the stress-strain relationships for the bonded CFRP sheet as measured from the DIC and load cells. This data was used to evaluate the dynamic increase

factor (DIF) of the material, as well as the effective bonded length of the CFRP sheet;

5. Comparison of the results found from this study to the previous studies reviewed;
6. Reporting of results from this study and recommendations for further research are listed.

The experimental work in this research study was limited to uniaxial double lap pull-out tests. The study focused on the effects of increasing strain rate from a static loading to the mid-range of what is considered dynamic loading, a target rate on the order of 1 s^{-1} representative of the approximate strain rate in flexure for far field blast design as specified in Canadian CSA S850 (2012). The tests and analyses concerning the static loading had already been completed by a previous researcher (Atunbi, 2018), who had also prepared the specimens used in the experimental work in this research study. Both the concrete and the carbon fibres used in the sheets remained constant throughout the experiment, with the concrete exhibiting 30 MPa of compressive strength, and a 1 mm thick coupon of carbon fibre composite exhibiting 642 MPa of tensile strength, with a 37,840 MPa modulus of elasticity.

1.4 Thesis Structure

This thesis is structured around two articles, which explore the dynamic increase factor (DIF) using both load cells and DIC techniques, the effective bonded length of CFRP sheets, and the maximum bond stresses between the CFRP sheet and concrete substrate.

Chapter 1 of this thesis provides an introduction to the entire thesis. Although there are subsequent introductions for the two articles mentioned previously, this chapter works to

bridge the two articles together. An overview of the experimental work is detailed, along with an outline of what this thesis aims to accomplish.

Chapter 2 details the literature review for the main body of the thesis. Again, there are separate literature reviews for the individual articles; however, the aim is for this to exist as a single body of work and the literature covers the entire study. The history of previous investigations into the field of externally bonded CFRP is reviewed, and by elaborating on what has been completed, an outline of how this study can help fill a knowledge gap is created.

Chapter 3 consists of the first article, *High strain properties of CFRP sheets surface bonded to concrete*. This article published in the American Concrete Institute (ACI) special publication, ACI SP-347: Recent Developments in High Strain Rate Mechanics and Impact Behavior of Concrete, (2021). The focus of this publication is on the DIF of CFRP sheets surface bonded to concrete. The DIF was calculated using two means: load acquired from traditional load cells, and surface strains using DIC techniques. Data using both methods was presented in a tabular and graphical format, comparing the results from the dynamic tests performed in this research project against the static loads found previously (Atunbi, 2018).

Chapter 4 presents the second article in the body of this thesis, *Experimental Analysis of CFRP Sheets Under High Strain Rates Surface Bonded to Concrete*. This unpublished article focuses on the effective bond length and the maximum bond stress found, compared against the static values from work by Atunbi (2018). Previous research into how strain rate impacts the aforementioned properties are discussed, and a discussion on how the findings of this study compares to the previous research is elaborated upon.

Finally, Chapter 5 serves to tie the two articles together. As with the introduction and literature review, each individual article has its own conclusions and discussions, although this chapter presents the two together as the findings of a single study. Conclusions from the two articles are presented and a discussion of the findings along with suggestions for future researchers in this field is presented.

1.5 Contributions of the Candidate

The candidate was the first and primary author of the two articles presented herein with co-authors, Dr. Alan Lloyd, and a previous researcher, Emmanuella Atunbi. Dr. Alan Lloyd presented the opportunity and aided in setting the initial scope of the project, along with providing guidance and technical insight throughout the course of this study. Emmanuella Atunbi (2018) a separate study on the static response to CFRP externally bonded to concrete substrate, which has been referenced extensively throughout this thesis as a comparison to the specimens studied within this experimental research programme. Additionally, the specimens used in this study had already been cast, with the CFRP sheets bonded. The candidate constructed the frame that supported the specimens during impact testing, carried out the experiments while obtaining data via load cells and DIC software, analyzed the data, and authored the articles.

REFERENCES

Atunbi, E. O., 2018. *Experimental Study on Bond Behaviour of CFRP Sheets Externally Bonded to Reinforced Concrete.* Fredericton(New Brunswick): University of New Brunswick.

Bizindavyi, L. & Neale, K. W., 1999. Transfer Lengths and Bond Strengths for Composites Bonded to Concrete. *Journal of Composites for Construction,* III(4), pp. 153-160.

Campbell, F. C., 2010. *Structural Composite Materials.* Materials Park(Ohio): ASM International.

Canadian Standards Association, 2012. *S850-12 Design and assessment of buildings subjected to blast loads.* Mississauga: Canadian Standards Association.

Ceroni, F., 2010. Experimental performances of RC beams strengthened with FRP materials. *Construction and Building Materials,* September, 24(9), pp. 1547-1559.

Correia, J. R., 2013. *The New FRP Materials for Civil Engineering Structural Applications [PowerPoint slides],* s.l.: s.n.

Harman, J., Atunbi, E. O. & Lloyd, A., 2021. High Strain Rate Properties of CFRP Sheets Surface Bonded to Concrete. *SP-347 Recent Developments in High Strain Rate Mechanics and Impact Behavior of Concrete,* pp. 21-38.

Kamaitis, Z., 2002. Damage to concrete bridges due to reinforcement corrosion. *Transport,* XVII(4), pp. 137-142.

Meier, U., 1996. Strengthening of structures using carbon fibre/epoxy composites. *Construction and Building Materials,* pp. 341-351.

Pesic, N. & Pilakoutas, K., 2003. Concrete beams with externally bonded flexural FRP-reinforcement: analytical investigation of debonding failure. *Composites Part B: Engineering,* XXXIV(4), pp. 327-338.

Pham, T. M. & Hao, H., 2016. Review of Concrete Structures Strengthened with FRP Against Impact Loading. *Structures,* Volume VII, pp. 59-70.

Zhu, H. et al., 2014. Digital image correlation measurement of the bond-slip relationship between fiber-reinforced polymer sheets and concrete substrate. *Journal of Reinforced Plastics and Composites,* XXXIII(17), pp. 1590-1603.

2. LITERATURE REVIEW

CFRP sheets have become a popular material used to retrofit old and degrading structures. The need for these externally bonded CFRP sheets has increased over time due to demand on structural members, such as bridge piers, dramatically increasing from heavier traffic flow, as well as from continual degradation of the concrete members (Al-Zubaidy et al., 2012). CFRP sheets have been used to strengthen the flexural capacity as well as the shear capacity of beams, as well as column strengthening by means of completely enveloping the column. CFRP has been found to be the ideal solution to increasing the structural capacity of these aging, failing members due to its high strength, ease of application, and low maintenance requirements (Correia, 2013). While this chapter covers the general uses, manufacturing, and background of CFRP sheets, the focus is on the dynamic properties and how these sheets can provide a superior alternative to other methods and materials at retrofitting existing structures to resist the effects of dynamic loads.

2.1 Alternatives to Retrofitting Against the Effects of Dynamic Loads

Dynamic loading covers a wide range of strain rates and causes. Unfortunately, recent history has shown many examples of dynamic loading in the form of blast loading. One such example comes from the Ronan Point gas explosion in 1968. Though new design regulations came into effect after this tragedy, specifically aimed at addressing progressive collapse, structures built before these regulations came into effect were exempt. In 2003, it was found that a similar gas explosion could occur in a building in Islington, located northwest of the Ronan Point tragedy in London, triggering a progressive collapse. When questioned, Islington council addressed that they wished that the walls had been

strengthened in the 1970s, after the Ronan Point explosion, though central government did not provide the necessary funds to retrofit these structures (Booth et al., 2003).

To combat failure from explosion induced dynamic loads, blast retrofitting can be employed. There are four main concerns when choosing a material to protect against dynamic loading: The increase in strength the material provides, the cost associated with its application, feasibility of installing the material on the structure, and how well the material contains debris under more extreme scenarios. These four attributes should always be taken into consideration when choosing what type of retrofitting material to use, whether it be CFRP, another FRP material, steel jacketing, engineered cementitious composites, or another solution (Goswami et al., 2019).

It has appeared as though blast retrofitting of columns, slabs, and walls has been much more pronounced and exhaustively covered than that of reinforced concrete beams. Goswami et al. (2019) attributes this to the fact that if such a dynamic load were to be applied, in the case of a blast, then typically a failure in one of columns, slabs, or walls could result in a much more catastrophic failure. This is elaborated on further by Malvar et al. (2007), where the researchers explain that a beam failure is more likely to result in a localized failure, as opposed to an entire system failure by means of progressive collapse. The researchers also point out that in a realistic scenario, where a slab is adjacent to the affected beam, the slab will provide substantial lateral support, resulting in higher strength and a lower likelihood of failure.

When reviewing various recent studies pertaining to retrofitting structures with various types of FRP sheets and steel jackets for increased blast performance, Goswami et al. (2019) found that one of the most frequently reported failure types was via debonding. As

such, the researchers concluded that not enough research has been performed in determining the bond behaviour of various FRP retrofitted materials. They recommended further studies at high strain rates, as the bond behaviour under high strain rates versus static loading is not adequately understood. Once a structural member has experienced a dynamically applied load, such as blast loading, the researchers also address the need to further studies into the members residual strength to aide in the safety and certainty when performing search and rescue operations.

2.2 Material Background

CFRP sheets externally bonded to concrete members tend to have a brittle failure mechanism. This is when the ductility has been reduced, resulting in a more sudden failure. The brittle CFRP failures tend to be caused by debonding at the ends of the CFRP sheets, known as plate end debonding, or by means of intermediate debonding, starting at a shear or flexural crack and propagating outwards. In contrast, when looking at internal FRP bars, the FRP bars provide a more ductile failure and the member usually fails due to crushing of the concrete, which tends to be more ductile than FRP debonding. Table 2.1 depicts the fibre material properties of the three most common FRP materials currently in use: glass, carbon, and aramid.

Table 2.1: Fibre Property Comparison.

Property	Glass	Carbon	Aramid
Strength (MPa)	2350-4600	2600-3600	2800-4100
Elasticity Modulus (GPa)	73-88	200-400	70-190
Strain at failure (%)	2.5-4.5	0.6-1.5	2.0-4.0
Density (g/cm^3)	2.6	1.7-1.9	1.4

Note: Data for FRP fibre material properties from Correia (2013).

As shown above, carbon provides a very high strength with a low ultimate strain. This presents difficulty in design as a member with low ductility has the risk of a very sudden failure. The values presented in the table above are solely for the fibre materials. When in use, the FRP sheets act as a composite material as the fibres are impregnated with an epoxy resin matrix, and thus the composite material properties differ from that of the fibre. CFRP composite testing performed by Zhang et al. (2016) covered static, quasi-static, and dynamic testing, with the strain rate varying from 7.00 x 10^{-5} s^{-1} up to 237.32 s^{-1}. Table 2.2 provides the average values for the tensile strength, modulus of elasticity, and ultimate strain obtained from Zhang et al. (2016).

Table 2.2: CFRP Sheet Composite Properties.

Property	CFRP Composite
Strength (MPa)	662.58
Elasticity Modulus (GPa)	47.85
Strain at failure (%)	1.05

Note: Data for FRP material properties from Zhang et al. (2016).

As with which material to use, the way in which the FRP composite is manufactured has a great impact on its material properties. The various products available can easily be split into two categories: Continuous, and discontinuous, shown in Figure 2.1 (Campbell, 2010).

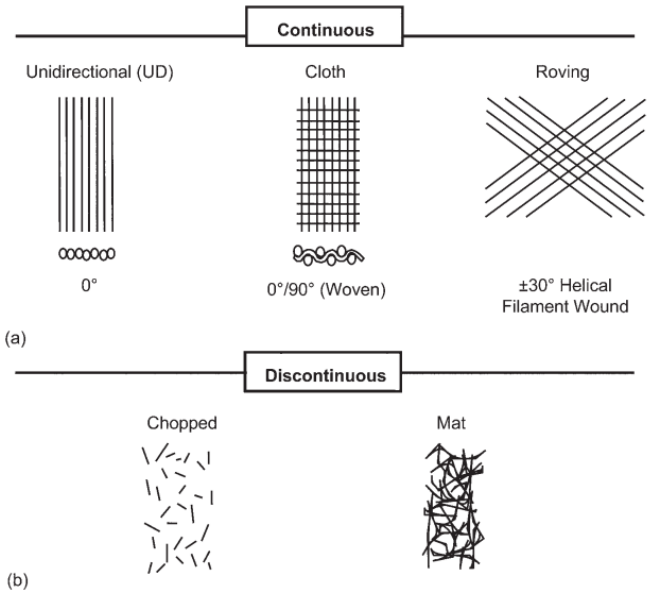

Figure 2.1: Continuous and discontinuous FRP manufacturing (Campbell, 2010).

Continuous FRPs use long, narrow fibers that are placed in a predetermined orientation. This orientation may be unidirectional, woven at a ninety-degree angle or at another predetermined angle. A study performed by Ekşi et al. (2016) compared the mechanical behaviour of woven and unidirectional fibre reinforced epoxy composites of carbon, glass, and aramid. Specimen groups were separated by material type and fibre orientation, with three (3) specimens per group. The data presented in Table 2.3 was obtained from this study.

Table 2.3: Fibre Orientation Tension Test Comparison.

Reinforcement Type	Density $\left({}^{g}/_{cm^3}\right)$	Modulus of Elasticity (GPa)	Tensile Strength (MPa)	Strain (mm/mm)
Woven Glass	1.55	14.35	220	0.016
Woven Aramid	1.20	19.09	357	0.019
Woven Carbon	1.31	42.00	340	0.009
Unidir. Glass (0º)	1.55	18.30	432	0.028
Unidir. Glass (90º)	1.55	7.94	52	0.0096
Unidir. Carbon (0º)	1.31	78.72	826	0.0100
Unidir. Carbon (90º)	1.31	4.93	37	0.0130

Note: Data for FRP material properties from Ekşi et al. (2016).

The researchers concluded from the data presented above that the modulus of elasticity and the tensile strength improved for all materials when using unidirectional fibres as opposed to their woven counterparts. Furthermore, they concluded that carbon composites performed significantly better in these metrics than aramid and glass. This however is not the case for all mechanical properties. While the composites with unidirectional fibres performed better than their woven counterparts in tension tests, the woven fibre samples outperformed the unidirectional fibres in shear (Ekşi et al., 2016).

It has been observed that the thinner the individual fibres are, the stronger the FRP composite will be. This is due to minimizing the surface area, and the surface level defects that are present on the fibres. Continuous FRPs are typically much stronger and have a higher modulus of elasticity than their discontinuous counterparts (Campbell, 2010). As this study focuses solely on continuous FRPs, discontinuous FRPs will not be covered further.

FRPs have a variety of structural uses, with the focus of this study being on externally laminated FRPs. The wet lay-up method of applying FRP sheets to existing structural

members has been the most common method of applying external FRP sheets to concrete and masonry members. This method utilizes FRP sheets that have been impregnated with a thermosetting resin, which acts to bind the FRP to the substrate material. One of the main advantages to this application method is that the FRP sheet can easily conform to a variety of surfaces. The main disadvantage of this application technique is in the curing of the resin. A high degree of control must be maintained during the curing process to ensure consistent reliability in the bond strength (Sciolti et al., 2010).

When manufacturing FRP shapes, the most popular method is by pultrusion. Pultrusion is the process of passing resin impregnated fibres through a curing die. This process provides very high consistency and has been shown to be very economical. This method can produce large quantities at once as the FRP passes through the curing die at speeds of up to 3 m/min, and can accommodate different sizes and shapes of FRP, such as open-section and single or multi-celled closed sections. Fibre volume for this manufacturing method is typically in the 35 % - 50 % range, and can consist of unidirectional, bidirectional, woven, braided, and stitched fibre fabrics. Prior to the 1970s, pultruded FRP shapes were primarily used for small scale, non-structural components. It was not until this time that larger pultruded FRP shapes began being developed for structural use (Bakis et al., 2002).

A newer FRP manufacturing technique, vacuum assisted resin transfer molding (VARTM), has been found to be very useful in civil engineering applications. VARTM has been used in retrofitting structures to increase girder or column strengths, as well as uses in the construction of lightweight bridges that also have the added benefit of being corrosion-free. VARTM has also been used to apply various FRP materials to steel, concrete, and masonry structures for blast protection. This manufacturing technique consists of four (4)

main steps. The reinforcing fibres are first placed over the molding surface, and then followed by a highly porous fabric used to distribute the resin. These layers are often separated by a thin layer of peel ply to help separate the reinforcing fibres from the distribution fabric once the curing process has completed. Next, tubes are placed into the mold. These tubes serve one (1) of two (2) purposes: Injecting the resin into the mold, and acting as a vent to allow air to escape and create a vacuum. The vacuum created during this process helps to ensure the resin is equally applied everywhere and is fully absorbed into the fabric. A vacuum bag made of nylon or equivalent material is then placed on top to ensure a vacuum tight seal. This vacuum bag is essential when injecting the resin and allowing air to escape through the tubes, as this is what creates the vacuum and applies equal pressure over the entire member during the curing process. This method can be used to apply FRP directly to a structural member, as shown in Figure 2.2, or create a mold of a member to produce multiple copies of the molded FRP, shown in Figure 2.3 (Uddin, 2013).

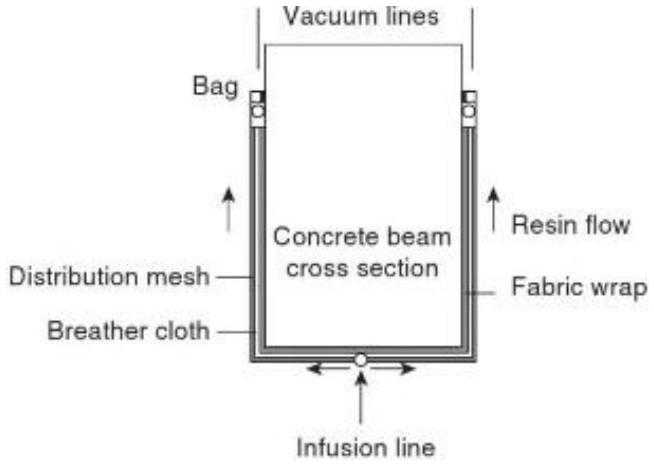

Figure 2.2: VARTM direct application to concrete member (Uddin, 2013).

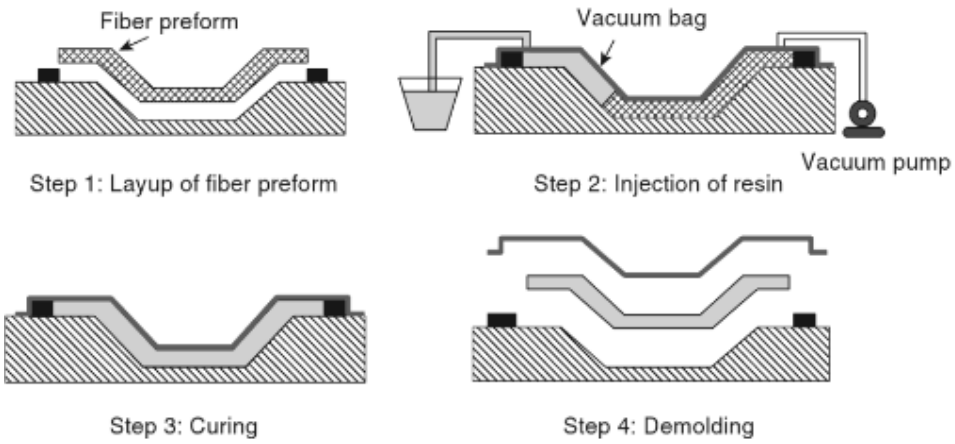

Figure 2.3: VARTM molding process (Uddin, 2013).

FRP has many advantages compared to more traditional rehabilitation materials, namely steel and concrete jacketing. FRPs provide high strength, corrosion resistance, as well as a high level of constructability due to the strength to weight factor. FRP is not, however, without its drawbacks, particularly when applied in harsh environments. The matrix resin that FRP materials are placed with have been found to exhibit severe reductions in tensile strength when exposed to freeze-thaw cycles. This behaviour appears to be more pronounced when salinity is high, which may be due to either being in close proximity to high saline water or other means (Frigione et al., 2018). When dealing with environments with high levels of salinity and alkaline solutions, polymers of aramid and glass are particularly impacted, whereas carbon is not nearly as impacted, with the most impact on the flexural strength being due to the adhesive bond (Frigione et al., 2018).

The factor that may cause the greatest negative impact on the FRP strength is poor curing of the adhesive. Ideally, the adhesive would be cured in very high, controlled temperatures with no moisture. This scenario, however, is not always practical for the expected use of

various FRP materials, mainly rehabilitation of existing structures. Due to this expected usage, FRP is widely applied on-site and outdoors, where it is more difficult and expensive to maintain a consistent and acceptable environment. Epoxy adhesives can take weeks to cure, especially when exposed to colder temperatures, which could extend this curing time even further. Added moisture during the curing process is difficult to avoid, whether from direct water such as rain or due to an increase in humidity, and has a sizeable impact on the adhesive properties (Frigione et al., 2018).

2.3 Dynamic Increase Factors in Structural Design

It is well known that common structural materials behave differently under dynamic loading conditions than static loading conditions. This change in response for a given loading type, is known as a dynamic increase factor (DIF). The CSA 850 (2012) design code lists equations to calculate the DIF for concrete under compressive and tensile loads, compared to a static strain rate of $30 \times 10^{-5}\ s^{-1}$, as well as for the yield and ultimate strength of steel reinforcement. The standard seems to group all types of FRP in one category and simply applies a DIF of 1.0 for both flexure and compression failure modes, implying no change in behaviour under dynamic loads. Meanwhile, no DIF is listed for diagonal tension shear, direct shear, or bond failures.

The increase in the apparent strength of both concrete and reinforcing steel has been shown to be quite substantial once strain rates between $10\ s^{-1}$ and $1000\ s^{-1}$ are achieved. In a review of published works on strain rate effects for concrete in tension by Malvar et al. (1998), they found that concrete has demonstrated an apparent increase in strength of 600 % under tension loading when compared to static strain rates. This study was used to inform CSA 850 (2012) on DIF formulas for concrete and steel reinforcement.

2.3.1 Concrete in Tension

Concrete under tensile loads is highly sensitive to strain rate. In order to account for the increase in strength that accompanies higher strain rates, the Comité Euro-International du Béton (CEB) published CEB Bulletin 187 in 1988, as stated by Malvar et. al (1998). This bulletin highlighted a distinct change to the slope of DIF to strain rate when examining concrete in tension at 30 s^{-1}. The formulas to approximate the DIF at a given strain rate are as follows in Equations [2-1] and [2-2].

[2-1] $$f_t/f_{ts} = \left(\frac{\dot{\varepsilon}}{\dot{\varepsilon}_s}\right)^{1.016\delta} \quad for\ \dot{\varepsilon} \leq 30\ s^{-1}$$

[2-2] $$f_t/f_{ts} = \beta\left(\frac{\dot{\varepsilon}}{\dot{\varepsilon}_s}\right)^{1/3} \quad for\ \dot{\varepsilon} > 30\ s^{-1}$$

Where β is defined by Equations [2-3] and [2-4]:

[2-3] $$log\,\beta = 7.11\delta - 2.33$$

[2-4] $$\delta = \frac{1}{10 + 6f'_c/f'_{co}}$$

Where δ is a unitless factor, f'_c is the specified compressive strength of the concrete in MPa, and f'_{co} = 10 MPa.

The CSA S850 (2012) uses the work performed by Malvar et. al (1998), a review of previous research studying the effects of concrete under tensile loads at varying strain rates,

to provide a more accurate material response than that given in the CEB Bulletin 187. The findings made by Malvar et. al (1998) led to proposing that in lieu of the change in slope occurring at 30 s^{-1}, it occurs at 1 s^{-1}, which better follows the empirical data covered in their study. It is noted, however, that CSA S850 (2012) still uses the original formulas for concrete in compression as the aforementioned review of previous research had found that the data match these formulas well. Figure 2.4 , obtained from Pyo et. al (2013) illustrates the original CEB formula for 30 MPa and 70 MPa concrete, along with the Modified CEB formula for similar strength concrete. These lines are accompanied by data points obtained from previous studies, listed on the figure, which the modified graphs follow much more closely.

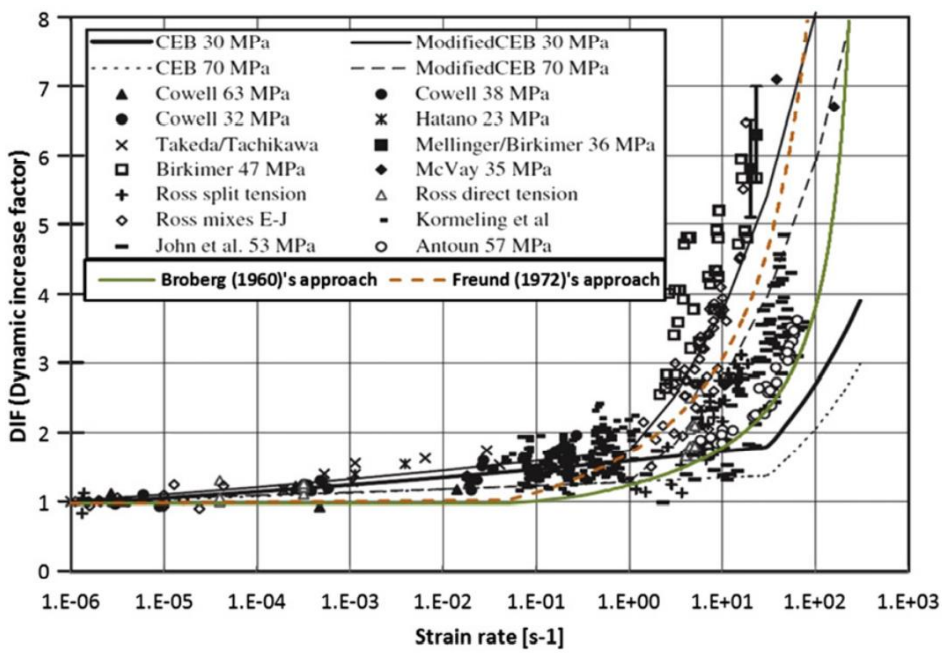

Figure 2.4: CEB concrete in tension DIF curve versus modified CEB curve.

2.3.2 Reinforcing Steel

Steel reinforcing bars, similarly to concrete, experience an increase in apparent strength, at both yield and ultimate, when subjected to higher strain rates. It has been shown that when experiencing strain rates in the order of 10 s^{-1}, reinforcing steel can see a DIF of 1.6 (Malvar, 1998). After obtaining data from various past research, Malvar (1998) was able to propose a formula for both yield and ultimate stress, that would then be adopted by CSA S850 (2012). Equations [2-5] to [2-7] show this formula and the change in yield versus ultimate.

[2-5] $$DIF = \left(\frac{\dot{\varepsilon}}{10^{-4}}\right)^{\alpha}$$

[2-6] $$\alpha_{fy} = 0.074 - 0.040\frac{f_y}{414}$$; for analysis at yield

[2-7] $$\alpha_{fu} = 0.019 - 0.009\frac{f_y}{414}$$; for analysis at ultimate

Where f_y is the yield stress, $\dot{\varepsilon}$ is strain rate, α_{fy} is the factor for analysing the DIF at yield, and α_{fu} is the factor for analysing the DIF at ultimate.

2.4 Experimental Studies of CFRP Sheets Bonded to Various Material Substrates

It is expected, as with the statically loaded members tested by Atunbi (2018), the failure mechanism will be bond failure on the concrete surface of the bond, as opposed to the CFRP or adhesive failing. Comparison studies between static and dynamic loading on concrete members have been conducted for many decades. A study performed by Hansen (1961) as cited by Ross (1983), conducted both static and dynamic shear tests on plain concrete and steel reinforced concrete members. It was observed that a plain concrete member exhibited a DIF of 1.15. This, meaning that the member withstood an average of

fifteen percent higher ultimate shear stress under dynamic loading conditions compared to the static loading conditions. While this study focused on flexure induced shear in plain and steel reinforced concrete, as opposed to the interfacial shear between CFRP and concrete, this study helped illustrate that the concrete response is sensitive to higher order strain rates.

2.4.1 Huo et al.

The experiments performed by Huo et al. (2016) involved the testing of CFRP externally laminated to a concrete interface and studying the bond behaviour under a variable load rate. The researchers utilized 30 MPa concrete prisms, with a cross section of 150 mm x 100 mm, and a length of 495 mm. Tests were comprised of two reinforced concrete prisms placed end-to-end with a 10 mm gap between, connected with two steel reinforcing bars in the compression zone. An illustration of their setup can be seen in Figure 2.5.

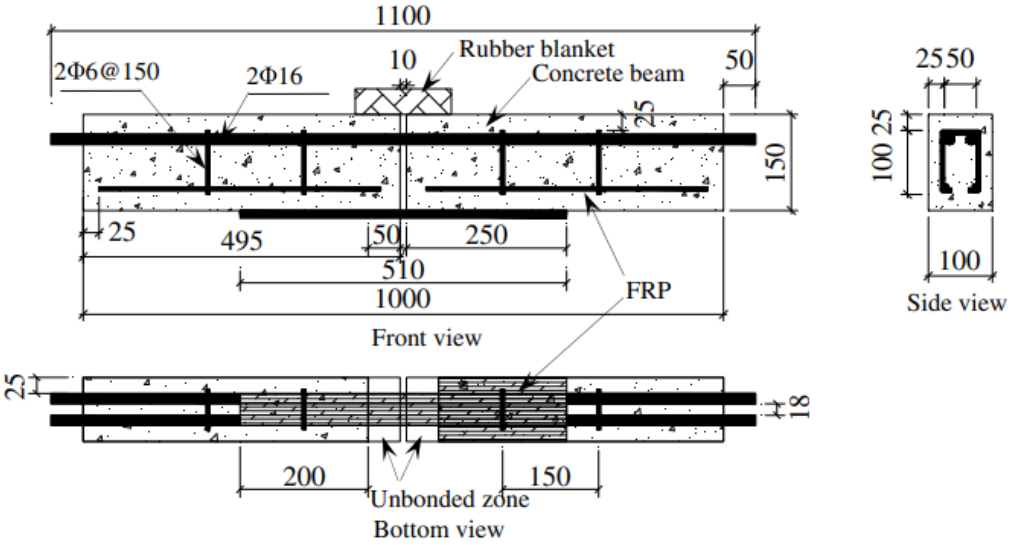

Figure 2.5: Specimen layout (Huo, et al., 2016).

The CFRP sheets in this experiment used unidirectional fibres, with a nominal thickness of 0.169 mm. Coupon samples of the CFRP were used to acquire static properties, and the researchers reported a tensile strength of 3,587 MPa, modulus of elasticity of 236 GPa, and an ultimate strain of 1.52 %.

Static testing along with impact testing was carried out using three-point bending tests. Static loading was applied by use of a manual hydraulic jack, with a load rate of roughly 2 kN/min. The impact tests, however, utilized a drop hammer. This drop hammer was lifted to a height varying from 200 mm to 600 mm with a mass of 198 kg. To capture the data acquired during these tests, strain gauges were placed along the bond length of the CFRP sheet, spaced at 25 mm, while a high-speed camera captured the loading and subsequent debonding at 1,000 hz.

The researchers found that for all static and dynamic testing, the failure method was via debonding, with the researchers noting that concrete flakes were still attached to the CFRP sheet after failure. When reviewing the data acquired from the strain gauges, they found

that the strain gauge closest to the 10 mm midspan gap was loaded prior to the subsequent gauges. This was as they had expected and indicates that debonding was initiated at this midspan gap. From this data, the researchers also noted the difference in ultimate strains from static to dynamic. They commented on how the specimens under dynamic loading experienced significantly higher ultimate strains as reported by the strain gauges on the CFRP bonded length, than the static counterparts.

The researchers noted that once the ultimate load was achieved, the maximum observed strains remained nearly constant throughout the remainder of the test. Once this maximum strain in the CFRP sheet was achieved, it began propagating away from the loaded end towards the free end. As mentioned previously, these strains were observed to be much greater under dynamic testing than static testing, and as CFRP has shown to exhibit a linear elastic behaviour until failure, it was reasoned that the stress in the CFRP is directly proportional to the increase in strains, and the ultimate load increased significantly under dynamic tests.

Though the ultimate strains, and by extension ultimate load, increased, it was noted that on the strain versus distance graphs the slope of the strain gradient was much steeper under dynamic loading. This change in strain gradient slope led to the observation of a shorter effective bond length, which contradicted the results found by Al-Zubaidy et al. (2012), as noted by the researchers.

2.4.2 Al-Zubaidy et al.

Al-Zubaidy et al. (2012), conducted an experiment studying the bond strength between CFRP sheets and steel under dynamic loading. The testing comprised of 160 test specimens tested at various loading rates. These loading rates ranged from, as reported by the

researchers, quasi-static to 5 m/s (250 s^{-1}). The main focus of this study was on the bond strength, effective bond length, strain distribution, and failure method.

The specimens used in this study consisted of two (2) steel plates, placed end-to-end, with a cross section of 50 mm x 5 mm and 210 mm in length. The CFRP sheets used in this study were comprised of unidirectional fibres, with a nominal thickness of 0.176 mm, a tensile strength of 1934 MPa, a modulus of elasticity of 206 GPa, and an ultimate strain of 1.02 %, tested under static loading conditions. To load the specimens at a dynamic load rate, the use of a drop-mass was employed. The researchers modified an existing apparatus at their testing facilities, to transfer the dynamic loading into an impact tensile load on the specimen. To record the data obtained from these tests, the researchers utilized a piezoelectric washer load cell, placed close to the upper grip of the apparatus to the specimen, as shown in Figure 2.6, illustrating the test setup.

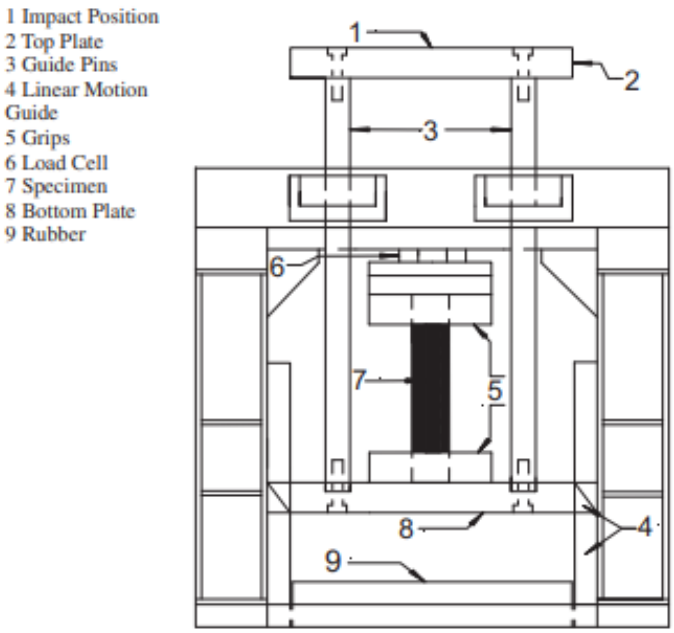

Figure 2.6: Test setup (Al-Zubaidy et al., 2012).

In addition to the load cell, strain gauges were placed along the CFRP sheet, in the centre of the shorter bonded length side. The strain gauges were placed every 15 mm, and both the strain gauges and load cell recorded data at a rate of 150 kHz. Finally, a high-speed camera was used to capture the impact and subsequent failure mode at a rate of 1,900 hz.

The researchers noted that the bond strength was sensitive to the loading rate. Their static loading rate was reported as 3.34 x 10^{-5} m/s, while their dynamic loading rate ranged from 3.35 m/s up to 5.0 m/s. These loading rate values, along with their respective effective bonded lengths, correspond with strain rates of 1 x 10^{-3} s^{-1} for the static loading, and 250 s^{-1} for the dynamic loading. When examining the data presented with a bond length of 100 mm, the statically loaded specimens exhibited an ultimate force of 46.73 kN, while the lowest dynamic loading rate specimens exhibited a strength of 56.99 kN. The failure mechanisms between these test groups differed. It was observed that when the bond length

was greater than the effective bonded length, for the statically loaded specimens, the failure mechanism was via CFRP rupture. This differed from the impact tests that were split between CFRP rupture and CFRP delamination caused by bond failure.

To analyze the effect of the loading rate on the effective bonded length, the researchers looked at all four load rates used in this experiment. When analyzed, the researchers found that the effective bond length is insignificantly influenced by the loading rate. The researchers noted that with a single CFRP layer under static loading, the effective bond length was approximately 30 mm, and the dynamically loaded counterpart had an effective bonded length of approximately 20 mm. While this reduction of 10 mm was deemed insignificant, this represents a decrease of 67 %, and the researchers attribute this decrease to the shear strength improvement of the adhesive used.

2.4.3 Li et al.

Li et al. (2020) conducted single-lap shear tests on seventy-five (75) specimens consisting of CFRP sheets externally bonded to a concrete substrate. These tests were performed under both quasi-static and dynamic load rates, ranging from approximately 0.02 mm/s to a load rate of 80 mm/s, as reported by the researcher. These loading rates correspond to a strain rate of approximately 2×10^{-4} s^{-1}, and 0.9 s^{-1}, respectively, when considering an effective bonded length of 90 mm, as reported by the researcher. The specimens were split into groups depending on the material and geometric features. While these specimens were split depending on the strength of the concrete, having a compressive strength of either 32 MPa or 53.8 MPa based on twenty-eight (28) day cylinder tests, this variable will not be covered in this paper. Concrete prisms with a cross section of 100 mm x 100 mm with a length of 190 mm were cast and loaded as per Figure 2.7, illustrating a distinction in how

the prisms were loaded for single and double-lap tests. The quasi-static and low loading-rate tests were both loaded using an MTS servo-hydraulic test machine, and the dynamically loaded specimens were loaded using a Split Hopkinson Pressure Bar apparatus that the researchers had modified for this experiment. A schematic, created by the researchers, of the modified Split Hopkinson Pressure Bar is shown in Figure 2.8.

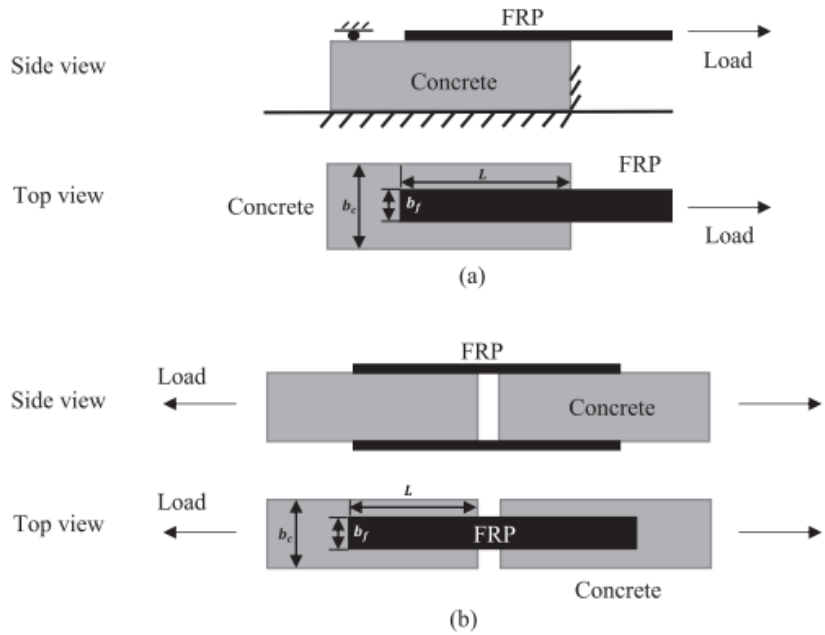

Figure 2.7: Test setup for single-lap (a) and double-lap (b) tests (Li, et al., 2020).

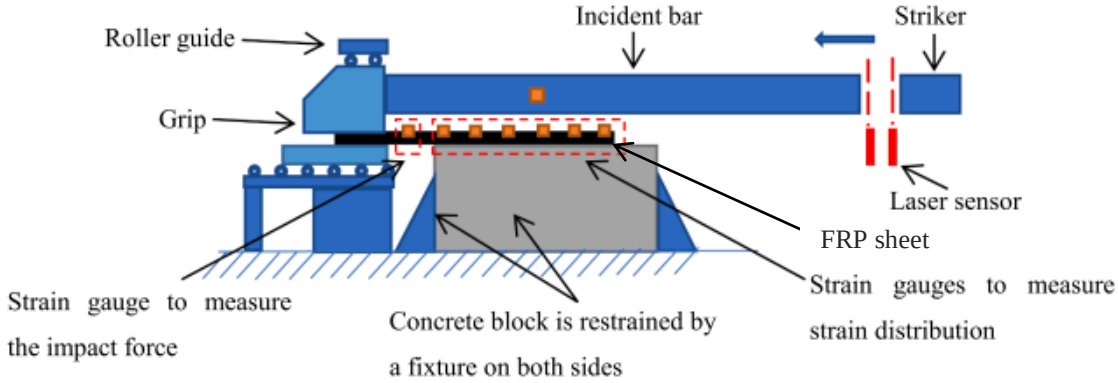

Figure 2.8: Modified Split Hopkinson Pressure Bar (Li, et al., 2020).

The CFRP sheets used by the researchers consisted of unidirectional fibres, and the researchers measured a tensile strength of 750 MPa, an elastic modulus of 82.7 GPa, and a thickness of 0.5 mm, for a single CFRP layer. The researchers investigated multiple variables with respect to the CFRP material, including the stiffness by using double layers, changing the bond width from 26 mm to 33 mm, and using three (3) different bonded lengths of 75 mm, 100 mm and 150 mm. The researchers used four (4), five (5), and six (6) strain gauges for the 75 mm, 100 mm, and 150 mm bonded length specimens, respectively. The researchers were not able to acquire a load cell for the specimens tested in the Split Hopkinson Pressure Bar, and therefore used one (1) additional strain gauge placed on the CFRP sheet ahead of the bonded length to measure the force. The data logger they used in this experiment recorded measurements at a rate of 1 MHz.

The observed failure method of the test specimens was mainly by debonding of the concrete, indicated by visually inspecting the specimens after the experiment and noting the concrete material still attached to the back of the CFRP sheet. Sixty (60) of the seventy-five (75) specimens failed in this manner.

Of the remaining fifteen (15) specimens, ten (10) failed by forming cracks in both the concrete and epoxy, all of which were in the dynamically loaded specimen group. The researchers noted that the concrete spalled at the loaded end, indicating that the failure began in the concrete as opposed to the epoxy. The researchers concluded that this failure mode occurred due to the dynamic load causing irregularities in the stress concentrations throughout the specimen. This was supported by their observation of the concrete spalling on the loaded end, which caused a stress concentration in the epoxy at that location.

One (1) of the remaining five (5) specimens failed in a similar manner to the other four (4), by CFRP failure along the fibre direction; However, it failed at a significantly lower ultimate load and was deemed that it probably failed due to either a material defect, or issue with installation. The other four (4), as mentioned, also failed by CFRP failure, or rupture of the CFRP. The researchers estimated the loads experienced and found that the loads had exceeded that of the CFRP fracture capacity, and the data was not useful for the focus of their study on the concrete to CFRP debonding process.

As the researchers tested both single and double-lap pullout tests, they were able to compare the strain rate effects on both sets of specimens. They noted that the strain rate had a much lesser effect on the bond stress in the single-lap pullout test than the double-lap pullout test. They noted specimens with increased stiffness respond much more to an increase in strain rate, to dynamic loading. This, they attributed to, was due to the dynamic response of the interfacial bond of the CFRP to concrete being much more dependent on the concrete than the CFRP, as shown in the failure modes. Additionally, they note that concrete is more sensitive to changes in strain rate than the CFRP material.

2.4.4 Atunbi

The data obtained through the experiments carried out in the research from this thesis were directly compared to the results obtained by Atunbi (2018) to observe noticeable changes in the bond behaviour of CFRP sheets bonded to a concrete substrate when subjected to increasing strain rates. Experiments similar to those carried out by Atunbi (2018) were modified for higher strain rates to be used for this thesis. The experiments used a double-lap pullout test of CFRP sheets bonded to a concrete substrate, though under static strain rates with loading rates of 0.5 mm/min. This static loading rate corresponds to a strain rate

of approximately 1.5 x 10^{-4} s^{-1}, when taking the average effective bonded length found by the researcher.

The test specimens consisted of two (2) concrete prisms positioned end-to-end, with a cross section of 150 mm x 150 mm and a length of 500 mm. Each prism was cast with a 20M reinforcing bar embedded in the centre. These reinforcing bars protruded from the ends of the prisms to provide a grip during the testing procedure. The carbon fibre sheets were unidirectional carbon fibres, with a nominal fibre thickness of 0.165 mm. Atunbi (2016) conducted static testing on CFRP coupon samples to confirm the tensile strength, modulus of elasticity, and ultimate strain, which were found to be 641.6 MPa, 37.84 GPa, and 1.9 %, respectively. These coupon samples were tested using a 250 kN capacity universal testing machine.

In carrying out the static testing of the CFRP sheets bonded to the concrete prisms, Atunbi (2016) followed the test method detailed in Annex N of the Canadian Standard Association's CSA S806 (2012). As mentioned, the prisms were placed end-to-end with CFRP bonded to opposing sides for the double-lap. A gap of approximately 3 mm was maintained between the prisms of each specimen by using a plaster material separated by a plastic film to eliminate any bonding between the two (2) prisms. Initially, to reliably know where to focus the instrumentation, the CFRP was bonded in a specific manner. On one (1) side of both prisms the CFRP was bonded the entire length, while on the opposing face, the CFRP was bonded along the entire length of one (1) prism, with a CFRP wrap on this end to anchor it in place, and the other prism was limited to one of 160 mm, 240 mm, or 350 mm of bonded CFRP, depending on the specimen group it was apart of. This CFRP orientation can be seen in Figure 2.9. After testing the first few specimens, the researcher

noted that some of the specimens had first failed on the side facing away from their instrumentation. The researcher attributed this phenomenon to the tension cracks in the concrete relieving the CFRP of stress on the shorter side, resulting in the side that is bonded down the entire length of both prisms taking the full load. This led the researcher to changing the layout of the CFRP specimens by bonding the CFRP on the remaining specimens symmetrically so that both sides were bonded down the entire length of one (1) prism, while both sides of the second prism had the CFRP terminate at the aforementioned bonded lengths of 160 mm, 240 mm, or 350 mm. This modified CFRP orientation can be seen in Figure 2.10.

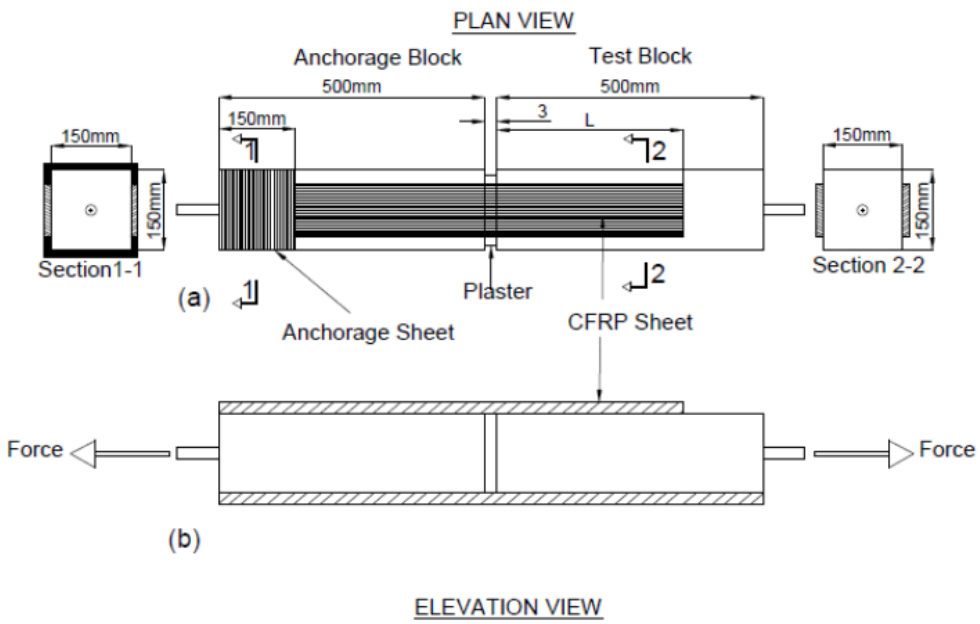

Figure 2.9: Initial CFRP layout on concrete specimens (Atunbi, 2018).

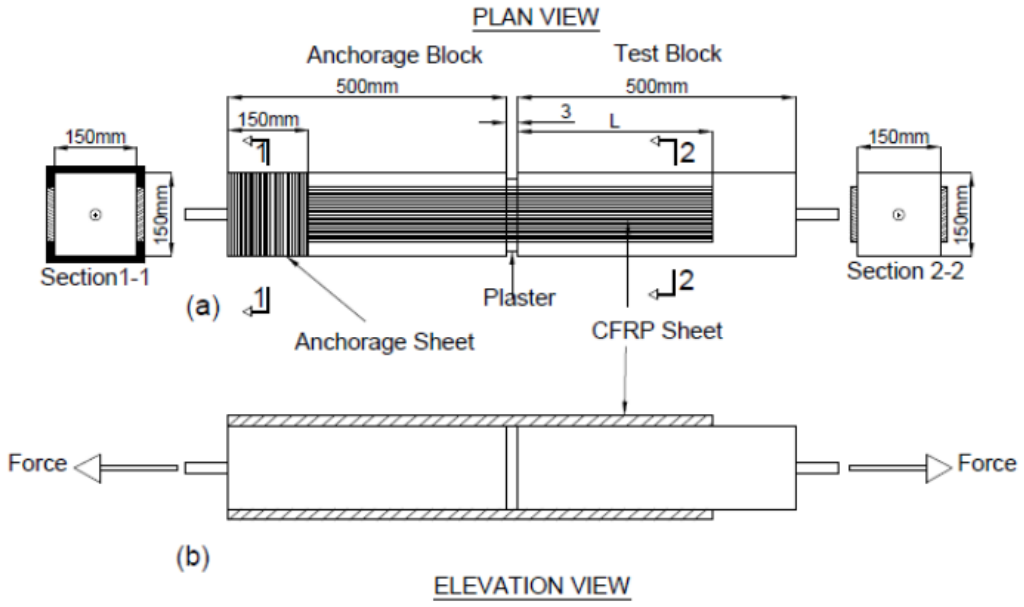

Figure 2.10: Modified CFRP layout on concrete specimens (Atunbi, 2018).

Instead of using traditional strain gauges as reported by the researchers detailed in sections above, Atunbi (2018) utilized DIC software to track black paint speckles on the CFRP. The researcher first painted the face of the specimen facing the cameras white to provide a uniform background colour for the tracking software. The researcher then applied the black paint speckles over this white background. The DIC software uses a reference image taken at the beginning of the test to base any movements of the black speckles on. As the DIC software tracks the movements of each speckle, pixel by pixel, it calculates the strain experienced by the CFRP over the entire field captured in the images. The researcher noted that using DIC software to calculate strains in such an experiment has large advantages over using traditional strain gauges. While strain gauges are able to accurately calculate the strain, they are only useful in determining the strain at the specific location that they are installed. In contrast, by using DIC, the researcher was able to obtain the strain at any location in the field of view observed by the cameras and software with great accuracy.

The testing apparatus for the specimens by Atunbi (2018) was a Universal testing machine, shown in Figure 2.11 without any specimen placed inside, showing the camera setup on the far side. Figure 2.12 shows the same apparatus with a specimen installed.

Figure 2.11: Empty Universal testing machine (Atunbi, 2018).

Figure 2.12: Specimen in Universal testing machine (Atunbi, 2018).

The researcher was interested in observing the failure mechanism for these statically loaded specimens, while recording the ultimate force, strain, and observed effective bond length. They noted that all specimens failed by means of progressive debonding, originating at the loaded end of the CFRP by means of a wedge crack formation. A wedge crack, as described by the researcher as tension cracks forming at the loaded end of the CFRP sheet that act to relieve the stress in the CFRP at that location. These wedge cracks typically caused the corners of the loaded end of the concrete to fall off.

The researcher noted from the strain graphs produced by the DIC software and further analysis, that once the peak bond strain was fully developed along the effective bonded length, no further bond length had a noticeable impact on the strength of the bonded member. Instead, once the peak strain was achieved, the effective bonded length shifted across the bonded length, away from the loaded end. This shift in effective bond length created a plateau at the peak bond strain, that diminished in strain as you travel down the effective bond length towards zero load.

REFERENCES

Al-Zubaidy, H. A., Zhao, X.-L. & Al-Mahaidi, R., 2012. Dynamic bond strength between CFRP sheet and steel. *Conposite Structures,* XCIV(11), pp. 3258-3270.

Atunbi, E. O., 2018. *Experimental Study on Bond Behaviour of CFRP Sheets Externally Bonded to Reinforced Concrete.* Fredericton(New Brunswick): University of New Brunswick.

Bakis, C. E. et al., 2002. Fiber-Reinforced Polymer Composites for Construction - State-of-the-Art Review. *American Society of Civil Engineers,* pp. 73-87.

Booth, R. & Gates, C., 2003. Ronan Point fears resurface. *Building Design,* 18 July, p. 1.

Campbell, F. C., 2010. *Structural Composite Materials.* Materials Park(Ohio): ASM International.

Correia, J. R., 2013. *The New FRP Materials for Civil Engineering Structural Applications [PowerPoint slides],* s.l.: s.n.

Ekşi, S. & Genel, K., 2016. Comparison of Mechanical Properties of Unidirectional and Woven Carbon, Glass and Aramid Fiber Reinforced Epoxy Composites. *Acta Physica Polonica A,* pp. 879-882.

Frigione, M. & Lettieri, M., 2018. Durability Issues and Challenges for Material Advancements in FRP Employed in the Construction Industry. *Polymers,* 10(3), p. 247.

Goswami, A. & Adhikary, S. D., 2019. Retrofitting materials for enhanced blast performance of Structures: Recent advancement and challenges ahead. *Construction and Building Materials,* pp. 224-243.

Hansen, R. J., 1961. Design of blast resistant structures. *Shock and Vibration Handbook,* Volume 3.

Huo, J. et al., 2016. Experimental Study on Dynamic Behavior of CFRP-to-Concrete Interface. *Journal of Composites for Construction,* October.20(5).

Li, G., Tan, K. H. & Fung, T. C., 2020. Experimental study on CFRP-concrete dynamic debonding behaviour. *Engineering Structures.*

Malvar, L. J., 1998. Review of Static and Dynamic Properties of Steel Reinforcing Bars. *ACI Materials Journal*, pp. 609-616.

Malvar, L. J., Crawford, J. E. & Morrill, K. B., 2007. Use of Composites to Resist Blast. *Journal of Composites for Construction,* pp. 601-610.

Malvar, L. J. & Ross, C.A., 1998. Review of Strain Rate Effects for Concrete in Tension. *ACI Materials Journal*, pp. 735-739.

Ross, T. J., 1983. *Direct Shear Failure In Reinforced Concrete Beams Under Impulsive Loading,* s.l.: Stanford University.

Sciolti, M. S., Frigione, M. & Aiello, M. A., 2010. Wet Lay-Up Manufactured FRPs for Concrete and Masonry Repair: Influence of Water on the Properties of Composites and on Their Epoxy Components. *Journal of Composites for Construction,* XIV(6), pp. 823-833.

Uddin, N., 2013. *Developments in fiber-reinforced polymer (FRP) composites for civil engineering.* Philadelphia: Woodhead Publishing.

Zhang, X. et al., 2016. Static and dynamic material properties of CFRP/epoxy laminates. *Construction and Building Materials,* pp. 638-649.

3. HIGH STRAIN RATE PROPERTIES OF CFRP SHEETS SURFACE BONDED TO CONCRETE[1]

Abstract

Many common building materials, such as concrete and steel, are expected to experience a change in apparent material properties under high strain rates. This effect is often incorporated into impact and blast design by using DIFs that modify properties of the material such as strength and stiffness when subjected to high strain rates. There is currently limited guidance on dynamic properties of FRP sheets bonded to concrete. Since FRP is a common retrofit material for structures that are vulnerable to blast and impact loads, it is important to have a full understanding on the behaviour of the FRP material and of the composite action between the FRP sheet and the substrate it is bonded to. Important parameters for blast and impact resistant design of reinforced concrete structures retrofitted with surface bonded FRP include dynamic measures of debonding strain, development length, and bond stress at bond failure. This paper presents the results of an experimental program measuring the dynamic properties of CFRP sheets bonded to concrete under impact induced high strain rates.

A series of rectangular concrete prisms were cast and fitted with surface bonded CFRP sheets to facilitate pull-out shear tests that directly measure the CFRP to concrete bond. The bonded length of the CFRP sheet was varied with three different lengths explored. A series of static tests were conducted to measure the strain fields on CFRP sheets under load

[1] Harman, J., Atunbi, E. O., & Lloyd, A. (2021). High Strain Rate Properties of CFRP Sheets Surface Bonded to Concrete. *ACI SP-347 Recent Developments in High Strain Rate Mechanics and Impact Behavior of Concrete*, 21-38.

up to failure. These strain fields, measured with digital image correlation (DIC) techniques, were used to determine development length, bond stress, and ultimate strain of the CFRP sheet prior to debonding. A companion set of prisms were also cast and tested under impact loading to measure the same properties at high strain rates of around 1 s^{-1}. Initial test results indicate a potential increase in both ultimate strain and bond stress, and a decrease in development length under high strain rates. The results of the larger study will be compiled and, when compared with the static companion set, be used to propose DIFs for CFRP sheets bonded to concrete for use in design in high strain rate applications.

3.1 Introduction

Fibre reinforced polymer (FRP) sheets are commonly used to reinforce and retrofit aging concrete structures (Meier, 1996). These FRP sheets are made of a variety of materials, including aramid, glass, and carbon (Correia, 2013), the focus of this study. There are a variety of reasons why a concrete structure may need to be reinforced with FRP.

A major contributor to the need for FRP sheet reinforcement is the corrosion of reinforcing steel. Over time the corrosion of reinforcing steel results in a smaller cross section of steel and the steel to concrete bond deteriorates. This leads to a lower ultimate capacity and potential sudden failure. This corrosion is mainly caused by poor design of the concrete structure, including inadequate cover, as well as poor quality of the concrete itself. Additionally, de-icing salts and exposure to other chlorides speed up the corrosion process (Kamaitis, 2002). As roads, and bridges, are seeing higher traffic flow than ever before, these structures are deteriorating at an even higher rate and require continual maintenance (Meier, 1996).

Carbon fibre reinforced polymer (CFRP) sheets can increase the stiffness and capacity of reinforced concrete (RC) structures, though often at the cost of brittle failures (Pesic et al., 2003). The most common cause of failure for various types of FRP is delamination where the FRP sheet prematurely peels off due to a failure in the bond between the FRP and the substrate material (Bizindavyi et al., 1999).

CFRP has many benefits over other reinforcing materials, as well as many disadvantages. The main advantages CFRP offers are its high strength to weight ratio and its elastic properties up until failure. The brittleness of the material is one of its disadvantages (Campbell, 2010).

Surface mounted strain gauges have often been used in experimental testing to measure the response of FRP sheets. Strain gauges, however, may be unreliable and can be inaccurate (Zhu et al., 2014). These inaccuracies are partly due to only measuring very localized strains, and when needing to measure across an entire field, the strains are an average of various points along the length of the field. The surface of CFRP is also not ideal for the use of strain gauges as it is very non-uniform. Other, more uniform materials may provide a better surface to attach strain gauges to, as the adhesive does not bond well when there are ridges and inconsistencies (Zhu et al., 2014).

Digital Image Correlation (DIC) offers an alternative to strain gauges and can capture an entire field of view, as opposed to a single location that the traditional strain gauges offer. Measuring the strains over an area is a much more accurate method to obtain valuable data than averaging between a number of known points. It is not only more accurate than contact gauges, it is also an easier process. Where strain gauges require a complete, level bond to be accurate, DIC requires no externally bonded materials to the surface and uses a speckle pattern painted onto the material that can be tracked using optical data measurement without the need of contact with the specimen (Zhu et al., 2014).

The dynamic increase factor (DIF) is defined as the ratio between the material strength at a given strain rate, to its static strength (Levi-Hevroni et al., 2018). The FRP tensile strength at bond failure will be the focus of this paper. When rates of approximately 1 s^{-1} are achieved, the slope of the DIF curve, for concrete in tension, drastically increases as the strain rates increase (Levi-Hevroni et al., 2018). Currently, there is more research data available focusing on the compressive response of concrete than the tensile response (Malvar et al., 1998). The aim of this research is to calculate the DIF when strain rates of

1 s^{-1} are achieved, using the strain data obtained by DIC correlated with the load data. The failure modes observed in this experiment will also be compared to that of the static experiments conducted by Atunbi (2018).

3.2 Literature Review

The use of CFRP sheets has become a common method to retrofit old, degrading structures in the past few decades. The need for these externally bonded CFRP sheets has increased due to demand on structure members, such as bridge piers, dramatically increasing from heavier traffic flow, as well as from continual degradation of the concrete members (Al-Zubaidy et al., 2012).

3.2.1 Material and Design Properties

CFRP has been used to strengthen the flexural capacity as well as the shear capacity of beams, as well as column strengthening by means of completely enveloping the column. CFRP has been found to be the ideal solution to increasing the structural capacity of these aging, failing members due to their strength, ease of application, and low maintenance (Correia, 2013).

Externally bonded CFRP sheets tend to have a brittle failure mechanism. This is when the ductility has been reduced, resulting in a sudden failure, which tends to be caused by debonding at the ends of the reinforcing sheets. In contrast, when looking at cast-in-place FRP bars, the FRP bars provide a more ductile failure and fail due to crushing of the concrete, which tends to be more desirable for design. Both methods, however, provide an increase in overall strength using equivalent amounts of reinforcing material (Ceroni, 2010).

3.2.2 Previous studies performed

Concrete prisms, tested in a double lap shear pull-out test configuration, with surface bonded CFRP strips on opposite sides were statically loaded by Atunbi (2018). In this experiment, the researcher found that the failure mechanism was due to concrete failure in tension at the substrate, as opposed to the CFRP or adhesive failing. The failure was initiated by a wedge crack in the concrete, described as a tension crack at the critical point of the CFRP sheet, leading to a bond failure. This failure can be seen in Figure 3.1. Three CFRP bonded lengths were tested by Atunbi (2018): 160 mm, 240 mm, and 350 mm. It was found that when increasing the bonded length, there was no significant increase in the maximum bond stress of the members. This conclusion fits well with other research conducted in the field (Al-Zubaidy et al., 2012), (Huo et al., 2016). Atunbi's experiment also confirmed that the use of DIC to measure strain was accurate when compared to the more traditional strain gauges used.

Figure 3.1: Wedge crack induced bond failure in static testing.
Image obtained from Atunbi (2018).

Comparison studies between static and dynamic loading on concrete members have been conducted for many decades. Under dynamic loading conditions, concrete is known to have a higher ultimate strength under compressive loads, and an even larger increase in strength in tensile loading (Pereira et al., 2017). Currently, the Canadian blast code CSA S850 (2012) uses a Dynamic Increase Factor (DIF) of 1.1 under compression, while the CEB-FIB Model Code for Concrete Structures (2010) and the UFC 3-340-02 Structures to Resist the Effects of Accidental Explosions (2008) both use a DIF of 1.12 for strain rates of 1 s^{-1}. For flexural design, these values are increased to 1.2 for the Canadian blast code, whereas the European and the US standards both use 1.19. The Canadian blast code (2012) also has a DIF of 1.0 for the tensile strength of FRP under flexural loading conditions, implying no change in behaviour under dynamic loads.

Huo et al. (2016) found that, when performing a three-point bending test on concrete specimens reinforced with CFRP sheets, the effective bond length of the CFRP sheet was shorter when the load was applied under impact conditions, as opposed to static. The effective bond length, as described by Huo et al. (2016), is the distance from the peak strain to the location where the measured strain is lower than 5 % of peak strain. This, however, has been contradicted in other research. A direct shear test on two steel members connected using CFRP sheets was carried out by Al-Zubaidy et al. (2012), where it was found that increasing the loading rates did not have the same substantial effect on the effective bond length as what was found by Huo et al. (2016).

3.3 Experimental Program

The conducted experimental program consisted of a total of twenty specimens with three different bonded lengths. Only three from each bonded length, however, are considered in

this paper. These specimens were tested in a double tab shear pull test on the CFRP sheet to concrete bond. This section of the paper details the specimens used, experimental setup, and the method for capturing all data obtained.

3.3.1 Specimen preparation

The specimens used in this experiment were prepared in conjunction with the static loading experiments conducted by Atunbi (2018) based on the experimental procedure detailed in Annex N of the CSA S806 standard (2012) by casting the prisms and applying the CFRP sheets to the specimens. Atunbi (2018) cast the concrete prisms, with dimensions of 500 mm in length and a cross-section of 150 mm by 150 mm, using ready-mix concrete. Each prism was cast with a 20M steel reinforcing bar embedded into the centre. These reinforcing bars extended out one end of the concrete prism and were used to facilitate loading and hold the specimen and load cells in place during tests. The naming convention for the specimens used in the experiments discussed in this paper uses two distinguishing identifiers. The naming convention used the following LX-# format, where the “X” denotes the bonded length being either 160 mm, 240 mm, or 350 mm. The “#” refers to the specimen number in the bonded length group. Figure 3.2 shows typical specimens after they had been cast and awaiting further preparation, as well as specimens after final preparations had occurred.

(a) Cast prisms.

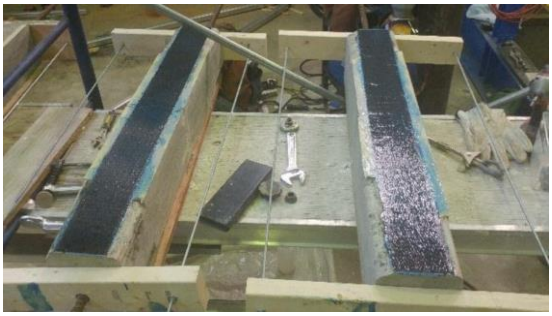

(b) Finished specimens.

Figure 3.2: Specimen Preparation by Atunbi (2016).

The CFRP used in this experiment was the same product used by Atunbi (2018), MasterBrace FIB 300-50CFS (BASF, 2019). This product is comprised of unidirectional carbon fibres with a thickness of 0.165 mm. The adhesive that bonds the CFRP to the concrete face was also manufactured by Master Brace, the adhesive was a combination of a primer, putty and a saturant (Atunbi, 2018).

To evaluate the compressive strength of the concrete used, standard cylinders of dimensions 100 mm in diameter, and 200 mm in height were tested. The compressive strength was found to be 32.3 MPa at the time of static testing (279 days) (Atunbi, 2018). The remaining cylinders were then tested at the time of testing for the experiments in this paper (27 months of age), where the compressive strength was found to be 29.4 MPa. The MasterBrace FIB 300-50CFS CFRP product (BASF, 2019) was applied to the concrete specimens at 51 days after the prisms were cast, by Atunbi (2016). The CFRP product has a tensile strength, elastic modulus, and ultimate strain of 642 MPa, 37.8 GPa, and 1.9 percent respectively. These values were measured from composite fibre and polymer matrix coupons that were representative of the composite CFRP strips bonded to the concrete specimens.

Each specimen consisted of two concrete prisms, which were set with a 3 mm gap between them and filled with plaster using a plastic sheet against each prism to reduce any bonds between them. As per Annex N of the CSA S806 standard (2012) the specimens were cleaned of any dirt or debris to allow the best possible bond between the CFRP and concrete as possible. After the surface cleaning, primer and putty were applied following the manufacturers' specifications, which creates a smoother surface for the bonding. Once the concrete surface was properly prepared, the CFRP sheets were cut into their respective lengths, and the resin was infused into the CFRP before being applied to two (2) opposing sides of the specimen. The CFRP sheets were bonded along the entire length of one (1) of the concrete prisms to act as an anchor, with the other end of the CFRP sheets being cut to length after bonding (Atunbi, 2018). Finally, another layer of resin was applied after the CFRP sheets were set.

3.3.2 Test set-up

The test apparatus, as shown in Figure 3.3 along with an accompanying sketch in Figure 3.4, supported the concrete specimens between the two posts shown. As the load is applied to the impact plate on the lefthand side of the image, the applied force rotates the impact plate about the hinges shown. The hinges allow the lefthand side post to rotate and transfer the downward load into a horizontal load, resulting in tension in the specimen.

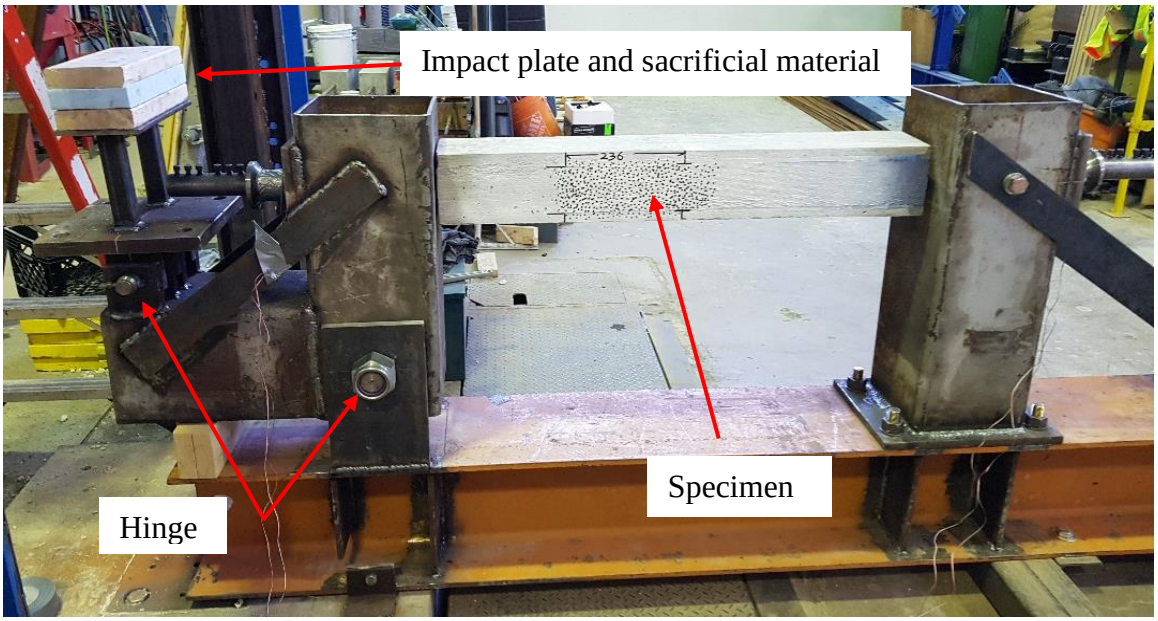

Figure 3.3: Test apparatus.

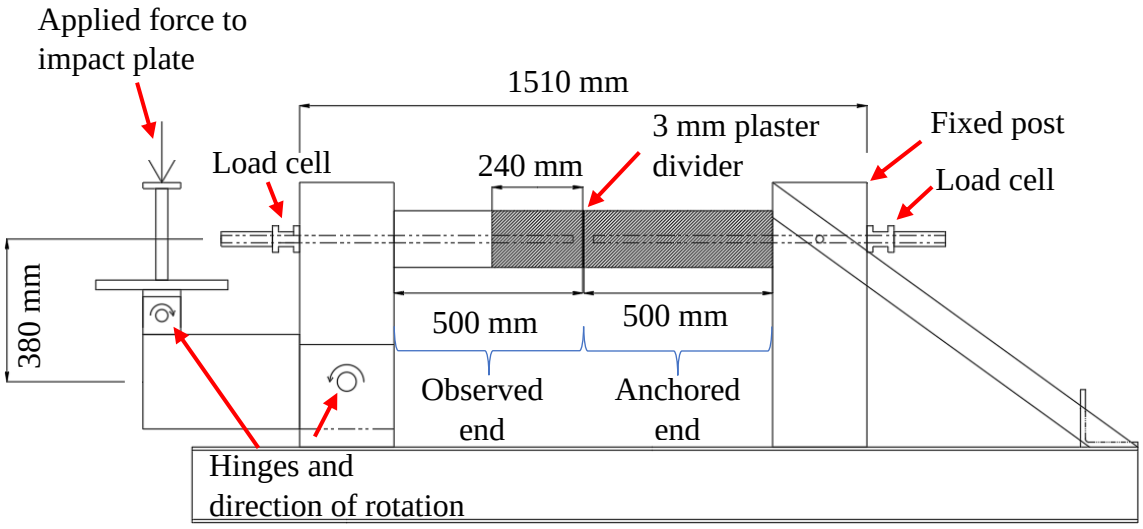

Figure 3.4: Apparatus sketch.

As can be seen in the above figures, the concrete specimen was placed between the two vertical posts, supported by the rebar. The rebar, embedded and extending from the prisms, fits through holes in both posts and is secured on the outside, using rebar couplers. Once the concrete specimen was placed in the apparatus, the load cells were placed on both ends,

with the rebar fitting through the load cells, and the high-speed camera put into position. This position was determined upon setup as lighting and safety for the equipment were the main concerns for the camera position. A large mass drop tower was used to load one end of the prisms. The mass was dropped onto the impact plate and two (2) hinges were employed to transfer the vertical impact force through the horizontal specimen. Calculations are shown in Appendix A to find the rotation experienced by the load cell placed on the exterior face of the hinged post, as well as the rotation of the specimen itself to demonstrate this rotation is kept to a minimum. A wood and expanded polystyrene layup was used as an impact damper on the impact plate. This damper allowed the force transfer to slow to a reasonable level to ensure the strain rates in the CFRP were close to to the goal of 1 s^{-1} (See Section 3.4.2 for information on strain rate). A strain rate of 1 s^{-1} was chosen to investigate the lower bound of the wide range covered under impact loading.

Before testing could occur, the concrete prisms were prepared for optical measurements with DIC. This was done by choosing one of the prisms faces with the CFRP and applying a thin coat of white spray paint. Once dry, large black dots were applied to create a high contrast speckle pattern. This paint and speckle pattern allowed the DIC software to detect and track deformations, which were used to calculate the strain fields. Figure 3.5 and Figure 3.6 show a typical test specimen before and after painting.

Four test specimens for each of the three bond lengths (160 mm, 240 mm, and 350 mm) were tested as static loading control specimens (Atunbi, 2018). A total of eight 160 mm, six 240 mm, and another six 350 mm bonded length specimens were tested under impact loads. Due to testing errors, only three impact tests from each group could be used for the purposes of this paper. Testing errors included the following: inadequate speckle pattern

due to light reflection, inadequate anchorage of the rebar by the rebar couplers, failure of the specimens to fail from the applied load, and load cells reporting drastically varied results, indicating an issue in the load cells leading to further diagnostics and adjustments.

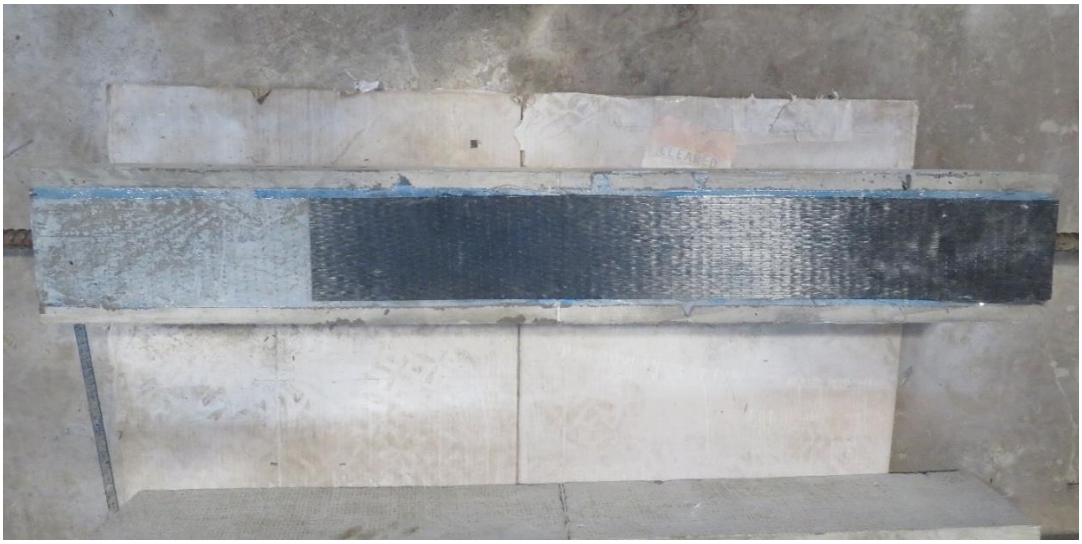

Figure 3.5: Typical test specimen (before painting).

Figure 3.6: Typical test specimen (after painting).

3.3.3 Data acquisition

During testing, there were two data acquisition systems in place. The first system measured the axial force in the reinforcement. Two load cells were used for testing, and were designed as cylindrical with hollowed centres, which the rebar could pass through, along with a rebar coupler pressed on the outside to hold in place. These load cells calculate the force using two quarter bridge strain gauges on each load cell, placed on opposite sides of the test specimen. To calculate the total force, the two strain gauges in each load cell were averaged and a calibrated relationship between measured strain and applied load was applied. For the load cells to accurately measure the peak of the impact, a sample rate of 50 kHz was used. Calibrating the load cells was completed using a 250 kN Instron universal testing machine.

Other data was acquired from a high-speed camera. To achieve a balance between high frame rate, and high resolution, a 16000 fps recording rate was used. Specimens were cleared of any dirt and debris before a light coating of white spray paint was applied. This provided a uniform background that contrasted against the black dot speckle pattern applied using a black permanent marker after the painting. The camera was placed at 4.5 m from the specimen face. At this distance, it was both safe from any debris that may have damaged the camera, as well as being able to capture the entire area of interest while keeping an adequate resolution for DIC. Data was recorded for a total of four seconds, with 50 % of the data occurring before the recording was triggered and the remainder after. This was to ensure that if the researcher either triggered the camera slightly early, or late, the impact would be captured within a reasonable range. Once the camera was placed in position, level and perpendicular to the test specimen, small marks were placed on the

specimen, close to the edge of the field of vision of the camera. The distance between these marks was measured, recorded, and written on one of the test specimens' faces. This distance was used to calibrate the DIC measurements during the analysis of the experiments.

The software used for the DIC calculations was VIC 2D (Correlated Solutions, 2018). This software takes each frame and tracks the changes in location of the previously mentioned black dots on the test specimen. For DIC to accurately calculate the strains, an initial reference image was required. The reference image used in each of the experiments was one of the frames just before the impact.

3.4 Experimental Results

Following each experiment, the failure of the specimen was observed and documented. As expected, debonding began at the joint between the two concrete prisms, referred to as the critical point, or loaded end, which extended outwards from this location. For the statically loaded specimens, tested by Atunbi (2018), the failure was initiated by the concrete failing in tension and the CFRP peeled back, removing a layer of concrete with it, indicating that the adhesive had fully bonded the CFRP sheet to the concrete face. The failure of the dynamically loaded specimens was also initiated by the concrete prisms failing in tension, however, the subsequent interfacial shear debonding was not as consistent. The CFRP sheets in the static testing were observed to have a full layer of concrete still attached after debonding, whereas the dynamically tested specimens did not always have concrete still attached to the majority of the CFRP sheet surface area after debonding. This means that some dynamically loaded specimens failed due to the capacity of the bonding agent, whereas others had failed in the concrete side of the bond. Far more specimens failed due

to the concrete failing than the adhesive failing; however, they were never as consistent or uniform of a failure as those tested under static conditions. Figure 3.7 shows the variation in failures, from a high percentage of adhesion failing to a very low percentage of adhesion failing, as well as a photo of a typical failure from the static loading scenario where it fails due to the concrete.

a) Dynamic test with mainly concrete failing.

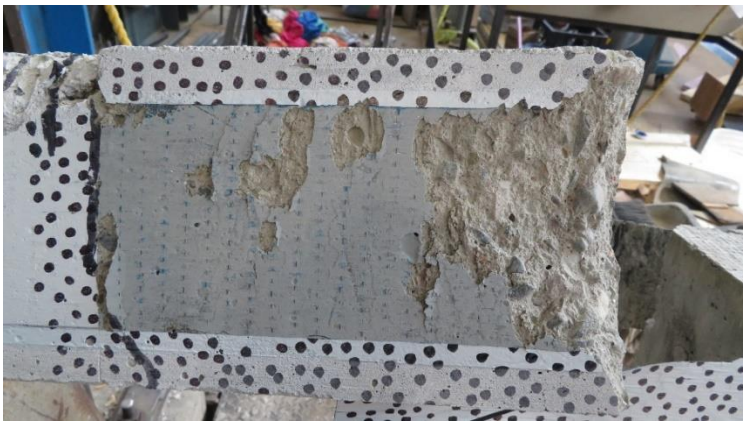

b) Dynamic test with mainly adhesive failing.

c) Typical static test with concrete failing.

Figure 3.7: Differing failure modes between dynamic tests and a typical static test.

As mentioned above, the CFRP began debonding at the critical point. This occurs due to a wedge crack, also referred to as a corner crack, forming at the critical point. These wedge cracks are believed to be formed from tension cracks occurring near the prism end and breaking off. An example of a prism with typical wedge cracks, along with a drawing to help illustrate the formation of wedge cracks, can be seen in Figure 3.8. Additionally, labels indicating the loaded side and unloaded side of a typical specimen is included.

a) Wedge cracks formed after dynamic testing.

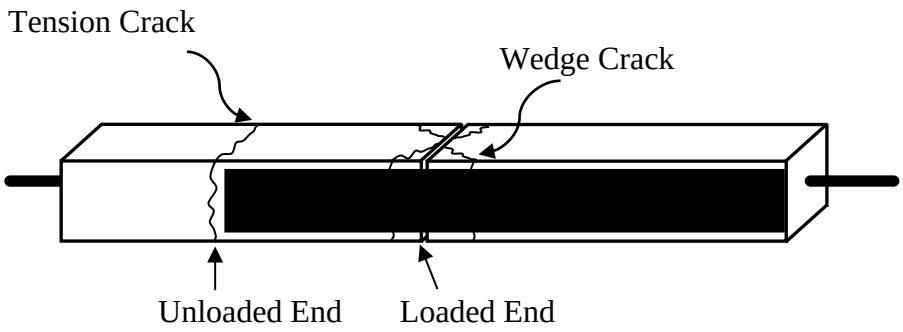

b) Depiction of cracks (Atunbi, 2018).

Figure 3.8: Typical cracks.

Tension cracks also appeared on the unloaded end of the specimens. This matches what was found in the static tests Atunbi (2018) conducted. Additionally, Atunbi (2018) found that these tension cracks were not present on the specimens with a bonded CFRP length of 350 mm. In the experiments conducted for this research, tension cracks were always present on the unloaded end of all specimens, regardless of bonded CFRP length. The two shorter bonded lengths, 160 mm and 240 mm, always cracked at or slightly beyond the end of the bonded CFRP. The average distance past the CFRP cut-off point was 26 mm and

16 mm, respectively. This was not the case for the specimens with a bonded length of 350 mm, where the tension crack occurred 220 mm beyond the critical point, on average.

3.4.1 Load cell data

The ultimate loads for each of the nine specimens, distributed among the various bonded lengths examined, is summarized in Table 3.1. The average ultimate force for the 160 mm, 240 mm, and the 350 mm bonded length specimens are as follows: 72.7 kN, 65.1 kN, and 76.8 kN, respectively. This shows that there was a drop in the average ultimate force between the 160 mm and the 240 mm bonded specimens. The load, as discussed in the experimental program chapter of this paper, was recorded using two independent load cells. The values obtained from these two load cells were averaged to give the final load over the period of the impact. As mentioned, the table below summarizes all nine specimens and their average peak load, standard deviation, and coefficient of variation for all three of the bonded lengths. The maximum loads obtained through static loading and their respective DIF values are also included. It should be noted that the standard deviation and coefficient of variance were calculated, and with these, it was found that the difference in results is not statistically significant, as shown in Figure 3.9. However, Bentler et. al (1987) suggest that for data that is either normally or elliptically distributed, a five to one ratio of samples to parameters is recommended. For data where the distribution is less certain, a ten to one ratio is recommended.

Table 3.1: Maximum recorded force compared to maximum force from static tests.

Specimen Dynamic	Max. Force (kN) Dynamic	Avg. Force (kN) Dynamic	SD*	COV*	Avg. Force (kN) Static**	DIF
L160-1	76.0					
L160-2	63.0	72.7	8.6	0.12	39.0	1.86
L160-3	79.2					
L240-1	57.2					
L240-2	67.0	65.1	7.0	0.11	43.4	1.50
L240-3	70.9					
L350-1	59.6					
L350-2	84.4	76.8	14.9	0.19	40.0	1.92
L350-3	86.4					

*SD = Standard Deviation, COV = Coefficient of Variation, Avg. = Average Values.
**Static loads taken from data obtained by Atunbi (2018).

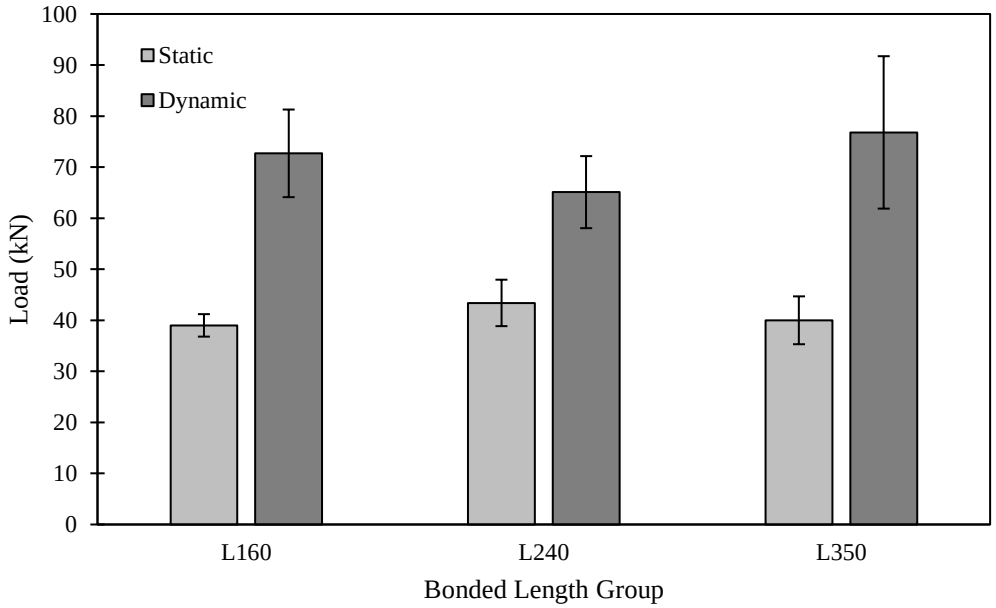

Figure 3.9: Statistical Analysis of Specimen Loading.

The average loads found during the dynamic tests appear to be much more varied than those found during the static testing; However, from calculating the standard deviation and a coefficient of variation, it was found that the difference in results was not statistically significant. With the static testing, the average peak loads were found to have a maximum variability of 4.4 kN, which is between the L160 and L240 bonded length groups. This

variability is increased drastically when looking at the dynamic testing groups, where the difference is increased to 11.7 kN. There are many factors that could lead to this drastic increase in variation, as there is a much higher level of control of the strain rate during static testing as opposed to dynamically. Figure 3.10, Figure 3.11, and Figure 3.12 show the force versus time graphs for L160-2, L240-3, and L350-1, respectively. Each graph shows a rapid increase in force during the elastic region, with a very short to no plastic region, before debonding. The force versus time graphs for all specimens can be found in Appendix B.

Figure 3.12, L350-1, shows the longest plastic region before failure, whereas L240-3 shows a very sudden failure. Each graph has the individual calculated load from both independent load cells along with the averaged force between the two with four points marked out, corresponding with the points that will be examined further on in this paper.

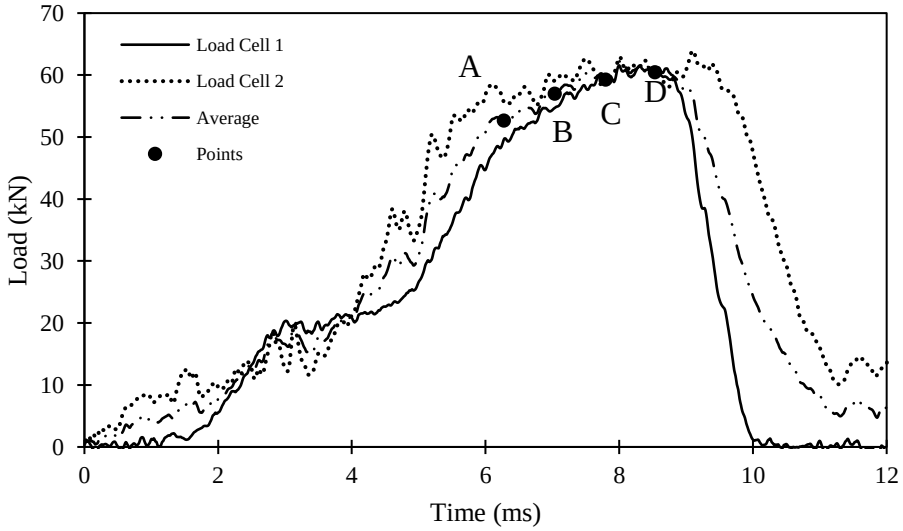

Figure 3.10: L160-2 force vs. time graph.

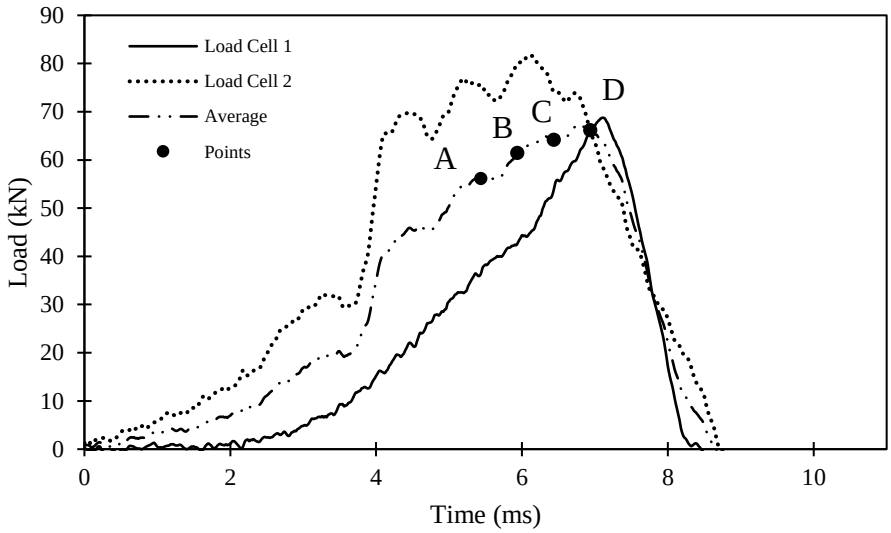

Figure 3.11: L240-3 force vs. time graph.

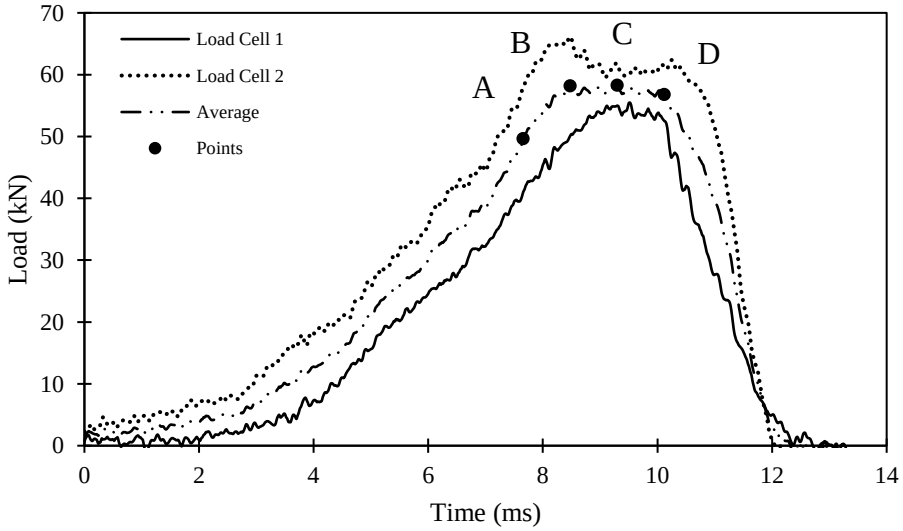

Figure 3.12: L350-1 force vs. time graph.

3.4.2 Strain data

Each of the specimens were also analyzed using the DIC software. This software takes each individual frame from the video file and tracks the movement of the markers placed on the specimen to detect the displacements across the field of vision. Once the debonding

occurred at the critical point, the strain readings reached a plateau and stayed relatively constant at that point. Figure 3.13, Figure 3.14, and Figure 3.15 are presented to show the strain rate, which was obtained by calculating the slope between the maximum strain and 40 % of the maximum. These graphs also show four markers listed as A, B, C, and D. These markers correspond to snapshots in time for each specimen to visualize the debonding process, shown in Figure 3.16, Figure 3.17, and Figure 3.18. The debonding occurred as described, by beginning at the critical point, at the loaded end, and propagating outwards away from the loaded end. This propagation is shown by the peak strain in the CFRP sheet reaching a point where a plateau begins to develop over time, until the CFRP sheet has completely debonded from the concrete prism. The strain profile for all specimens can be found in Appendix B.

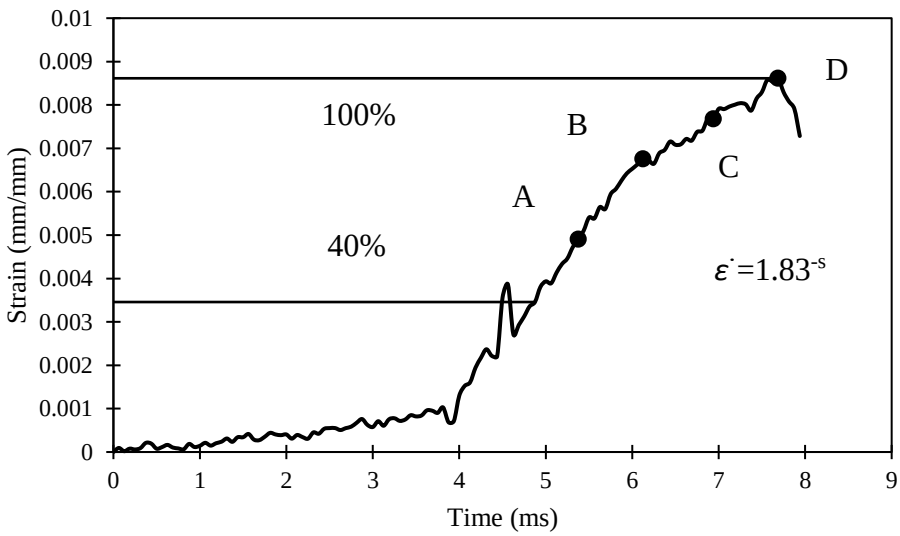

Figure 3.13: L160-2 strain time history.

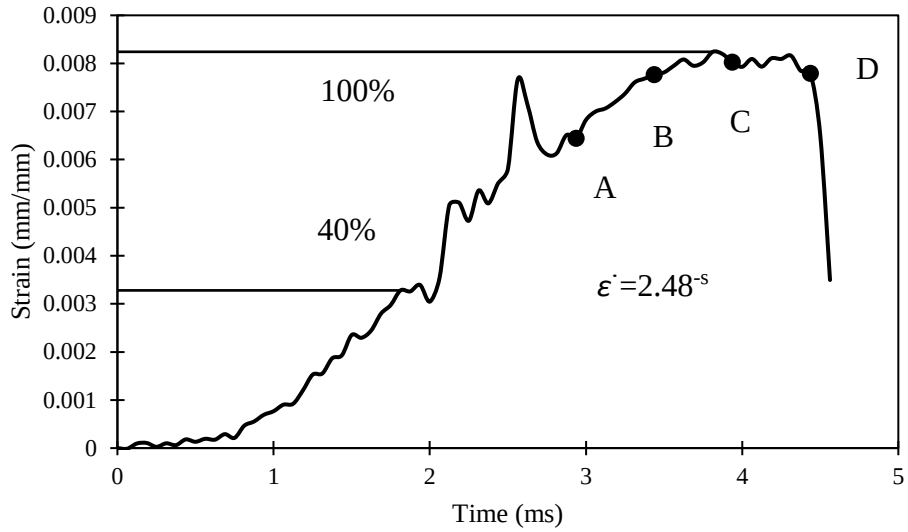

Figure 3.14: L240-3 strain time history.

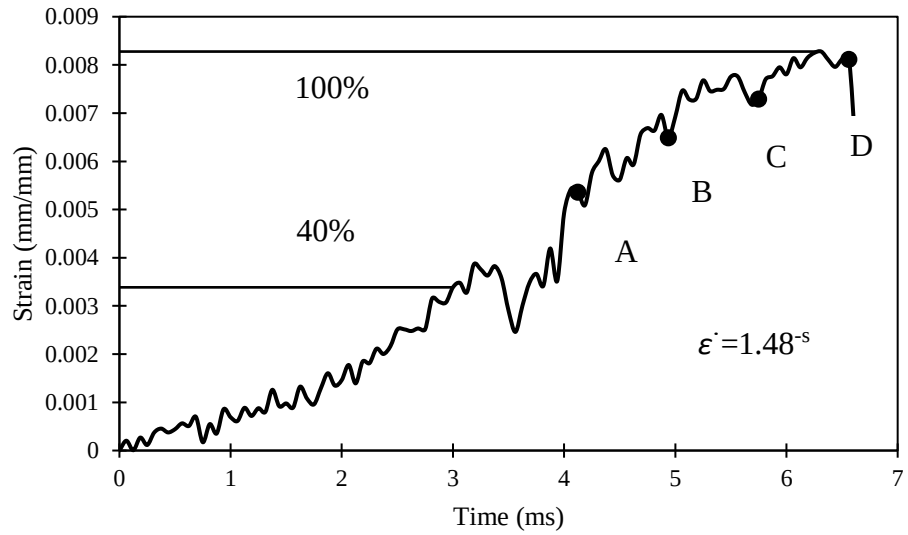

Figure 3.15: L350-1 strain time history.

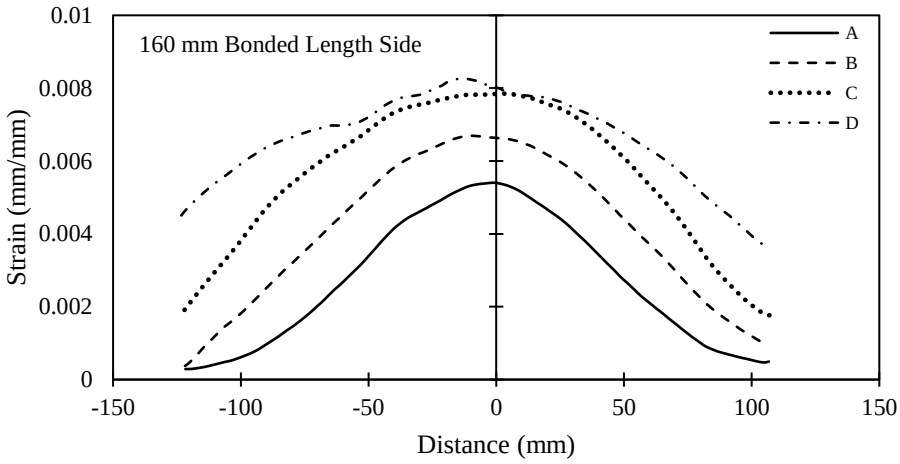

Figure 3.16: L160-2 strain distribution at four distinct times.

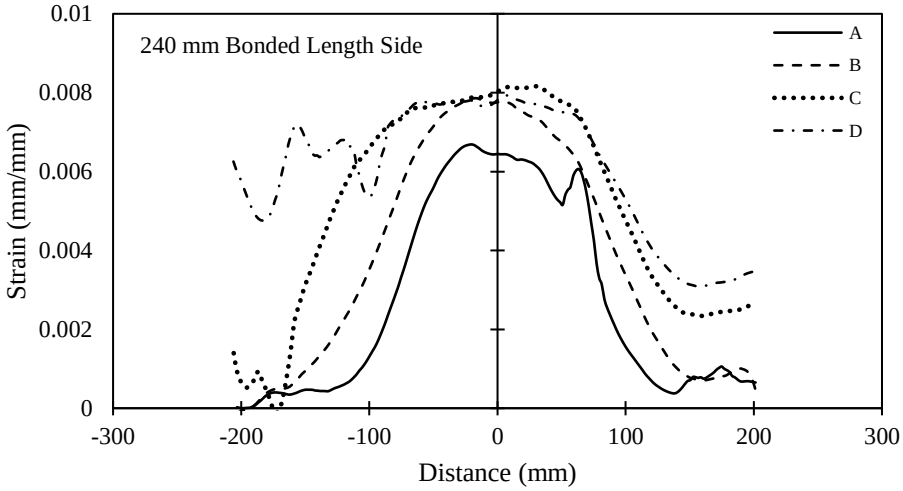

Figure 3.17: L240-3 strain distribution at four distinct times.

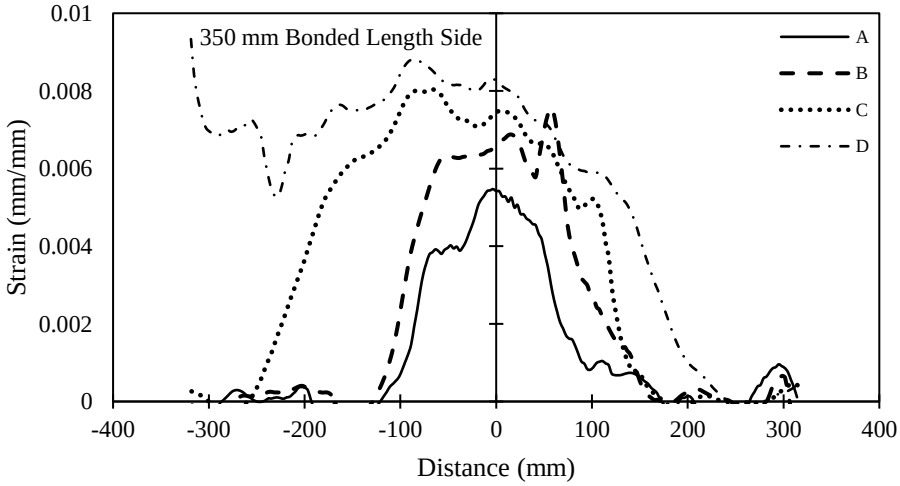

Figure 3.18: L350-1 strain distribution at four distinct times.

From Figure 3.16, Figure 3.17, and Figure 3.18, the maximum strains can be seen for specimens L160-2, L240-3, and L350-1. These graphs were created in the software VIC 2D and used a single axial inspection line across the area of interest of the relevant specimen. When compared to the statically loaded specimens tested by Atunbi (2018), these values are much higher. This was expected as materials loaded dynamically tend to have a higher ultimate capacity than those loaded statically. The plateaus beginning at the critical point and extending outwards tend to form very rapidly near the end of the impact. Strain versus time graphs show that the strains continue to grow throughout the impact, and the strain plateau slowly levels off until it reaches the peak strain at which time the remaining CFRP reaches that peak in a short period of time.

As previously discussed, materials loaded under dynamic conditions may exhibit a higher ultimate capacity than those loaded statically, which can be accounted for using a DIF. Table 3.2 shows the average maximum strains for each specimen group for the tests performed for this paper, against the statically loaded specimens by Atunbi (2018). The average maximum strains for the dynamically loaded group in the L160, L240, and L350 bonded length groups are 0.80 %, 0.84 %, and 0.92 %, respectively. These maximum strain values are higher than those reported from the static groups, as expected. The DIF values calculated for the L160, L240, and L350 are 1.78, 1.47, and 1.61, respectively. These DIF values are much higher than what was expected, as reported by the relevant codes (Canadian Standards Association, 2012; Unified Facilities Criteria, 2008; Fédération internationale du béton, 2010). This, however, is supported by the data collected from the load cells. Table 3.2 shows both the DIF calculated from the strain data, as well as the DIF

calculated from the load data, for each of the three specimen groups. The DIF values calculated are very similar. These two measurement systems were fully independent of each other and produced similar DIF values.

Table 3.2: Average maximum strain comparison between dynamic and static tests.

Specimen Group	Dynamic Maximum Strain (%)	Avg. Dynamic Maximum Strain (%)	Static Maximum Strain (%)	DIF (Strain Data)	DIF (Load Cells)
L160	0.91 0.78 0.71	0.80	0.45	1.78	1.86
L240	0.88 0.82 0.82	0.84	0.57	1.47	1.50
L350	0.83 0.94 0.98	0.92	0.57	1.61	1.92

3.5 Conclusions and Recommendations

This paper explored the results of experiments investigating the bond between CFRP sheets and concrete under dynamic loading conditions. Two load cells were used in this experiment, which were placed on either end of the specimen and averaged over the course of the experiments. DIC was used to measure the strains across the specimens. Using these two methods of obtaining data, the following conclusions and recommendations can be drawn:

1. The failure mode observed in this experiment was initiated by the concrete failing in tension, by means of a wedge crack. From there, it was expected that debonding would occur due to the interfacial shear failure of the concrete. While this was

observed to be the case for the majority of the specimens, matching what was observed by Atunbi (2018), by the back face of the fully debonded CFRP sheet retaining a layer of concrete, this was not always the case. It was observed that the interfacial shear failure did not always occur in the concrete, but would also happen in the adhesive. By observing the back of the debonded CFRP sheets, it could be seen that some of the area had adhesive failure, while other areas had concrete failure. It is believed that, as the DIF was higher than expected, the ultimate capacity of the concrete increased beyond the strength of the adhesive bond in some of the specimens. Further experimentation with different adhesives is recommended, as this adhesive may not be forming the complete bond as was expected and assumed.

2. Much higher DIF values were found than expected when examining both the load data and strain data. These DIFs ranged from 1.47 to 1.78, which differs greatly from the 1.19 to 1.20 for concrete in flexure, and the 1.0 for FRP in flexure, as prescribed by the relevant codes (Canadian Standards Association, 2012; Fédération internationale du béton, 2010; Unified Facilities Criteria, 2008). Further dynamic tensile tests should be conducted with a larger sample size to find a more precise DIF for CFRP sheets externally bonded to concrete.
3. The strain plateaus observed by Atunbi (2018) were observed in this experiment as well. These plateaus formed, starting at the critical point located at the loaded side and propagated outwards, as the concrete to CFRP bond was broken, and continued along the length of the specimen during the propagation of debonding.

4. There was a small difference in ultimate bond strength between the three bonded lengths, 160 mm, 240 mm, and 350 mm. These values were 72.7 kN, 65.1 kN and 76.8 kN, respectively. The 240 mm bonded length specimens had an average ultimate capacity lower than either the 160 mm or 350 mm bonded groups. This is reflected in the calculated DIF values from both the load cells and strain data of 1.5, which was lower than the other specimen groups. Further tests with a larger sample size are recommended as this was an unexpected result and may have been due to an outlier specimen.
5. Tension cracks were always found at or near the unloaded ends for the 160 mm, and 240 mm specimens. As for the 350 mm specimens, the tension crack was found at an average of 220 mm along the length of the CFRP, measured from the critical point. This differs from the statically loaded specimens tested by Atunbi (2018), where the tension cracks always formed on the unloaded side, though no cracks were found on the 350 mm bonded length group. This difference in tension cracks occurring in the 350 mm bonded length group could be attributed to the inertial effects present in dynamic testing.

Further studies where the specimens are loaded dynamically is recommended. This study has shown that the use of DIC is a useful, reliable method of measuring the strain fields under dynamic conditions, so it is suggested to continue the use of this method. Future studies should involve more specimens per bonded length group, along with multi-layered CFRP specimens. As the failure mode of the specimens was expected to be solely due to the concrete failing, an investigation into the reason for the adhesive failing would be

essential. This investigation should include different adhesives, as well as attempting different strain rates to find at what point the adhesive begins to fail over the concrete.

REFERENCES

Al-Zubaidy, H. A., Zhao, X.-L. & Al-Mahaidi, R., 2012. Dynamic bond strength between CFRP sheet and steel. *Conposite Structures,* XCIV(11), pp. 3258-3270.

Atunbi, E. O., 2018. *Experimental Study on Bond Behaviour of CFRP Sheets Externally Bonded to Reinforced Concrete.* Fredericton(New Brunswick): University of New Brunswick.

BASF, 2019. *MasterBrace FIB 300/50 CFS.* [Online].

Bentler, P.M. & Chou, C.P., 1987. Practical issues in structural modeling. *Sociological Methods & Research,* XVI(1).

Bizindavyi, L. & Neale, K. W., 1999. Transfer Lengths and Bond Strengths for Composites Bonded to Concrete. *Journal of Composites for Construction,* III(4), pp. 153-160.

Campbell, F. C., 2010. *Structural Composite Materials.* Materials Park(Ohio): ASM International.

Canadian Standards Association, 2012. *S806-12 Design and construction of building structures with fibre-reinforced polymers.* Mississauga: Canadian Standards Association.

Canadian Standards Association, 2012. *S850-12 Design and assessment of buildings subjected to blast loads.* Mississauga: Canadian Standards Association.

Ceroni, F., 2010. Experimental performances of RC beams strengthened with FRP materials. *Construction and Building Materials,* September, 24(9), pp. 1547-1559.

Correia, J. R., 2013. *The New FRP Materials for Civil Engineering Structural Applications [PowerPoint slides],* s.l.: s.n.

Correlated Solutions, 2018. *Vic-2D.* s.l.:s.n.

Fédération internationale du béton, 2010. *Model Code for Concrete Structures.* Lausanne: Ernst & Sohn.

Huo, J. et al., 2016. Experimental Study on Dynamic Behavior of CFRP-to-Concrete Interface. *Journal of Composites for Construction,* October.20(5).

Kamaitis, Z., 2002. Damage to concrete bridges due to reinforcement corrosion. *Transport,* XVII(4), pp. 137-142.

Levi-Hevroni, D. et al., 2018. Experimental and numerical investigation on the dynamic increase factor of tensile strength in concrete. *International Journal of Impact Engineering,* April, Volume CXIV, pp. 93-104.

Malvar, L. J. & Crawford, J. E., 1998. *Dynamic Increase Factors for Concrete,* Port Hueneme, CA: Naval Facilities Engineering Service Center.

Meier, U., 1996. Strengthening of structures using carbon fibre/epoxy composites. *Construction and Building Materials,* pp. 341-351.

Pereira, L. F., Weerheijm, J. & Sluys, L. J., 2017. A new effective rate dependent damage model for dynamic tensile failure of concrete. *Engineering Fracture Mechanics,* Volume CLXXVI, pp. 281-299.

Pesic, N. & Pilakoutas, K., 2003. Concrete beams with externally bonded flexural FRP-reinforcement: analytical investigation of debonding failure. *Composites Part B: Engineering,* XXXIV(4), pp. 327-338.

Unified Facilities Criteria, 2008. *Structures To Resist The Effects Of Accidental Explosions.* s.l.:National Institute of Building Sciences.

Zhu, H. et al., 2014. Digital image correlation measurement of the bond-slip relationship between fiber-reinforced polymer sheets and concrete substrate. *Journal of Reinforced Plastics and Composites,* XXXIII(17), pp. 1590-1603.

4. EXPERIMENTAL ANALYSIS OF THE CFRP SHEET TO CONCRETE SUBSTRATE BOND UNDER HIGH STRAIN RATES[2]

Abstract

The need to account for dynamic loading in structures, by impact, blast, or other means is important for safe and effective design in high strain rate applications. Not only does new construction need to account for these types of loading, but existing structures that were not originally designed to handle such loads have needed to be retrofitted to handle such extreme loading. CFRP sheets have shown to be a versatile, inexpensive, and easy to install solution to retrofitting aging structures for a variety of reasons. While this material is used extensively in the civil engineering world to retrofit existing structures, an adequate understanding that has been accepted by the engineering world on how this composite material behaves under higher strain rates has not been achieved. As previous research has indicated, the failure mechanism of CFRP sheets, and other FRP products, is most often by delamination. This type of a failure shows that while having an understanding of how the fibres react under high strain rates versus lower strain rates is important, it is imperative that studies continue to evaluate the composite action of CFRP sheets bonded to common building materials such as concrete and steel. This paper explores the bond stresses developed in CFRP sheets to concrete substrate specimens when subjected to strain rates in the order of 1 s^{-1}. These bond stresses are compared against values found in static testing

[2] Harman, J., & Lloyd, A. (2022). Experimental Analysis of CFRP Sheets Under High Strain Rates Surface Bonded to Concrete. *Unpublished.*

carried out by a previous researcher using identical specimens with similar testing procedures.

The specimens used in this study consist of concrete prisms cast with CFRP sheets bonded to opposing faces and tested in a double-lap pullout experiment. The specimens were split into three (3) groups of varying bonded lengths, and the strain fields were measured using digital image correlation techniques (DIC) and software. The DIC results are compared with load from load cells installed on each end of the specimens to validate the values found by the DIC technique. As the strains experienced in the static and dynamically loaded specimens were both measured using DIC techniques, a comparative analysis was performed to compute dynamic increase factors (DIF) for the bond stresses achieved under high strain rates. The goal of this study is to obtain these DIF values to further the understanding of CFRP sheet behaviour with respect to strain rate in order to facilitate the adoption of DIF values in design and analysis of concrete structures that are expected to experience high strain rates.

4.1 Introduction

As the use of externally applied fibre reinforced polymers (FRP) have shown positive results for strengthening structural members, studies have been focusing on the effective bond length of these FRPs. The effective bond length of an FRP sheet can be described as the bonded length associated with the maximum strength of the FRP reinforcing, regardless of additional bonded material. Through these studies, it has been demonstrated that the most common methodology of failure has been due to delamination, initiating from high stress concentrations at the critical stress point (Franco et al., 2013).

As structures are subjected to a vast array of loading scenarios, it is imperative to understand how the bond between FRP sheets and the substrate material behaves under different strain rates. Through rigorous testing, it has been shown that the bond strength between FRP sheets and concrete will increase as strain rate increases (Shen et al., 2015), (Li et al., 2020). Although it is known that the bond strength increases as strain rate increases, further studies are required to have a full understanding of the bond behaviour across a wider spectrum of strain rates (Shen et al., 2015).

Developing an understanding of the bond stress at different strain rates is an important part in the debonding behaviour of CFRP sheets. Specifically, by understanding the bond stress, and knowing the ultimate strength of a material, models can be created to predict the failure method. Currently, there are numerous models that exist to predict the bond stress distribution of a member. These models vary in their complexity due to the assumptions made by the researcher (Buyukozturk et al., 2004). In order to develop the models used to determine failure modes and predict the bond stress distribution, experimental investigations have been conducted over the years. Li et al. (2020) performed a dynamic

experimental study on the debonding behaviour of CFRP sheets adhered to concrete. In this investigation the researchers utilized seventy-five (75) specimens to isolate a variety of variables including: CFRP sheet stiffness, bond width, bond length, the concrete strength, and the strain rate. After analyzing the interface bond behaviour, the researchers concluded that increasing the loading rate increases the ultimate load and the peak bond stress significantly. Such results led the researchers to conclude that the limiting factor of the bond strength could be the CFRP material load capacity as the failure mode switches from debonding to CFRP fracture.

There have been contradicting studies over the years when identifying the effects of increasing strain rates on the bond length. Shen et al. (2015) found that the specimens subjected to dynamic loading had a significant decrease in the effective bond length, when compared to the specimens subjected to static testing. This is reinforced by Huo et al. (2016); their study, a three-point bending test, found that the effective bond length was shorter under impact loading compared to static loading. Additionally, they found that the strain distribution had a steeper curve, indicating a higher interfacial shear stress between FRP and concrete (bond stress) under dynamic loading. The findings with regards to the effective bond length shortening during high strain rate events was contradicted by Al-Zubaidy et al. (2012).

This paper covers the experimental research program studying the bond stress and effective bonded length behaviour of CFRP sheets under dynamic loading conditions compared to statically loaded specimens. Specimens were tested in a CFRP sheet-to-concrete double lap pull-out shear test, with data obtained via load cells, as well as Digital Image

Correlation (DIC) software. The effective bonded length and bond stresses are summarized and compared against one another for the different bonded lengths and strain rates.

4.2 Experimental Program

There were nine (9) dynamically loaded specimens tested in this experimental program. Each specimen consisted of two (2) concrete prisms with a 150 mm x 150 mm cross-section, and 500 mm in length. Data was obtained using load cells, as well as a highspeed camera used for DIC techniques to calculate the strain across the field of interest on the specimen.

4.2.1 Specimen Preparation

The specimens were all prepared prior to the commencement of the dynamic tests by Atunbi (2018). This preparation was part of the statically loaded specimen tests that are used to compare the results of the dynamically loaded specimens against, presented in this paper. The specimens prepared for this experimental program followed the recommendations laid out by CSA S806 Annex N, Test methods for bond strength of FRP sheet bonded to concrete (2012).

The concrete prisms had one (1) 20 mm diameter rebar embedded into the centre of each prism, with the rebar extending out one (1) end of the prism. The prisms were placed end-to-end with a 3 mm gap between, maintained using plaster on each concrete prisms end and a sheet of plastic between to ensure a bond break between ends. CFRP sheets were then applied to two (2) opposing sides of the specimen; both CFRP sheets were bonded along the entire length of one (1) of the concrete prisms to act as an anchor, with the other end of the CFRP sheets being cut to length after bonding (Atunbi, 2018). Shortly before testing occurred, the dynamic specimens had both CFRP sheets cut to a length of 160 mm,

240 mm, or 350 mm on the prism not acting as the anchor. An example of how the CFRP sheet was applied and cut to the proper length can be seen in Figure 4.1.

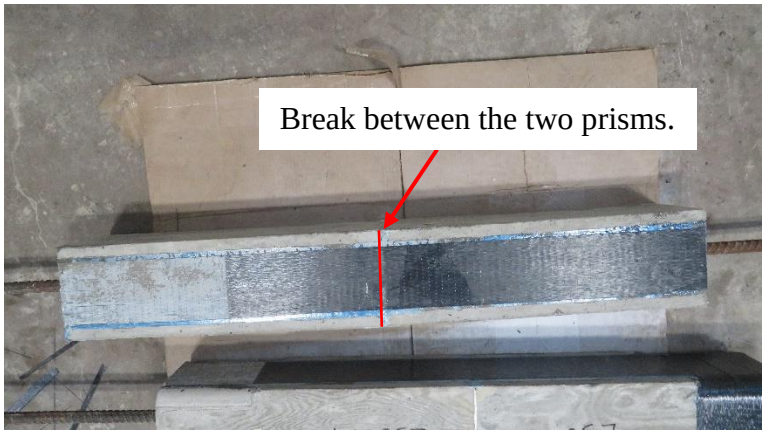

Figure 4.1: Typical specimen after CFRP cut on one (1) end.

The concrete used for the specimens had a compressive strength of 29.4 MPa at the time of testing (27 months), measured from testing standard concrete cylinders with a 100 mm diameter. The concrete prisms were cast and left for 48 hours and were then moist cured for seven (7) days. The CFRP sheets were applied to the prisms at 51 days of age (Atunbi, 2018).

The CFRP sheets used are a dry unidirectional carbon fibre sheet. The material was tested by Atunbi (2018), adhering to the directions laid out in Annex F of CSA S806-12. The CFRP coupons were tested using a 250 kN universal testing machine. The results of five (5) coupon tests and their average results can be found in Table 4.1 and plotted in Figure *4.2* (Atunbi, 2018). These CFRP sheet coupons had a length of 340 mm and a width of 38 mm. The adhesive used to adhere the CFRP to the concrete consisted of three (3) composite strengthening systems consisting of primer, putty and a saturant provided by the manufacturer.

Table 4.1: CFRP coupon properties from 1 mm thick layups.

Specimen	Ultimate Load (kN)		Ultimate Strain (mm/mm)		Tensile Strength (MPa)		Modulus of Elasticity (GPa)	
	Indiv.	Avg.	Indiv.	Avg.	Indiv.	Avg.	Indiv.	Avg.
Coupon 1	23.3		0.019		613.7		38.42	
Coupon 2	24.2		0.018		636.1		35.66	
Coupon 3	24.0	24.4	0.020	0.019	632.4	641.6	37.94	37.84
Coupon 4	26.2		0.019		689.5		38.39	
Coupon 5	24.2		0.019		636.1		38.81	

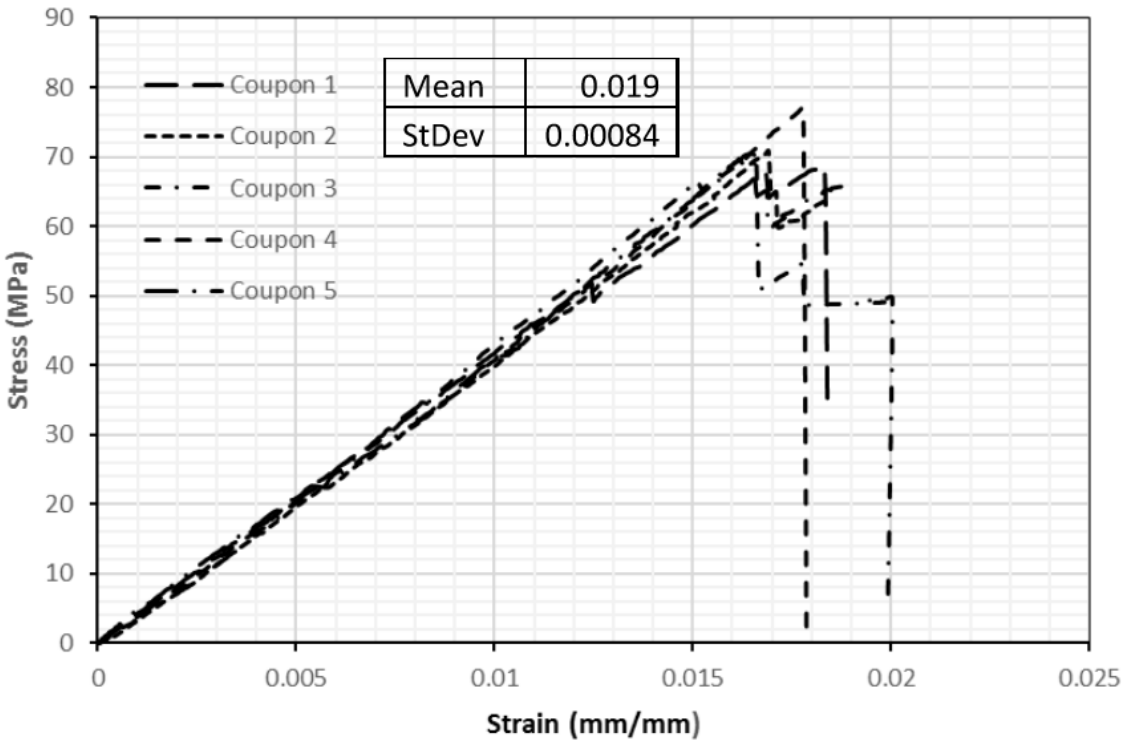

Figure 4.2: CFRP Coupon Stress vs. Strain.

Prior to testing the specimens, the side facing the high-speed camera required further preparation. Each sample had white spray-paint applied in a thin layer; thin layers were applied as a thicker layer of paint has the possibility of cracking and flaking off during testing, impacting the final strain data results. Once the paint dried, a random speckle pattern using a matte black marker was applied for the camera and data tracking software

to use. A typical specimen prior to painting, and the painting and speckling process is shown in Figure 4.3 to Figure 4.5.

Figure 4.3: Typical specimen prior to painting.

Figure 4.4: Typical painted specimen.

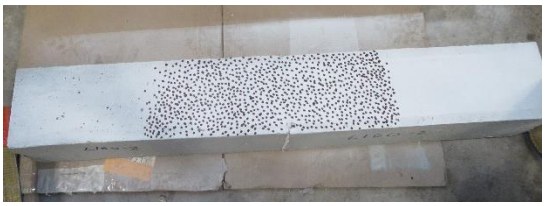

Figure 4.5: Typical specimen ready for testing.

4.2.2 Test Setup

The specimens were tested in a double lap pull-out shear method under dynamic loading conditions. For this to be achieved, the specimens were placed horizontally below a mass drop frame in an apparatus that was able to convert the vertical force delivered by the drop frame to a horizontal axial force applied to the specimen. This apparatus can be viewed in Figure 4.6 and Figure 4.7

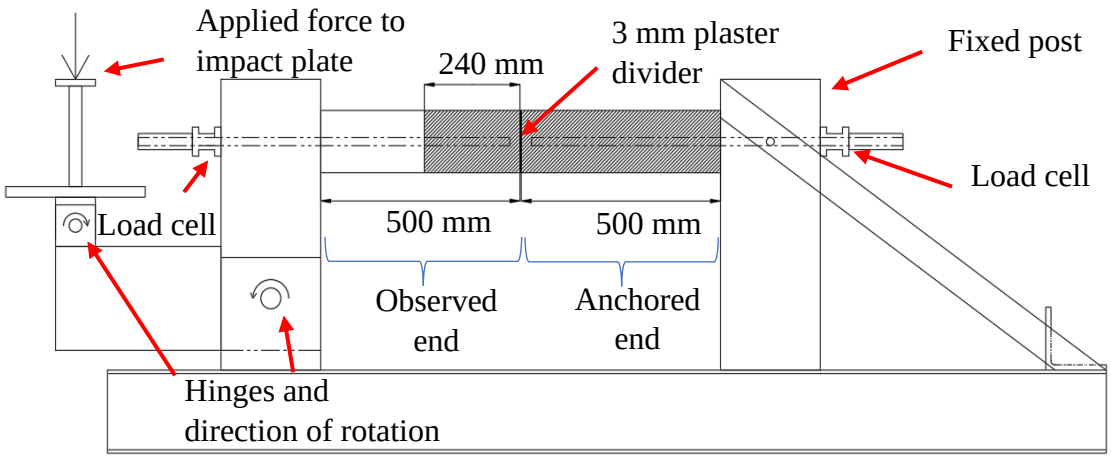

Figure 4.6: Sketch of Apparatus.

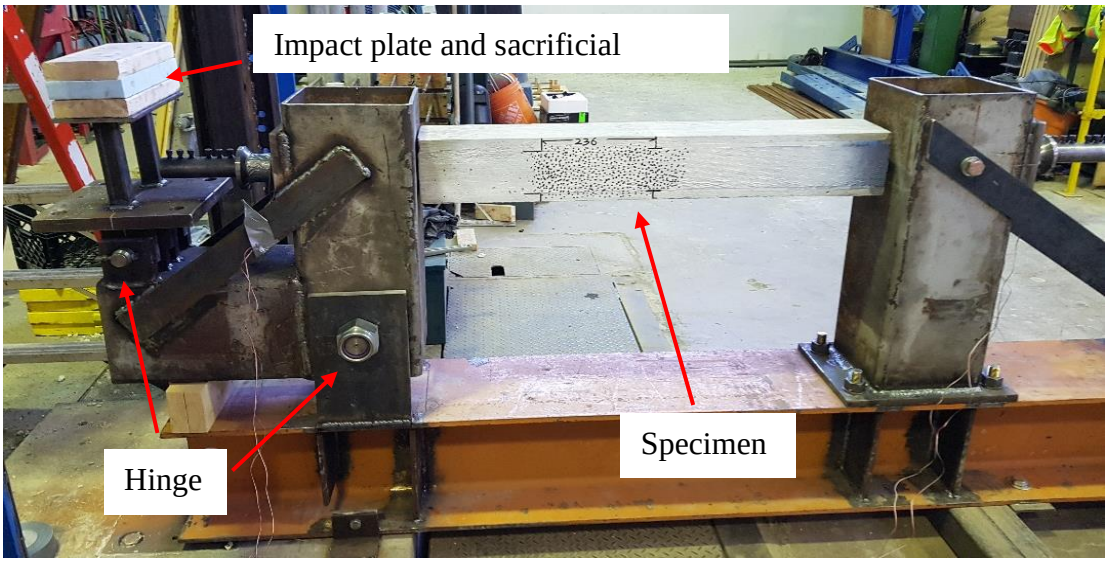

Figure 4.7: Apparatus with loaded specimen.

The apparatus holds the specimen horizontally between two (2) vertical posts. The post on the right was fixed in place with bracing attached to ensure the post did not deflect due to the dynamic loads applied. The post on the left is hinged at the bottom to allow the post to rotate, transferring the vertical force applied to the impact plate into a horizontal force on the specimen. Calculations are shown in Appendix A to find the rotation experienced by

the load cell placed on the exterior face of the hinged post, as well as the rotation of the specimen itself to ensure this rotation is kept to a minimum. When the drop mass makes contact with the impact plate, a sacrificial material, as shown above, modified the impact impulse in order to achieve the desired strain rate of approximately 1 s^{-1}. A strain rate of 1 s^{-1} was chosen to investigate the lower bound of the wide range covered under impact loading. The sacrificial material used in this experiment consisted of 51 mm rigid insulation protected and secured with wood on either side. This material was readily available and upon testing, was found to adequately reduce the strain rate to the aforementioned 1 s^{-1}. Additionally, a hinge was installed below the impact plate to allow it to rotate as the impact occurs. By allowing rotation about this hinge, the impact plate was in full contact with the sled throughout the duration of the impact. The specimen was then centred between the posts with the rebar extending through holes in both posts. With the rebar extending outwards, the load cells were placed on either end, and fixed in place using rebar couplers. This termination using load cells and rebar couplers can be seen in Figure 4.8.

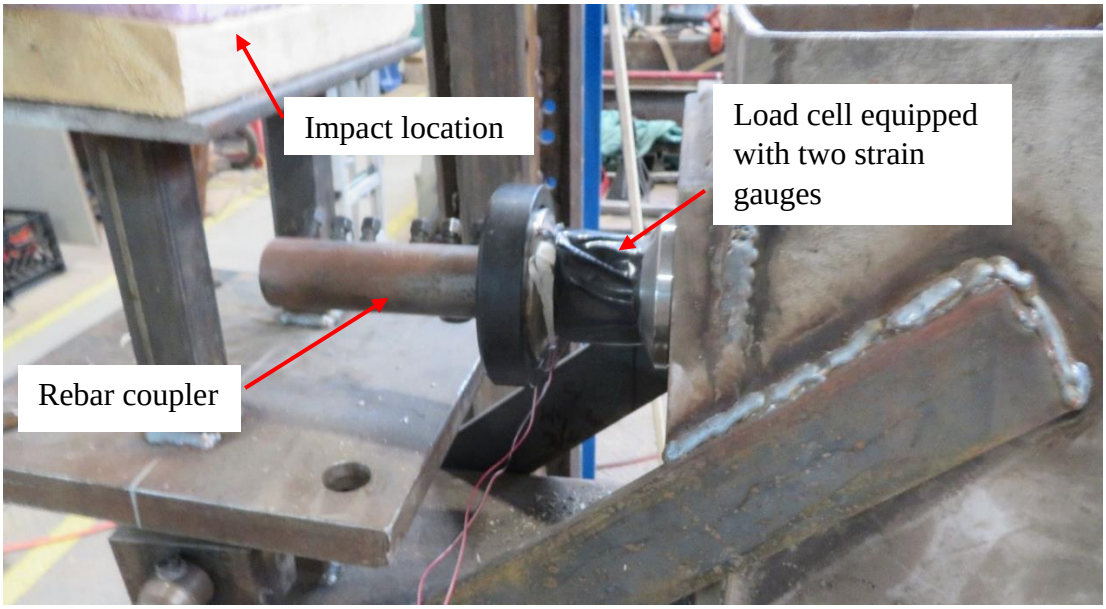

Figure 4.8: Typical rebar termination.

Once the specimen was fixed in place, the highspeed camera was adjusted to view the face of the specimen with the speckle pattern applied. The edges of the camera view were marked on the specimen, and the distance between the two points was then measured and recorded. This distance was used later for the software analysis to set a gauge length for every specimen.

4.2.3 Data Acquisition & Analysis

Two (2) types of data were recorded; strain data using a highspeed camera and DIC software (Correlated Solutions, 2018), and loads obtained through two (2) load cells positioned on either side of the specimen.

The white paint and black speckle pattern were due to the use of the DIC techniques to obtain strain data. The highspeed camera recorded at a rate of 16 kHz, and by using DIC software, the speckles were tracked across each frame during the impact. The camera was set to record prior to the impact, though only began saving the recording once the trigger

was pressed. This was set to save two seconds prior to the trigger and the following two seconds to ensure the impact was recorded and saved. An example of the data recorded by use of the DIC technique is provided in Figure 4.9.

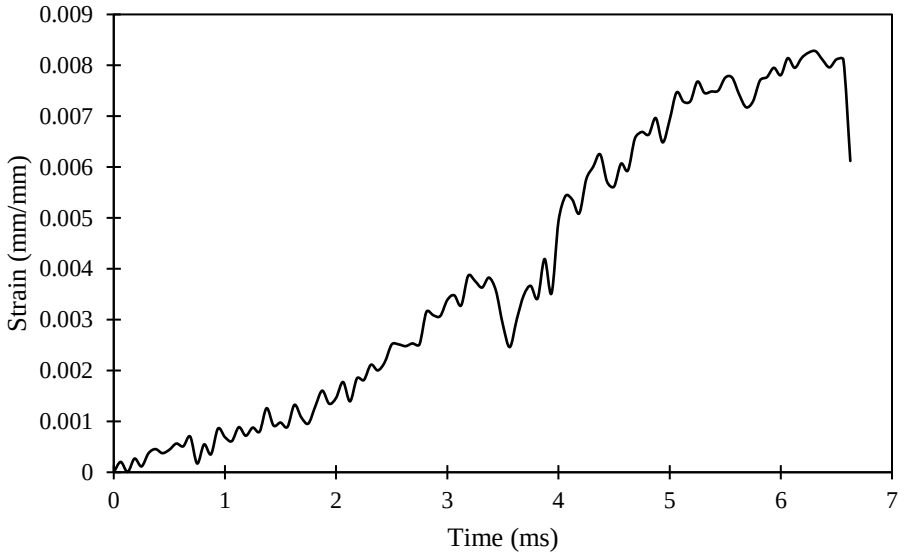

Figure 4.9: L350-1 DIC strain data.

The two (2) load cells were positioned on the outside of the posts and held in place using rebar couplers. The data acquisition system measuring the load was triggered just before the load was released and ran for five (5) seconds at a frequency of 50 kHz to ensure the load was captured. The loads obtained from each load cell were compared to ensure there was not a significant error occurring in either the timing or the magnitude of the load. The loads were then averaged to obtain the final ultimate load of each specimen. The load results for one (1) of the test specimens can be seen in Figure 4.10. Although this paper focuses on the data obtained from the DIC technique, the load cell data was used to verify the data obtained via DIC.

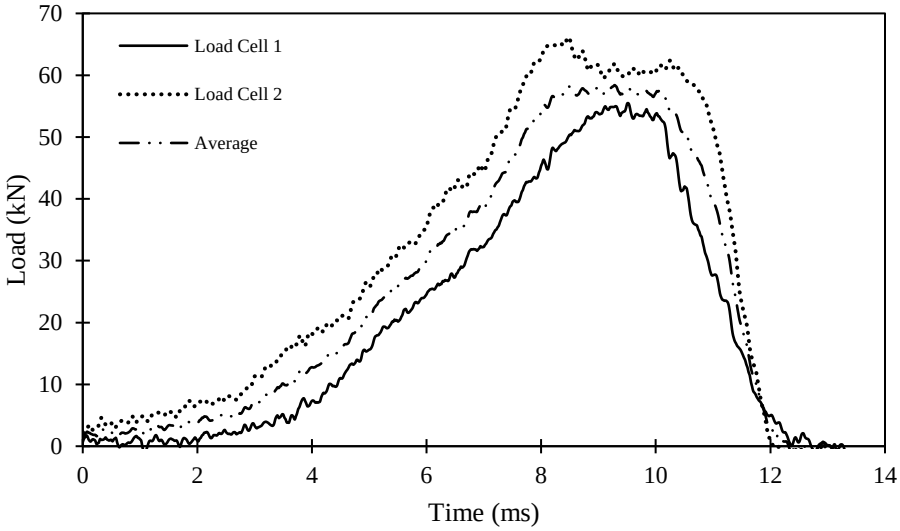

Figure 4.10: L350-1 load cell data.

An example of a test specimen after loading can be seen in Figure 4.11. The cracking pattern at the end of the debonded area has been marked in black marker.

Figure 4.11: Specimen L240-2 post debonding.

4.3 Experimental Results

4.3.1 Data Validation

As previously mentioned, there were two (2) methods of data acquisition used in this research study, using separate data acquisition systems: Two (2) load cells, and DIC techniques focusing on the strains across a field. This study focuses on the strains obtained via DIC techniques, though the use of DIC in dynamic strain rate research applications has been minimal. Therefore, load cells were used to verify the data by calculating the Dynamic Increase Factor (DIF) for both the load and strain data. This comparison can be seen in Table 4.2.

Table 4.2: Data validation.

Specimen Group	Max. Strain (%)*		Max. Load (kN)*		DIF	
	Dynamic	Static	Dynamic	Static	DIF_{ε}	DIF_{Load}
L160	0.80	0.45	72.7	39.0	1.78	1.86
L240	0.84	0.57	65.1	43.4	1.47	1.50
L350	0.92	0.57	76.8	40.0	1.61	1.92

*Average of three tests.

4.3.2 Strain Rates

The goal of the research presented herein was to determine bond stresses, effective bonded lengths, and strains loaded at a strain rate, $\dot{\varepsilon}$, close to 1 s^{-1}. It is known that many materials behave and react differently when dynamically loaded compared to statically. The statically loaded specimens were loaded at a rate of 0.5 mm/min, or a strain rate of approximately 1.5 x 10^{-4} s^{-1}, in a universal testing machine in the structures laboratory of the University of New Brunswick (Atunbi, 2018). This reported velocity represents the crosshead motion of the testing machine, relative to the displacement between the ends of the rebar grips. Using the graphs presented in Atunbi's (2018) paper, a strain rate in the

order of 1 x 10^{-5} s^{-1} was calculated. These statically loaded specimens are what the results of the dynamically loaded specimens will be compared against. The strain versus time data for each of the test specimens was analyzed to determine a strain rate per specimen. To calculate the strain rate of the CFRP sheet, a point was taken at the peak strain and another at 40 % of the peak strain. From there, by knowing how much time has passed based on the number of frames and the 16 kHz rate, the slope of the line could be calculated. An illustrative example for each of the test groups: L160, L240, L350, can be seen in Figure 4.12 through Figure 4.14.

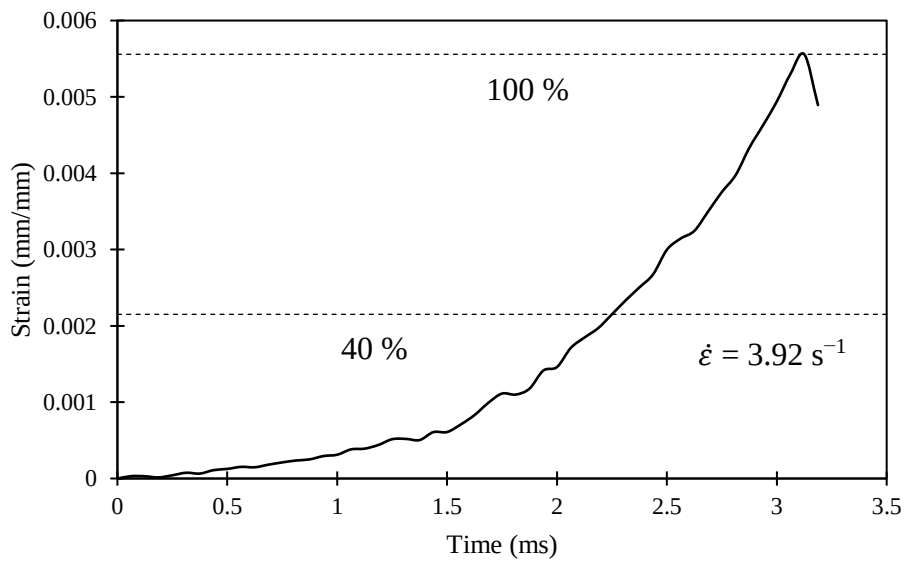

Figure 4.12: L160-1 strain versus time.

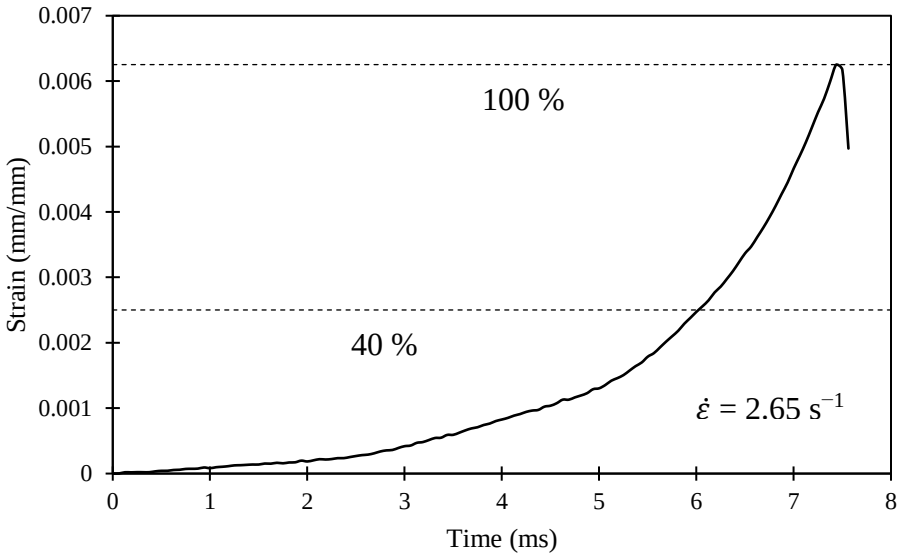

Figure 4.13: L240-1 strain versus time.

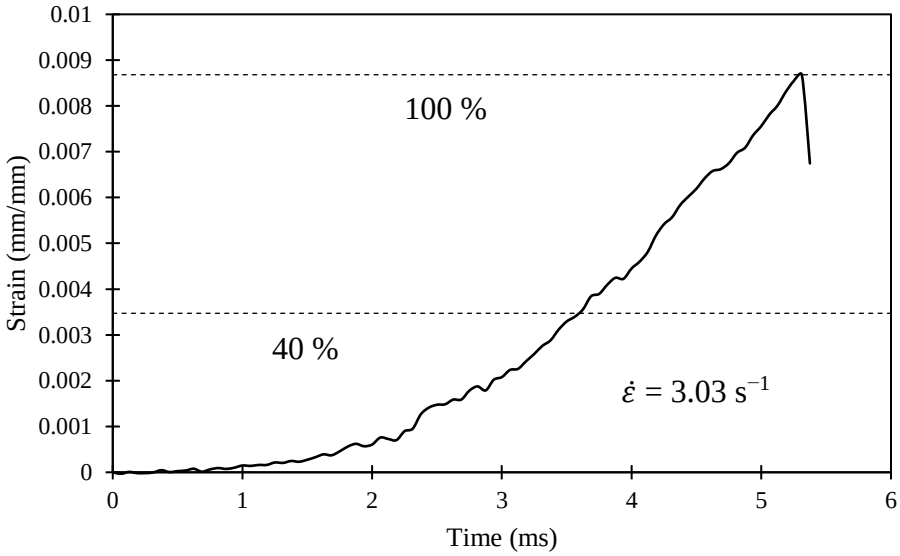

Figure 4.14: L350-3 strain versus time.

Each specimen used the secant slope between peak strain and 40 % of the peak to calculate the strain rate. This method of obtaining the strain rate was used as the region presented as linear in all tests. Table 4.3 below lists all the calculated strain rates, and the average strain rate for each of the bonded length groups.

Table 4.3: Strain rates.

Specimen	Strain Rate (s^{-1})	
	Individual	Average
L160-1	3.92	2.74
L160-2	1.83	
L160-3	2.46	
L240-1	2.65	2.60
L240-2	2.66	
L240-3	2.48	
L350-1	1.48	2.47
L350-2	2.91	
L350-3	3.03	

4.3.3 Bond Stress

The average bond between two given points along an axial line created using DIC software, which travelled along the centre of the specimen was calculated using Equation [4-1] (Shen et al., 2015).

$$\tau_i = E_f t_f \frac{d\varepsilon_i}{dx_i} \quad [4\text{-}1]$$

The elastic modulus of the CFRP sheet (E_f) and CFRP composite thickness (t_f) were constant at 37,840 MPa and a nominal 1 mm, respectively, staying consistent with the statically loaded specimens. The strains and positions along the length of the test specimen were provided by the DIC software, spaced and measured at roughly every 2.16 mm. Using this method, the average bond stress was calculated between every virtual point created by the DIC software for a frame in time just prior to failure. This frame, for each specimen, was selected by starting at the frame in which failure occurred and worked backwards. The data was extracted from the closest frame to failure where the end of the bonded length was experiencing little to no strain. This was done in order to ensure there was a full

effective bonded length, and the maximum strain in that frame was still approximately equal to the maximum strain at failure. The data between 30 % and 70 % of the peak strain was extracted to get an average bond stress, as the goal was to eliminate any noise or uncertainty of where the effective bonded length began or ended. There was one specimen, however, that exhibited a short plateau in the strain data, in all frames from the DIC, located in the approximate centre of the effective bonded length. For this specimen, L350-3, the aforementioned 30 % and 70 % bounds were extended based on a visual inspection so as to take a more accurate calculation of the average bond stress. Figure 4.15 illustrates the extracted region of bond stress data obtained from a point in time, 1.00 ms prior to failure corresponding to 87.4 % of the peak load. This bond stress data overlays the strain field at that time to illustrate the correlation between the effective bonded length in the strain data with the peak bond stress.

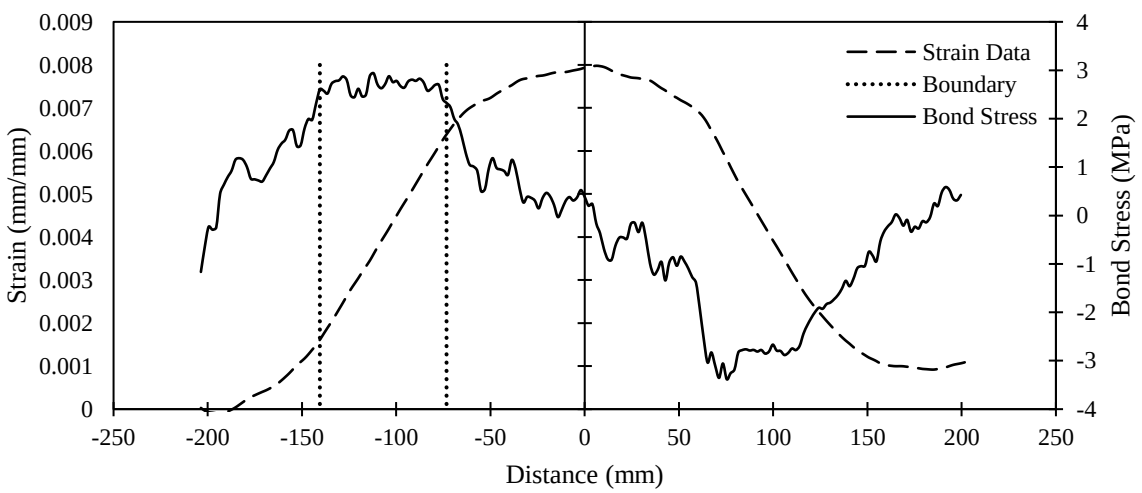

Figure 4.15: L240-3 bond stress overlaying strain.

The bond stress between the two (2) boundaries shown above was averaged over the length to find an average maximum bond stress, which was then used to calculate the effective bond length, described further in Section 4.3.4. These values were then compared against

those found during the static testing (Atunbi, 2018). An example of the bond stress between the 20 % and 80 % peak strain limits from each of the bonded groups: L160, L240, and L350 is shown in Figure 4.16 through Figure 4.18.

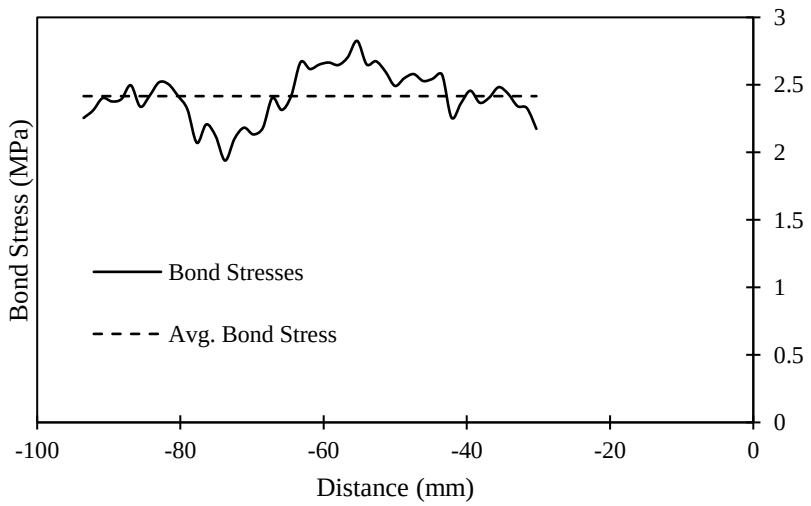

Figure 4.16: L160-3 bond stress.

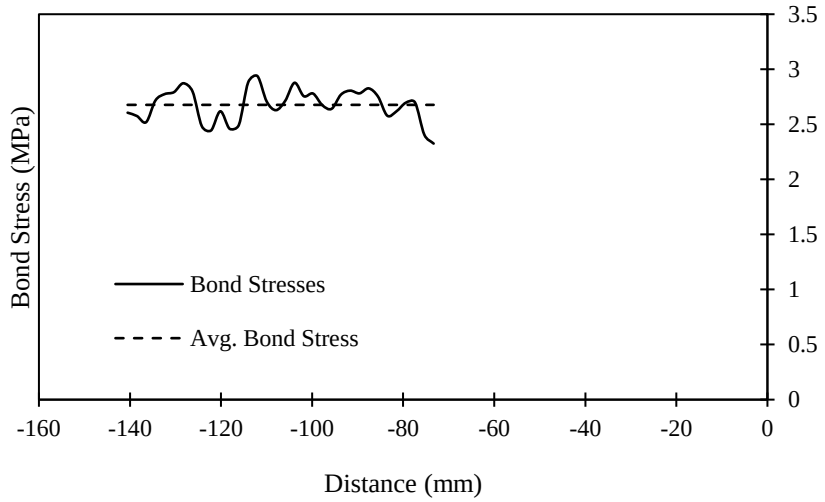

Figure 4.17: L240-3 bond stress.

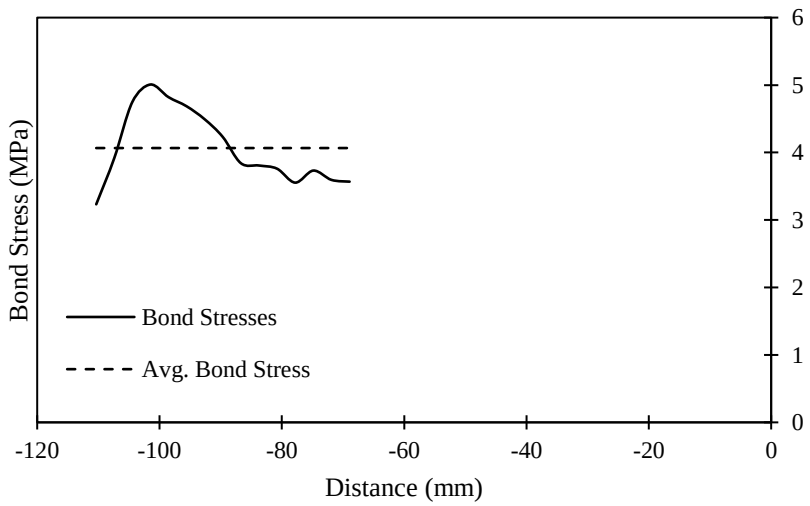

Figure 4.18: L350-2 bond stress.

The process of establishing the 30 % and 70 % boundaries of the maximum tensile strain, followed by calculating the bond stresses and averaging those values between the boundary points was completed for all specimens except for the discussed L350-3 specimen. These averages were then compared against the values which were calculated using from the data obtained during the static testing (Atunbi, 2018), and a DIF value was calculated. When reviewing the analyzed work of Atunbi (2018), inconsistencies in the bond stress values were found when performing basic slope calculations of the effective bonded length. The values found were substantially different than the values presented by the researcher, therefore, the graphs presented in their paper were imported to a computer-aided design software in order to scale the image and calculate the slope of the strain profile. It should be noted that the graph figure showing the strain profiles for L240-S-3 was removed from the average bond stress calculation as the same profile was presented for specimen L240-S-2. To remain as consistent as possible, a strain profile close to failure was used for all specimen calculations. The bond stresses, their respective maximum strain for the given frame, and their DIF values are presented in Table 4.4.

Table 4.4: Bond stress comparison.

Specimen	$\tau_{dynamic}$ (MPa)		$\varepsilon_{dynamic}$ (%)		τ_{static} (MPa)	ε_{static} (%)	DIF_{τ}	DIF_{ε}
	Individual	Average	Individual	Average				
L160-1	3.13		0.909					
L160-2	3.02	2.93	0.785	0.802	3.64	0.450	0.80	1.78
L160-3	2.63		0.714					
L240-1	3.13		0.881					
L240-2	2.79	3.05	0.817	0.837	3.97	0.570	0.75	1.47
L240-3	3.24		0.815					
L350-1	3.09		0.828					
L350-2	2.85	2.91	0.944	0.918	2.69	0.570	1.08	1.61
L350-3	2.78		0.981					

The bond stresses calculated above were then used to calculate the expected effective bonded lengths. Attempts were made to use the graphical representations of the strain data to visually establish the boundaries from where the effective bonded length begins and terminates. This was found to be ineffective, however, as noise in the data prevented consistent, reliable distinctions in determining the ends of the effective bonded lengths.

4.3.4 Effective Bonded Length

The relevant data for this experiment came from DIC analysis. DIC provided a strain profile along the member, showing a rise in the strain at the point of interest. When loading increased, the peak strain extended out from the point of interest at the loaded end, creating a plateau in the strain graph. A diagram depicting the loaded and unloaded ends can be seen in Figure 4.19. This was the expected result as the static testing (Atunbi, 2018) showed similar results. Three (3) regions can clearly be seen in the strain data, shown in Figure 4.20. The first region is the unloaded zone, followed by the effective bonded length, and then the peak strain along the plateau.

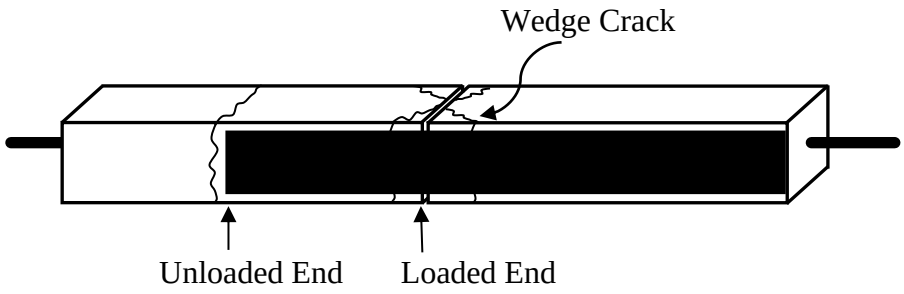

Figure 4.19: Loaded and unloaded ends of prism.

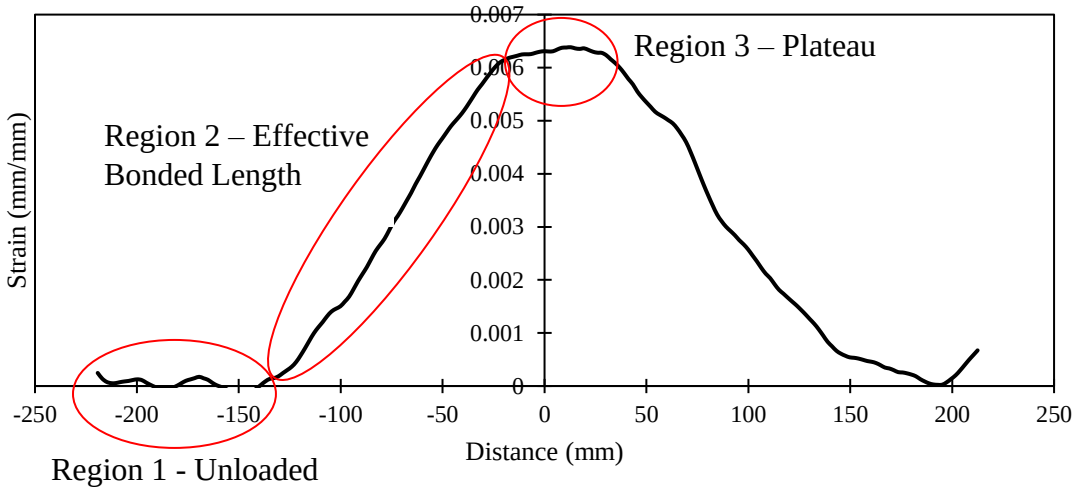

Figure 4.20: Regions of strain data (L240-2).

As mentioned, the static testing (Atunbi, 2018) demonstrated these three (3) regions as well. Below, in Figure 4.21, is a comparison between the dynamic strains found in this experiment, and the static strains found in the static testing for a specimen in the L240 test groups. The data for the dynamic specimen, L240-1, was taken 0.688 ms prior to failure, or at 88.9 % of the peak load. The data for the static specimen, L240-S-3, was obtained from the data recorded just at failure (Atunbi, 2018).

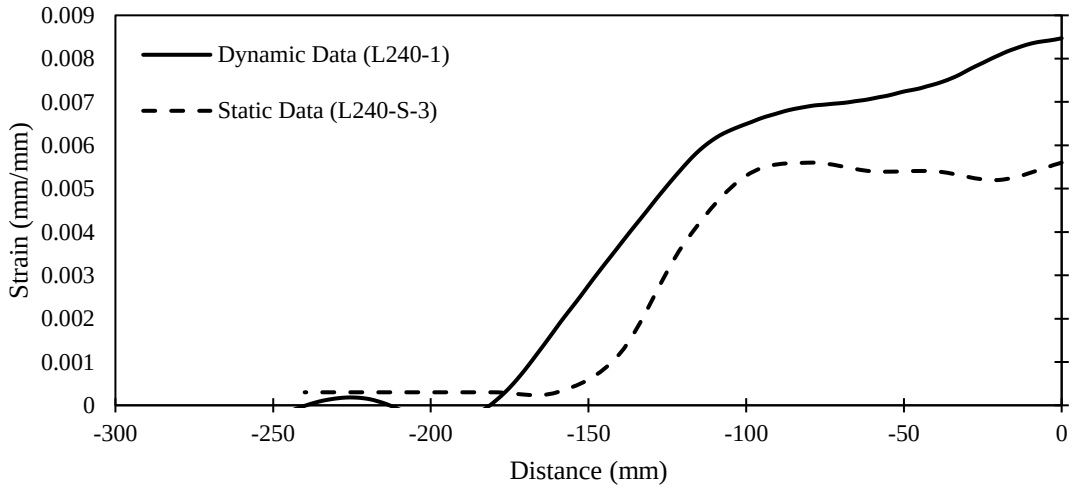

Figure 4.21: Strain vs. Distance Comparison.

Throughout the course of the impact, the peak strain increased until it hit the plateau elevation; The peak then began propagating outwards, forming the plateau. The slope descending from the plateau to the unloaded region is the length it took the CFRP material to develop its maximum tensile strength. As it was found to be difficult to visually determine where the effective bonded length, L_e, begins and ends for all of the specimens, the effective bonded length was calculated using the bond stress. Equation [4-2] was used to calculate the effective bonded length.

$$L_e = \frac{E_f \varepsilon_{max} t_f}{\tau_{avg}} \quad [4\text{-}2]$$

The modulus of elasticity for the CFRP sheets, and the CFRP sheet composite thickness of the was taken as 37,840 MPa, and 1 mm, respectively. The peak strain, ε_{max}, was taken as the maximum strain in the frame chosen prior to failure, as discussed in Section 4.3.3. Finally, the maximum average bond stress, τ_{avg}, was taken as the average bond stress between 30 % and 70 % of the peak strain for the specimen.

As previously discussed, there are three (3) distinct regions in the strain profile data: Unbonded region, effective bonded length, and the plateau. Figure 4.22 below shows how these sections change throughout the course of the impact response. Note that Reading #1 occurred 6.125 ms after impact, with data labelled Reading #2 taken 0.875 ms after, and Reading #3 taken another 0.375 ms after that.

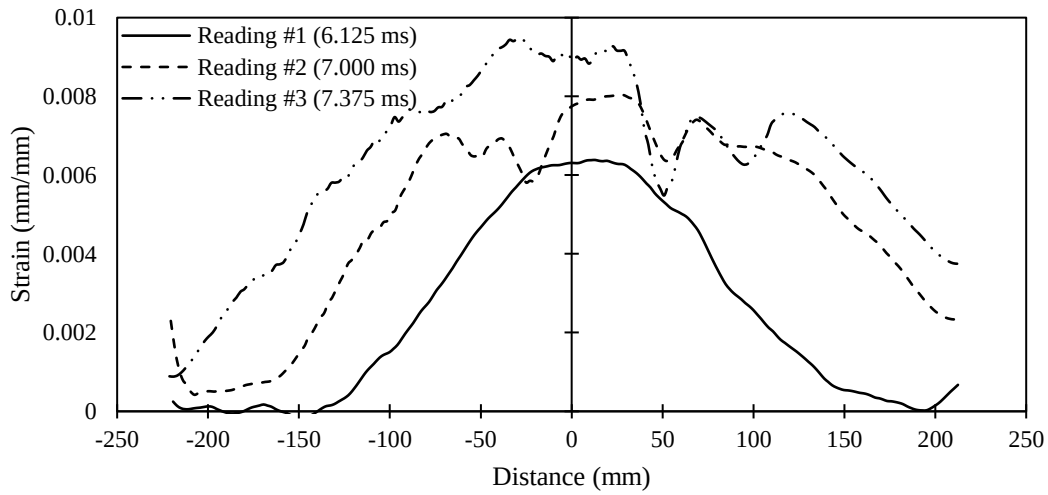

Figure 4.22: Strain profile example at different times after impact load (L240-2).

As shown in the figure above, though the peak strain continues to increase, the plateau extends further, and subsequently the effective bonded length is shifted over.

The effective bonded length for each of the specimens was calculated and compared against the effective bonded lengths found in the static testing (Atunbi, 2018). These values and their respective DIF can be found in Table 4.5.

Table 4.5: Effective bonded length comparison.

Specimen	$L_{e,dynamic}$ (mm)		$L_{e,static}$ (mm)	DIF_{Le}
	Individual	Average		
L160-1	109.8			
L160-2	98.2	103.5	50.0	2.07
L160-3	102.5			
L240-1	112.6			
L240-2	110.6	106.6	55.0	1.94
L240-3	96.6			
L350-1	101.5			
L350-2	125.2	120.0	57.5	2.09
L350-3	133.4			

The above table lists the calculated effective bonded lengths and compares it against the statically tested specimens. The DIF values range from 1.76 to 2.03.

4.3.5 Comparisons to Literature

Table 4.6 provides the DIF values for the ultimate strain, the bond stress, and the effective bonded length for ease of comparison, below.

Table 4.6: DIF summary.

Specimen Group	DIF_{ε}	DIF_{τ}	DIF_{Le}
L160	1.78	0.80	2.07
L240	1.44	0.75	1.94
L350	1.61	1.08	2.09
All	1.62	0.88	2.03

The table above provides the data obtained through the experimental research and analysis conducted and is a comparison to the values obtained through statically loaded prisms of identical characteristics by Atunbi (2018). As was expected, the strain experienced by the specimens tested dynamically was significantly higher than the statically loaded specimens. The bond stress was found to generally decrease with an increase in strain rate,

though the L350 bonded length group experienced a modest increase in bond stress. The bond stress DIF ranged from 0.75 – 1.08. When comparing the effective bonded lengths obtained from the dynamically loaded double lap pull-out shear test against the experiments ran by Atunbi (2018), an increase factor ranging from 1.94 to 2.09 was found. This result contradicts what was observed by Shen et al. (2015). It should also be noted that by substituting in the DIF values for stress and strain into the formula presented in Section 4.3.4, the DIF for the effective bonded length should range between 1.49 and 2.22. These values would average to 1.88, which is similar to of the range of values found.

Specimens in the experiments performed by Shen et al. (2015) had a consistent bond length of 200 mm while changing the strain rate, $\dot{\varepsilon}$, from 0.61 x 10^{-3} s^{-1} to 0.63 s^{-1}. As the strain rate was incrementally increased, the effective bonded length, L_e, decreased from 71.8 mm to 56.7 mm. This drop in effective bonded length results in a reduction factor of approximately 0.79. While this difference in results cannot be explained, it was found that the change in bond strength with respect to strain rate provided similar results as that shown in the data presented herein.

As shown in Table 4.6, the bond stress, τ, had a DIF that ranged from 0.75 to 1.08. The results of the experiment by Shen et al. (2015) shows differing results, where there is an increase in bond strength as strain rate increases. The bond strength at a strain rate of 0.61 x 10^{-3} s^{-1} was found as 3.27 MPa, which increased up to 5.75 MPa at a strain rate of 0.63 s^{-1}. When using these results, a DIF for the bond stress is equal to 1.76, a significant increase in bond strength, as opposed to the apparent reduction in bond stress from the experiment presented herein.

When looking at the results found in the experiment presented in this paper, a correlation between the maximum strain, bonded length, and bond stress can be drawn. Table 4.6 shows that by significantly increasing the maximum strain, a similar increase in the effective bonded length can be observed, while a noticeable, though less significant decrease can be seen in the bond stress. As mentioned, the results from the effective bonded length by Shen et al. (2015) does not match these findings, though an increase in the bond stress was observed.

Huo et al. (2016) obtained similar results as Shen et al. (2015) with respect to the effective bonded length. While these researchers analyzed an additional variable, being the number of layers of CFRP, when looking at only the results from a single layer of 50 mm wide CFRP strips, the effective bonded length drops with an increase in strain rate. The results provided by Huo et al. (2016) shows that the effective bonded length drops from 90 mm at a strain rate in the magnitude of 10^{-5} s^{-1} to 80 mm when using a strain rate ranging from 2.67 s^{-1} to 4.90 s^{-1}. The effective bonded length in the research conducted by Huo et al. (2016) was recorded by measuring the distance between the locations of peak strain and 5 % of the peak strain.

The maximum bond stresses found by Huo et al. (2016) contradict the findings in this study, similar to Shen et al. (2015). The researchers had two (2) specimens that used a single layer of CFRP that were tested at strain rates in the magnitude of 10^{-5} s^{-1}. These specimens provided bond stresses of 3.50 MPa and 4.05 MPa. There were six (6) dynamically loaded counterparts. These six (6) specimens were split into two (2) groups based on the height at which the drop hammer was dropped from: 200 mm, and 400 mm. The strain rate ranged from 2.67 s^{-1} to 4.90 s^{-1} with some overlap in strain rate between

these two (2) dynamically loaded groups. The bond stresses for the six (6) dynamically loaded specimens ranged from 5.40 MPa to 6.93 MPa, which coincidentally both occurred from the 200 mm drop hammer group. A summary of the data obtained by Huo et al. (2016), including maximum strain, effective bonded length, and maximum bond stress can be found in Table 4.7.

Table 4.7: Specimen data from Huo et al. (2016).

Specimen	$\dot{\varepsilon}$ ($^{-s}$)	ε_{max} ($\mu\varepsilon$)		L_e (mm)		τ_{max} (MPa)	
		Indiv.	Avg.	Indiv.	Avg.	Indiv.	Avg.
C50-1-S-1	10^{-5}	6.459	6.252	90	90	4.05	3.78
C50-1-S-2		6.046		90		3.50	
C50-1-D200-1	3.12	8.110		80		5.40	
C50-1-D200-2	2.67	6.930	8.053	80	80	6.93	6.12
C50-1-D200-3	4.56	9.120		80		6.02	
C50-1-D400-1	4.10	10.260		80		6.39	
C50-1-D400-2	4.90	9.790	10.760	80	80	5.47	6.10
C50-1-D400-3	4.70	12.230		80		6.45	

Data collected from Huo et al. (2016).

The data presented above has been used to calculate the average DIF values as a comparison to the DIF values found from the experiment presented in this paper. Table 4.8 shows these comparison DIF values using the statically loaded specimens, and the specimens using a drop distance of 200 mm, as this produced strain rates closest to the strain rates found in the experiment presented herein. The DIF values presented that were obtained through the experiments carried out in this paper are shown as the average of all three (3) bonded length groups, from Table 4.6, as in theory any bonded length beyond that of the effective bonded length provides no additional strength and should be comparable.

Table 4.8: DIF comparison to literature.

Data Source	DIF_{ε}	DIF_{τ}	DIF_{Le}
Huo et al. (2016)	1.29	1.62	0.89
Data presented	1.62	0.88	2.03

Data collected from Huo et al. (2016).

4.4 Conclusions and Recommendations

Based on the results presented, the following conclusions can be made regarding the effective bonded length and the peak bond stress:

1. As strain rate increased, the peak strain and the effective bonded length increased at similar rates, while the maximum bond stress experienced a modest decrease. This contradicts previously observed research that found a decrease in the effective bonded length, with an increase in bond stress as the strain rate increased. It was noted that when inputting the DIF values for stress and strain in the CFRP sheet into the effective bonded length formula, the DIF for the effective bonded length should range between 1.49 and 2.22 for the three (3) bonded length groups. This envelope encompasses the 1.94 to 2.09 DIF found for the effective bonded length. Previous research has shown that the effective bonded length should decrease with an increase in strain rate, however. An explanation for the difference in the correlation between effective bond length, bond stress, and peak strain, with what was reported from previous researchers cannot be determined as the number of specimens in this experiment, along with those in the comparison experiments, was fairly low for each bonded length group.
2. The use of DIC techniques to calculate the strains experienced across a field under dynamic loading conditions was used in this study. The strain data from the DIC

technique, along with load data obtained from two (2) load cells was compared against data from the statically tested specimens. The greatest difference in DIF values produced by the two (2) independent data collecting methods, that being the DIC bonded length group. The DIF value obtained through use of the DIC techniques was 1.61, while the DIF obtained via the load cells was 1.92. While this difference in value is significant, the shorter bonded length groups had a difference between the DIC and load cell data of 0.08 and 0.03, showing much less significant differences.

Further testing is required with a focus on the effective bonded length. The small sample size of data may have been detrimental in finding an accurate effective bonded length, particularly with the L160 bonded length group. It is believed that this bonded length group was particularly difficult in obtaining data as the ends of the effective bonded length tended to reach the unloaded end of the CFRP much quicker than the longer bonded length groups. This provided less useable data as the true effective bonded length could not be observed. It is recommended that future testing utilize more specimens to negate this issue.

It is also recommended to introduce additional, incrementally higher, strain rates. This study compared static strain rates against strain rates in the magnitude of 1 s^{-1}, which only provides one position along the dynamic spectrum. An analysis of the behaviour as the strain rate increases proportionately would be a logical progression of this study.

REFERENCES

Al-Zubaidy, H. A., Zhao, X.-L. & Al-Mahaidi, R., 2012. Dynamic bond strength between CFRP sheet and steel. *Conposite Structures,* XCIV(11), pp. 3258-3270.

Atunbi, E. O., 2018. *Experimental Study on Bond Behaviour of CFRP Sheets Externally Bonded to Reinforced Concrete.* Fredericton(New Brunswick): University of New Brunswick.

Buyukozturk, O., Gunes, O. & Karaca, E., 2004. Progress on understanding debonding problems in reinforced concrete and steel members strengthened using FRP composites. *Construction and Building Materials,* pp. 9-19.

Canadian Standards Association, 2012. *S806-12 Design and construction of building structures with fibre-reinforced polymers.* Mississauga: Canadian Standards Association.

Correlated Solutions, 2018. *Vic-2D.* s.l.:s.n.

Franco, A. & Royer-Carfagni, G., 2013. Effective bond length of FRP stiffeners. *International Journal of Non-Linear Mechanics,* Volume 60, pp. 46-57.

Huo, J. et al., 2016. Experimental Study on Dynamic Behavior of CFRP-to-Concrete Interface. *Journal of Composites for Construction,* October.20(5).

Li, G., Tan, K. H. & Fung, T. C., 2020. Experimental study on CFRP-concrete dynamic debonding behaviour. *Engineering Structures.*

Shen, D., Shi, H., Ji, Y. & Yin, F., 2015. Strain rate effect on effective bond length of basalt FRP sheet bonded to concrete. *Construction and Building Materials,* Volume 82, pp. 206-218.

5. GENERAL CONCLUSIONS AND RECOMMENDATIONS

This study presents the findings of an experimental investigation into the bond behaviour of CFRP sheets surface mounted to concrete substrate. This experiment involved the use of double lap pull-out shear tests under dynamic loading conditions and served as a comparison study to similar tests under static loading conditions. A DIC technique was utilized to capture the strain data and was validated using load cells to ensure accurate results. The data obtained through this experiment leads to the following conclusions:

1. The use of DIC has shown to be an effective tool in measuring the strains over a field. There were, however, issues in obtaining clear data for a number of specimens that prevented the measurement of a clear effective bonded length. It is believed that better data could be obtained with an improved experimental setup. Further research and use of DIC may discover more effective methods of mitigating these difficulties.
2. The failure mode observed in this experiment was initiated by the concrete failing in tension, by means of a wedge crack. From there, it was expected that debonding would occur due to the interfacial shear failure of the concrete. While this was observed to be the case for the majority of the specimens, matching what was observed by Atunbi (2018), by the back of the fully debonded CFRP sheet retaining a layer of concrete, this was not always the case. It was observed that the interfacial shear failure did not always occur in the concrete but would also happen in the adhesive. By observing the back of the debonded CFRP sheets, it could be seen that some of the area had adhesive failure, while other areas had concrete failure. It is believed that, as the DIF was higher than expected, the ultimate capacity of the

concrete increased beyond the strength of the adhesive bond in some of the specimens.

3. The effective bonded length appears to increase as strain rate is increased. This contradicts previously observed research that found either no difference, statistically, or a decrease in effective bonded length.
4. An average decrease in bond stress was observed with an increase in strain rate. This, however, differed depending on which bonded length group is examined. While the L160 and L240 bonded length groups experienced DIF values of 0.80 and 0.75, respectively, the L350 group experienced an increase in bond stress with a DIF of 1.08. This difference in DIF between the shorter two (2) bonded length groups versus the longer L350 bonded length group was unexpected. When examining the empirical results, it can be seen that the bond stress in the L350 group was significantly lower than the other two (2) in the static testing. The fact that the L350 group displays the far lowest bond stress in the static testing indicates that there may have been either instrumentation, workmanship, or analytical errors in one or multiple bonded length groups. Further testing is recommended.
5. Much higher DIF values were found than expected when examining both the load data and strain data. These DIFs ranged from 1.47 to 1.78, which differs greatly from the 1.19 to 1.20 for concrete in flexure, and the 1.0 for FRP in flexure, as reported by the relevant codes (Canadian Standards Association, 2012; Fédération internationale du béton, 2010; Unified Facilities Criteria, 2008).
6. There was a small difference in ultimate bond strength between the three bonded lengths, 160 mm, 240 mm, and 350 mm. These values were 72.7 kN, 65.1 kN and

76.8 kN, respectively. The 240 mm bonded length specimens had an average ultimate capacity lower than either the 160 mm or 350 mm bonded groups. This is reflected in the calculated DIF values from both the load cells and strain data of 1.47, which was lower than the other specimen groups.

7. Tension cracks were always found at or near the unloaded ends for the 160 mm, and 240 mm specimens. As for the 350 mm specimens, the tension crack was found at an average of 220 mm along the length of the CFRP, measured from the critical point. This differs from the statically loaded specimens tested by Atunbi (2018), where the tension cracks always formed on the unloaded side, though no cracks were found on the 350 mm bonded length group. This difference in tension cracks occurring in the 350 mm bonded length group could be attributed to the inertial effects present in dynamic testing.

It is recommended that further studies be carried out on CFRP surface bonded to concrete substrate. Future studies should utilize a greater number of specimens per bonded length group, to decrease the effect of the results on one specimen to the average. Additionally, it is recommended that future experiments investigate the effects of a varied strain rate further. This study focused on a comparison between statically loaded and a strain rate in the order of 1 s^{-1}. While this is a starting point, incremental experiments between and beyond these rates should be investigated to develop of deeper understanding of the effects of increasing strain rate.

While it was found that a combination of the concrete and the adhesive was the failure mechanisms in these experiments, other materials such as Glass FRP, Aramid FRP, and

Basalt FRP should be tested to identify any variations in the bond strengths of these alternate materials.

REFERENCES

Al-Zubaidy, H. A., Zhao, X.-L. & Al-Mahaidi, R., 2012. Dynamic bond strength between CFRP sheet and steel. *Conposite Structures,* XCIV(11), pp. 3258-3270.

Atunbi, E. O., 2018. *Experimental Study on Bond Behaviour of CFRP Sheets Externally Bonded to Reinforced Concrete.* Fredericton(New Brunswick): University of New Brunswick.

Bakis, C. E. et al., 2002. Fiber-Reinforced Polymer Composites for Construction - State-of-the-Art Review. *American Society of Civil Engineers,* pp. 73-87.

BASF, 2019. *MasterBrace FIB 300/50 CFS.* [Online].

Bentler, P.M. & Chou, C.P., 1987. Practical issues in structural modeling. *Sociological Methods & Research,* XVI(1).

Bizindavyi, L. & Neale, K. W., 1999. Transfer Lengths and Bond Strengths for Composites Bonded to Concrete. *Journal of Composites for Construction,* III(4), pp. 153-160.

Booth, R. & Gates, C., 2003. Ronan Point fears resurface. *Building Design,* 18 July, p. 1.

Buyukozturk, O., Gunes, O. & Karaca, E., 2004. Progress on understanding debonding problems in reinforced concrete and steel members strengthened using FRP composites. *Construction and Building Materials,* pp. 9-19.

Campbell, F. C., 2010. *Structural Composite Materials.* Materials Park(Ohio): ASM International.

Canadian Standards Association, 2012. *S806-12 Design and construction of building structures with fibre-reinforced polymers.* Mississauga: Canadian Standards Association.

Canadian Standards Association, 2012. *S850-12 Design and assessment of buildings subjected to blast loads.* Mississauga: Canadian Standards Association.

Ceroni, F., 2010. Experimental performances of RC beams strengthened with FRP materials. *Construction and Building Materials,* September, 24(9), pp. 1547-1559.

Correia, J. R., 2013. *The New FRP Materials for Civil Engineering Structural Applications [PowerPoint slides],* s.l.: s.n.

Correlated Solutions, 2018. *Vic-2D.* s.l.:s.n.

Ekşi, S. & Genel, K., 2016. Comparison of Mechanical Properties of Unidirectional and Woven Carbon, Glass and Aramid Fiber Reinforced Epoxy Composites. *Acta Physica Polonica A,* pp. 879-882.

Fédération internationale du béton, 2010. *Model Code for Concrete Structures.* Lausanne: Ernst & Sohn.

Franco, A. & Royer-Carfagni, G., 2013. Effective bond length of FRP stiffeners. *International Journal of Non-Linear Mechanics,* Volume 60, pp. 46-57.

Frigione, M. & Lettieri, M., 2018. Durability Issues and Challenges for Material Advancements in FRP Employed in the Construction Industry. *Polymers,* 10(3), p. 247.

Goswami, A. & Adhikary, S. D., 2019. Retrofitting materials for enhanced blast performance of Structures: Recent advancement and challenges ahead. *Construction and Building Materials,* pp. 224-243.

Hansen, R. J., 1961. Design of blast resistant structures. *Shock and Vibration Handbook,* Volume 3.

Harman, J., Atunbi, E. O. & Lloyd, A., 2021. High Strain Rate Properties of CFRP Sheets Surface Bonded to Concrete. *SP-347 Recent Developments in High Strain Rate Mechanics and Impact Behavior of Concrete,* pp. 21-38.

Huo, J. et al., 2016. Experimental Study on Dynamic Behavior of CFRP-to-Concrete Interface. *Journal of Composites for Construction,* October.20(5).

Kamaitis, Z., 2002. Damage to concrete bridges due to reinforcement corrosion. *Transport,* XVII(4), pp. 137-142.

Levi-Hevroni, D. et al., 2018. Experimental and numerical investigation on the dynamic increase factor of tensile strength in concrete. *International Journal of Impact Engineering,* April, Volume CXIV, pp. 93-104.

Li, G., Tan, K. H. & Fung, T. C., 2020. Experimental study on CFRP-concrete dynamic debonding behaviour. *Engineering Structures.*

Malvar, L.J., 1998. Review of Static and Dynamic Properties of Steel Reinforcing Bars. *ACI Materials Journal*, pp. 609-616.

Malvar, L. J. & Crawford, J. E., 1998. *Dynamic Increase Factors for Concrete,* Port Hueneme, CA: Naval Facilities Engineering Service Center.

Malvar, L.J. & Ross, C.A., 1998. Review of Strain Rate Effects for Concrete in Tension. *ACI Materials Journal*, pp. 735-739.

Malvar, L. J., Crawford, J. E. & Morrill, K. B., 2007. Use of Composites to Resist Blast. *Journal of Composites for Construction,* pp. 601-610.

Meier, U., 1996. Strengthening of structures using carbon fibre/epoxy composites. *Construction and Building Materials,* pp. 341-351.

Pereira, L. F., Weerheijm, J. & Sluys, L. J., 2017. A new effective rate dependent damage model for dynamic tensile failure of concrete. *Engineering Fracture Mechanics,* Volume CLXXVI, pp. 281-299.

Pesic, N. & Pilakoutas, K., 2003. Concrete beams with externally bonded flexural FRP-reinforcement: analytical investigation of debonding failure. *Composites Part B: Engineering,* XXXIV(4), pp. 327-338.

Pham, T. M. & Hao, H., 2016. Review of Concrete Structures Strengthened with FRP Against Impact Loading. *Structures,* Volume VII, pp. 59-70.

Ross, T. J., 1983. *Direct Shear Failure In Reinforced Concrete Beams Under Impulsive Loading,* s.l.: Stanford University.

Sciolti, M. S., Frigione, M. & Aiello, M. A., 2010. Wet Lay-Up Manufactured FRPs for Concrete and Masonry Repair: Influence of Water on the Properties of Composites and on Their Epoxy Components. *Journal of Composites for Construction,* XIV(6), pp. 823-833.

Shen, D., Shi, H., Ji, Y. & Yin, F., 2015. Strain rate effect on effective bond length of basalt FRP sheet bonded to concrete. *Construction and Building Materials,* Volume 82, pp. 206-218.

Uddin, N., 2013. *Developments in fiber-reinforced polymer (FRP) composites for civil engineering.* Philadelphia: Woodhead Publishing.

Unified Facilities Criteria, 2008. *Structures To Resist The Effects Of Accidental Explosions.* s.l.:National Institute of Building Sciences.

Zhang, X. et al., 2016. Static and dynamic material properties of CFRP/epoxy laminates. *Construction and Building Materials,* pp. 638-649.

Zhu, H. et al., 2014. Digital image correlation measurement of the bond-slip relationship between fiber-reinforced polymer sheets and concrete substrate. *Journal of Reinforced Plastics and Composites,* XXXIII(17), pp. 1590-1603.

APPENDIX A – MAXIMUM APPARATUS ROTATION CALCULATIONS

Calculations to determine the rotation of the load cell with respect to the specimens are presented in Appendix A. These calculations were carried out to ensure the applied loading remained in-line with the specimen up to debonding failure.

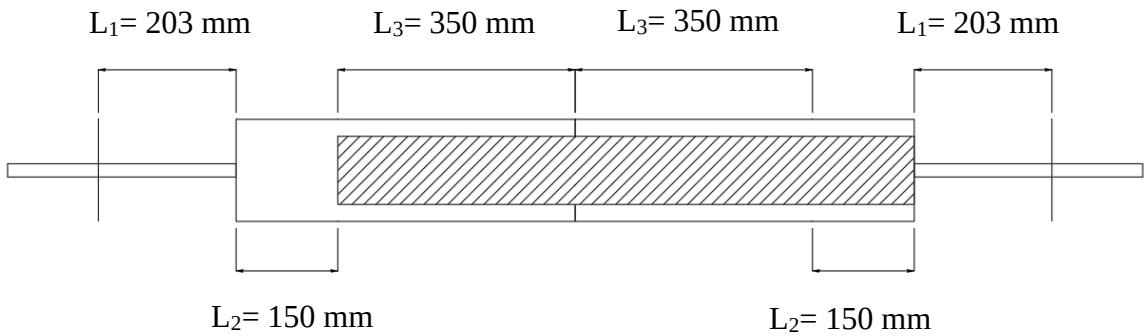

L_1 = Length of rebar to coupler = **406 mm**

L_2= Length of transformed concrete section = **300 mm**

L_3= Length of unbonded L350 test specimen CFRP = **700 mm**

$$\Delta_{tot} = \Delta_1 + \Delta_2 + \Delta_3 = \frac{PL_1}{A_s E_s} + \frac{PL_2}{\left[A_g + (n-1)A_s\right] \times E_c} + \frac{PL_3}{A_f E_f}$$

From Table 3.1, P_{avg} = **76.8 kN** for L350 bonded length group

A_s = **300 mm²**

E_s = **200 GPa**

E_c = **25456 MPa**

$A_g = 150\text{mm} \times 150\text{mm} = \mathbf{22,500mm^2}$

$$n = \frac{200{,}000\text{MPa}}{4500 \times \sqrt{32\text{MPa}}} = \mathbf{7.857}$$

$A_f = 2 \times 1\text{mm} \times 100\text{mm} = \mathbf{200mm^2}$

E_f = **37840 MPa**

$$\Delta_{tot} = 76{,}800 \times \left[\frac{406}{300 \times 200{,}000} + \frac{300}{(22{,}500 + (7.857 - 1) \times 300) \times 25456} + \frac{700}{200 \times 37840}\right]$$

$$\Delta_{tot} = 7.66 \text{ mm}$$

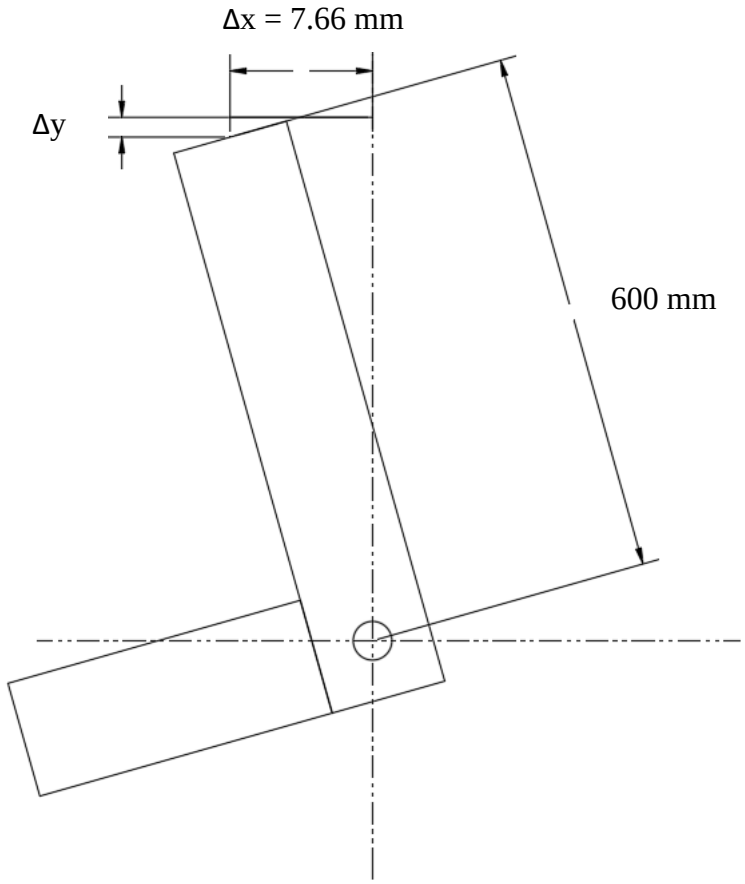
Δx = 7.66 mm
Δy
600 mm

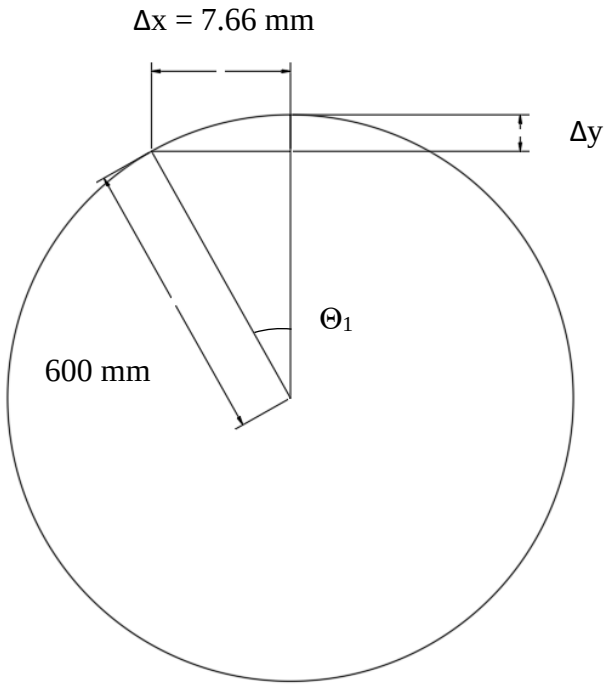
Δx = 7.66 mm
Δy
Θ1
600 mm

$$\Delta y = 600 - \sqrt{600^2 - 7.66^2} = \mathbf{0.049mm}$$

$$\Theta_1 = \sin^{-1}\left(\frac{7.66}{600}\right) = \mathbf{0.731}°$$

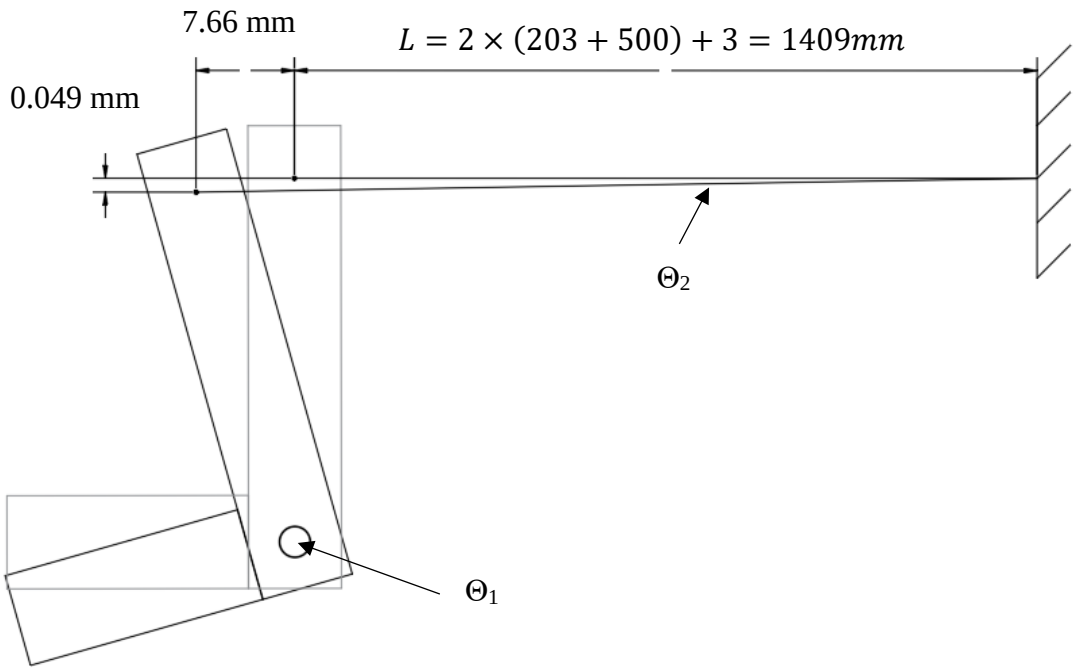

$$\Theta_2 = \sin^{-1}\left(\frac{\Delta y}{L + \Delta x}\right) = \sin^{-1}\left(\frac{0.049}{1409 + 7.66}\right)$$

$$\Theta_2 = \mathbf{0.002}°$$

<u>Difference in Rotation</u>

$$\boldsymbol{\Theta = \Theta_1 - \Theta_2 = 0.731° - 0.002° = 0.729°}$$

As reinforcing steel is a ductile material, it is expected that the steel was able to elastically deform to remain orthogonal with the load cell after a maximum difference of 0.729 º of rotation.

APPENDIX B – EXPERIMENTAL LOAD DATA

B.1 Load Data for Specimens L160

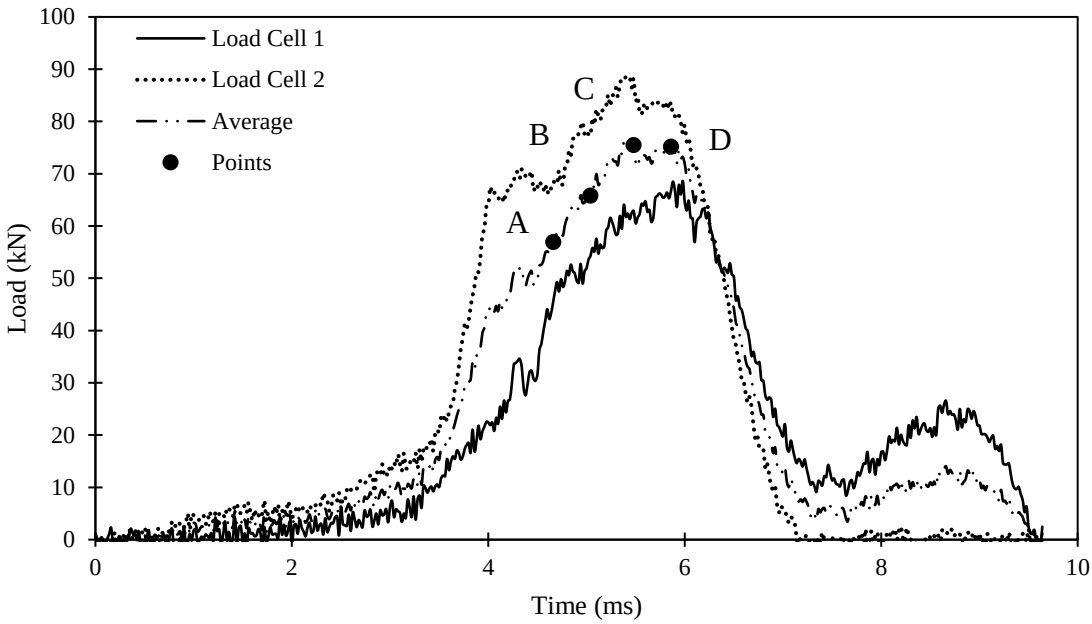

Figure B1.1: Specimen L160-1 Load Data.

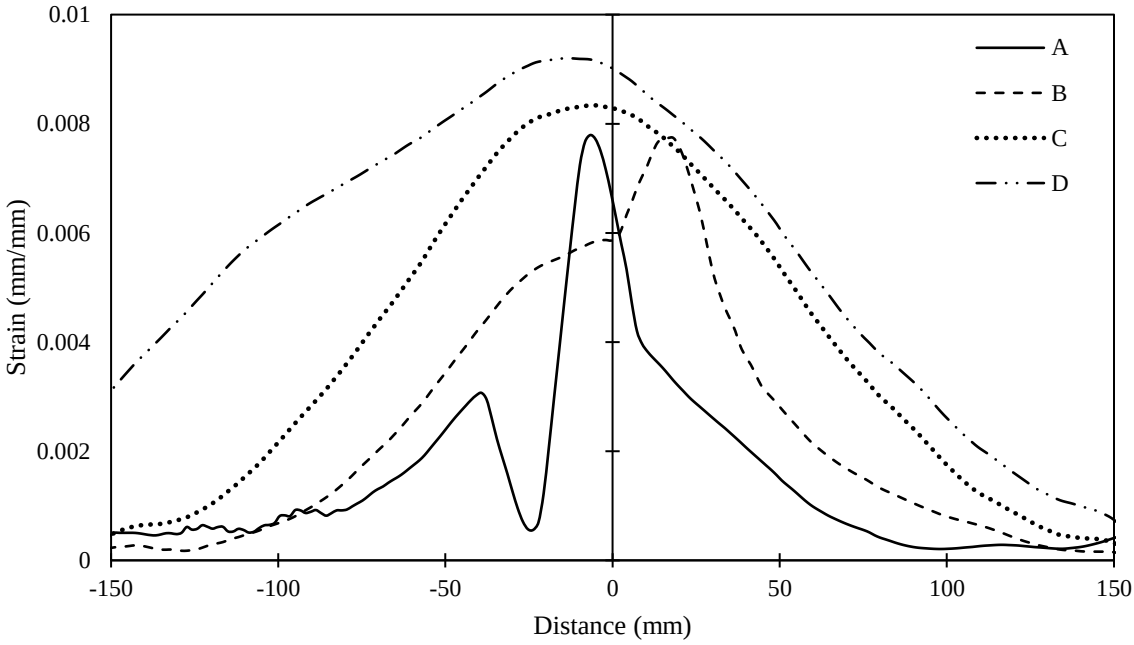

Figure B1.2: Specimen L160-1 Strain Data.

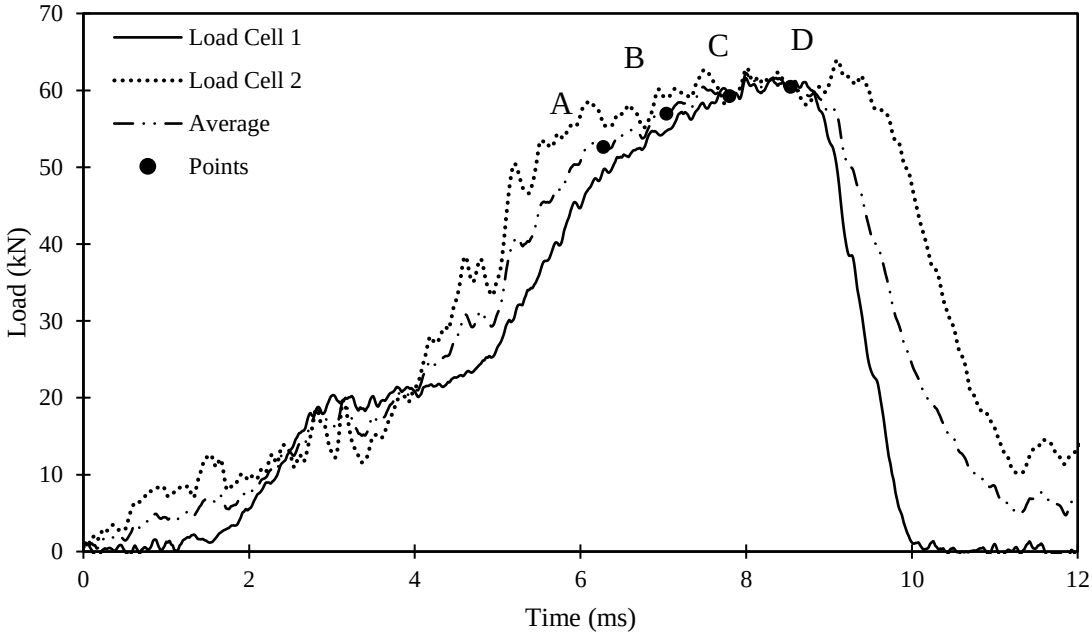

Figure B1.3: Specimen L160-2 Load Data.

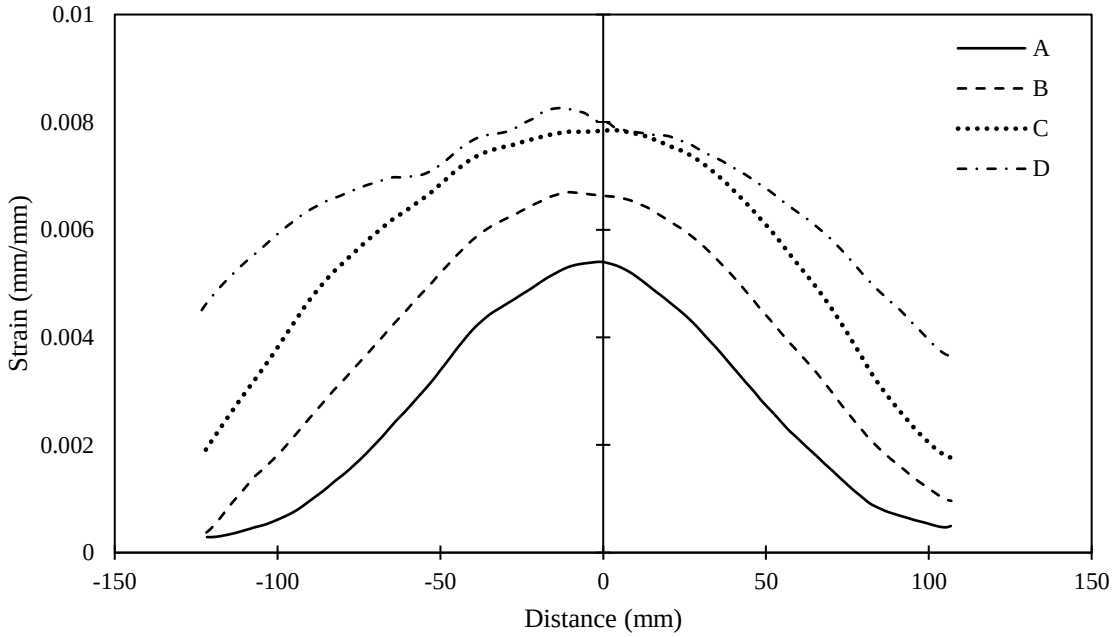

Figure B1.4: Specimen L160-2 Strain Data.

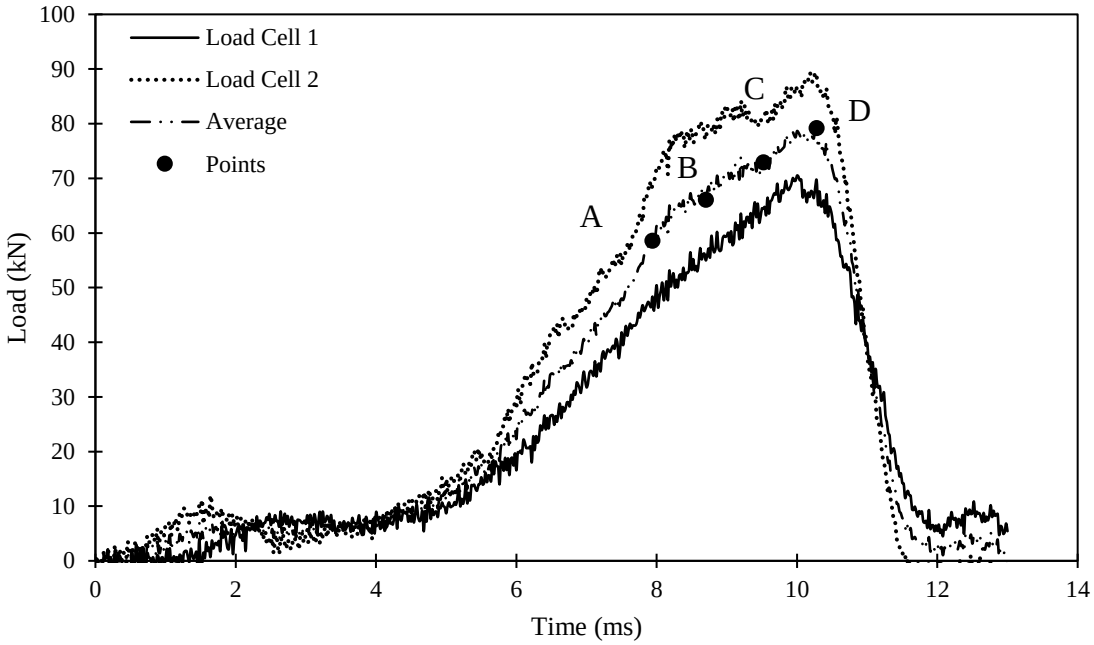

Figure B1.5: Specimen L160-3 Load Data.

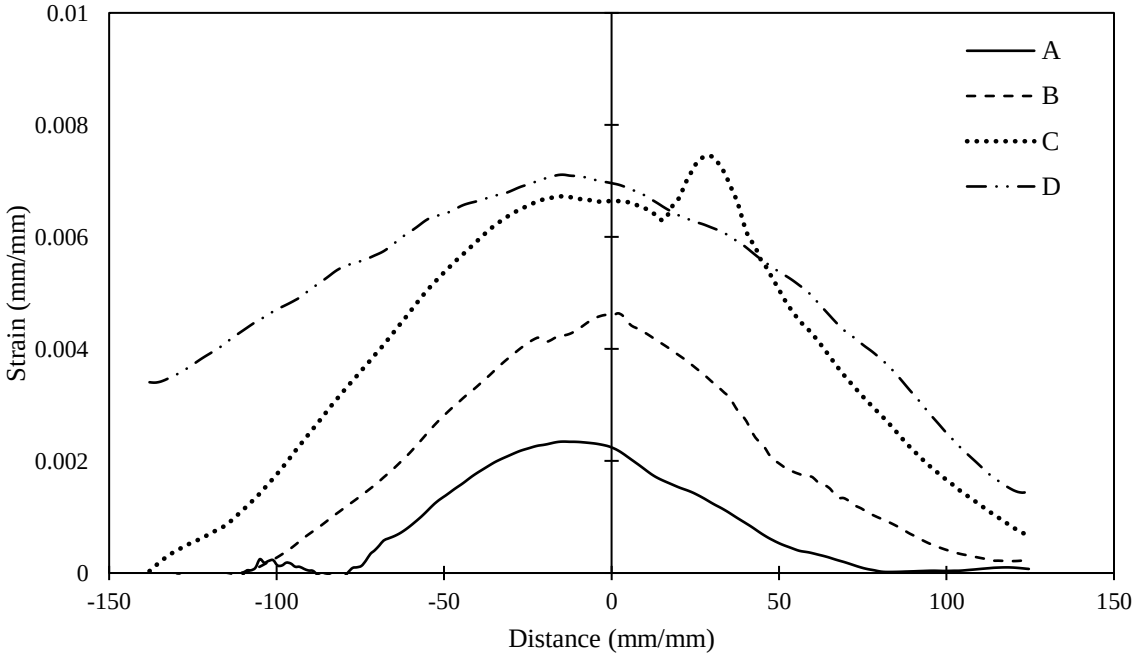

Figure B1.6: Specimen L160-3 Strain Data.

B.2 Load Data for Specimens L240

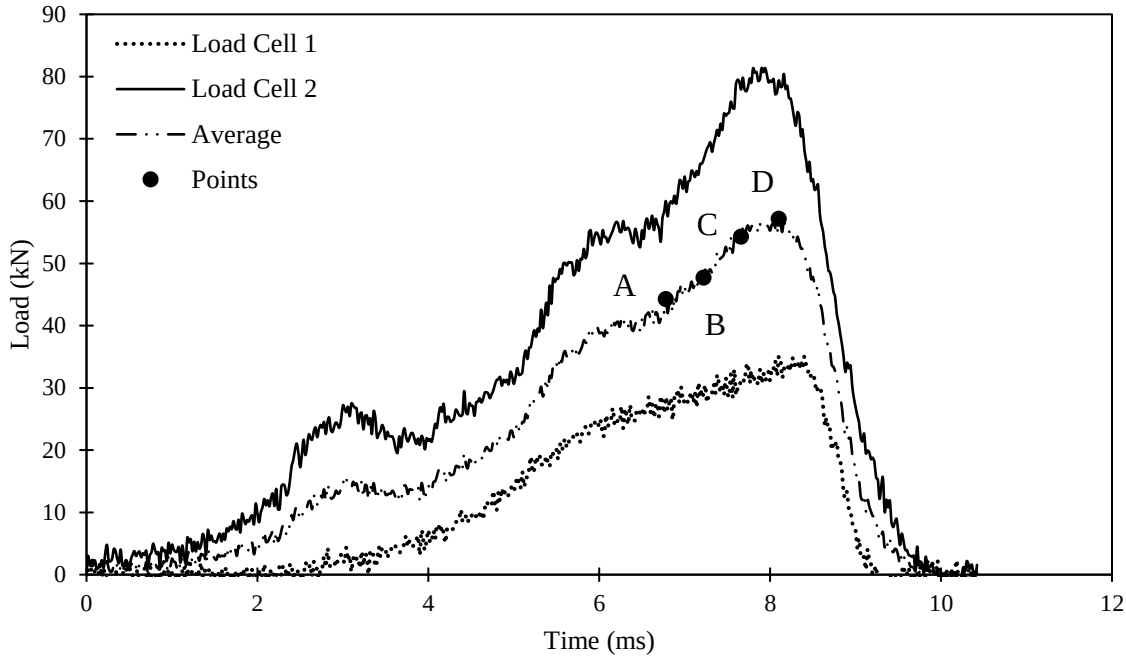

Figure B2.1: Specimen L240-1 Load Data.

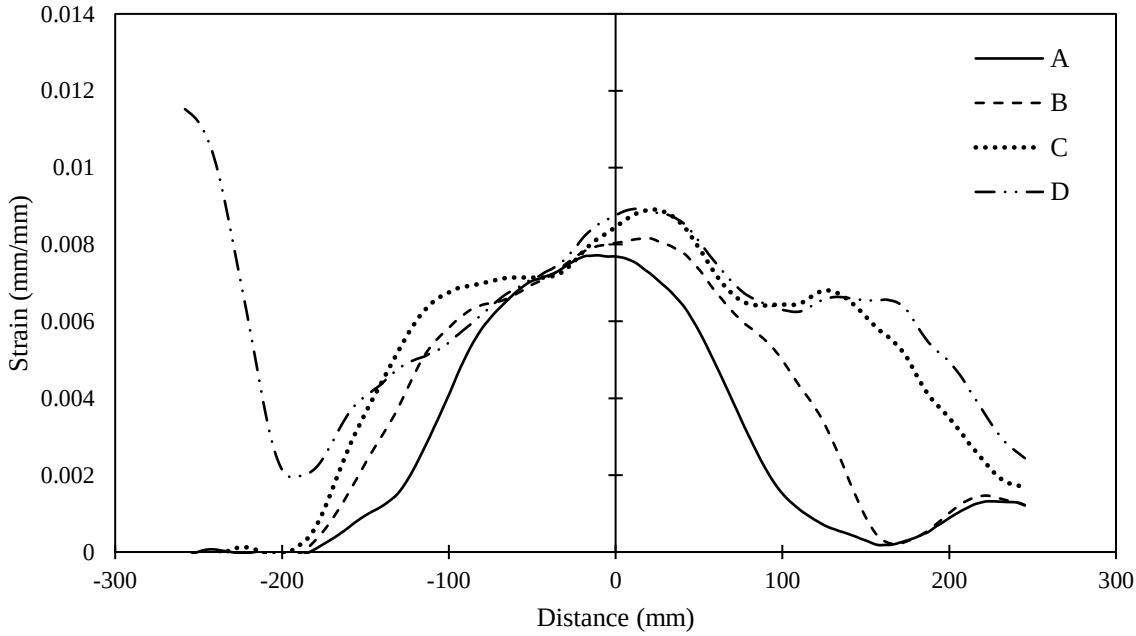

Figure B2.2: Specimen L240-1 Load Data.

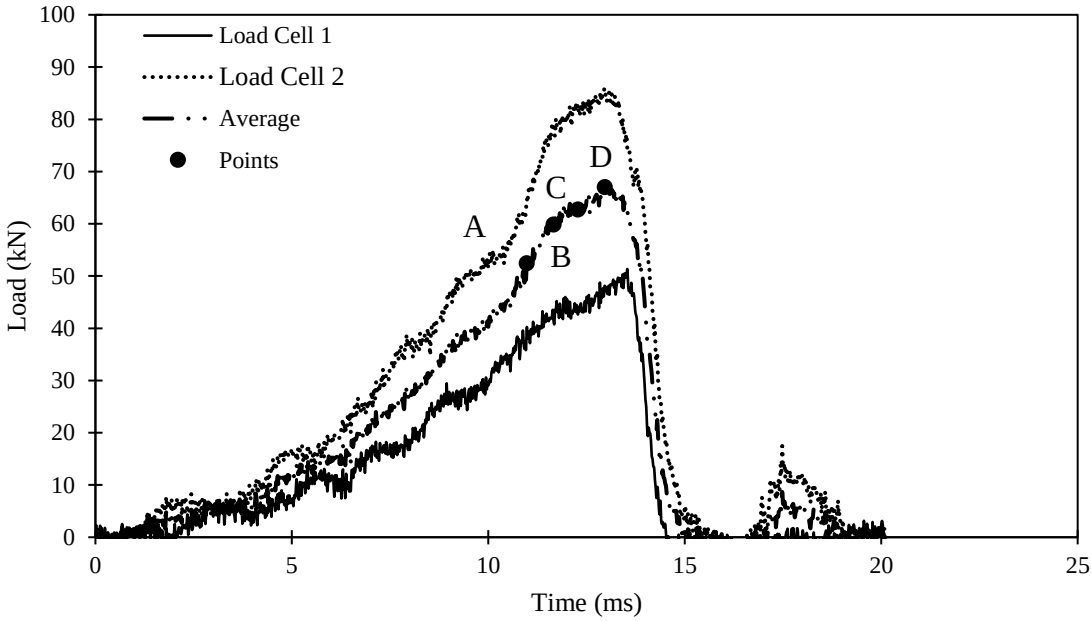

Figure B2.3: Specimen L240-2 Load Data.

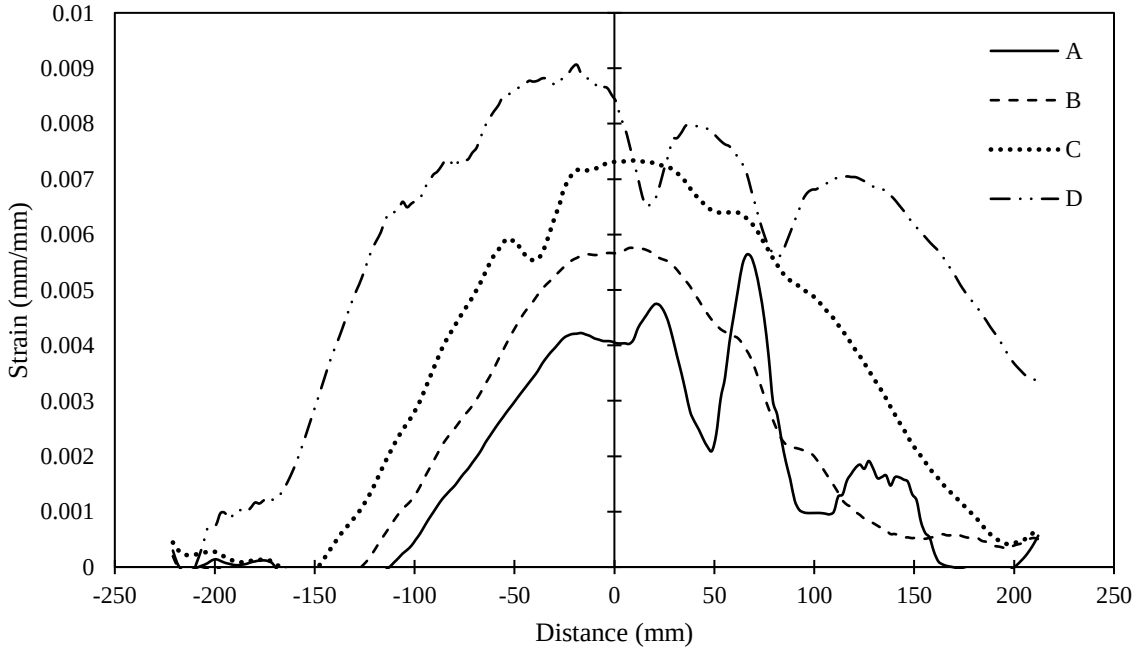

Figure B2.4: Specimen L240-2 Strain Data.

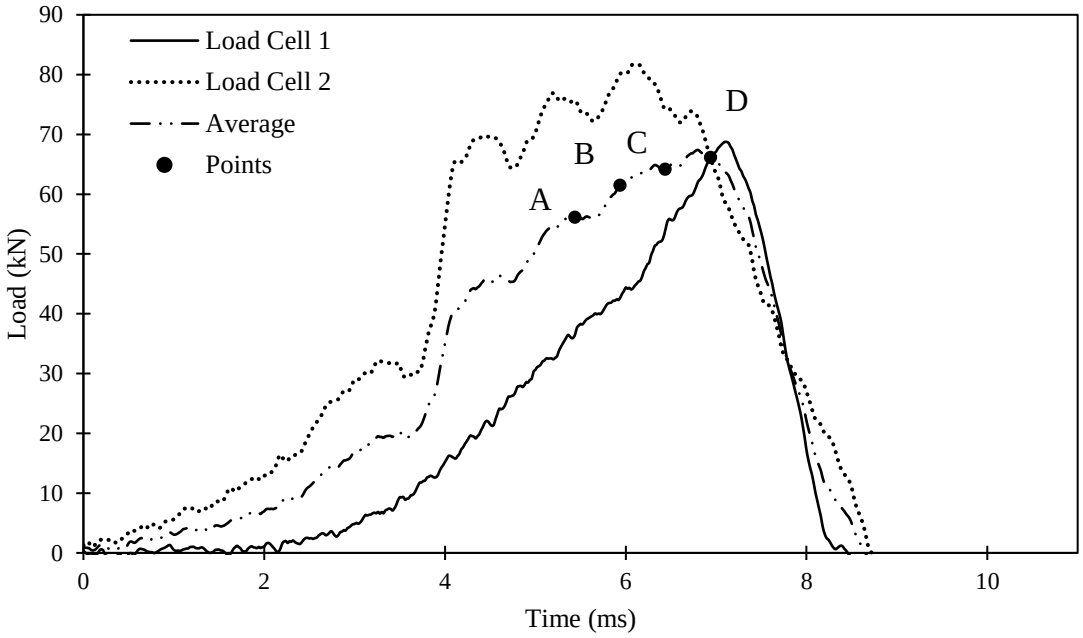

Figure B2.5: Specimen L240-3 Load Data.

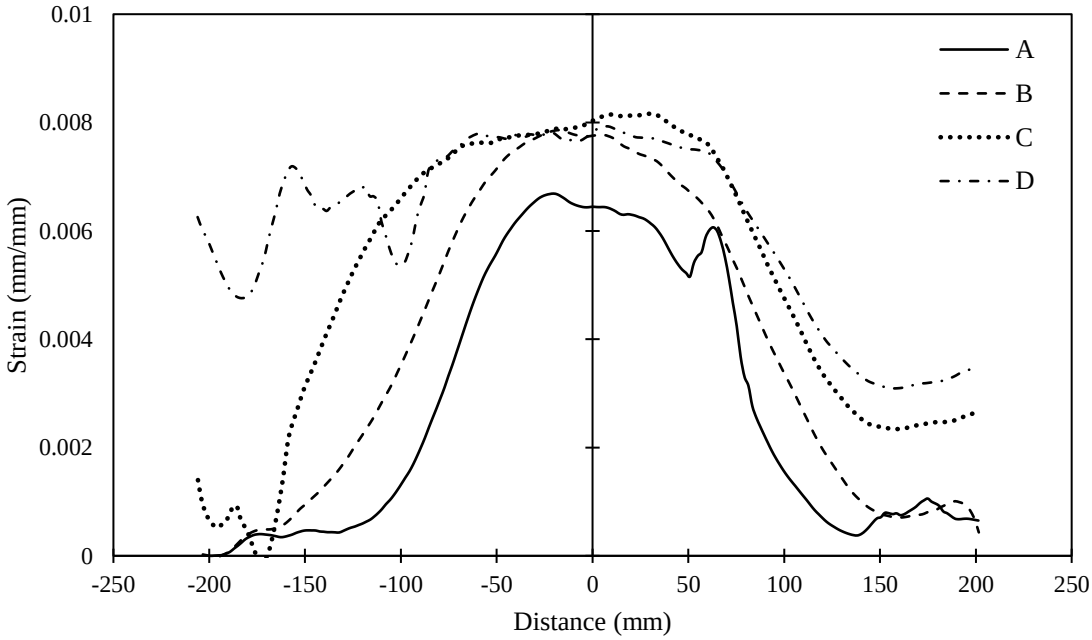

Figure B2.6: Specimen L240-3 Strain Data.

B.3 Load Data for Specimens L350

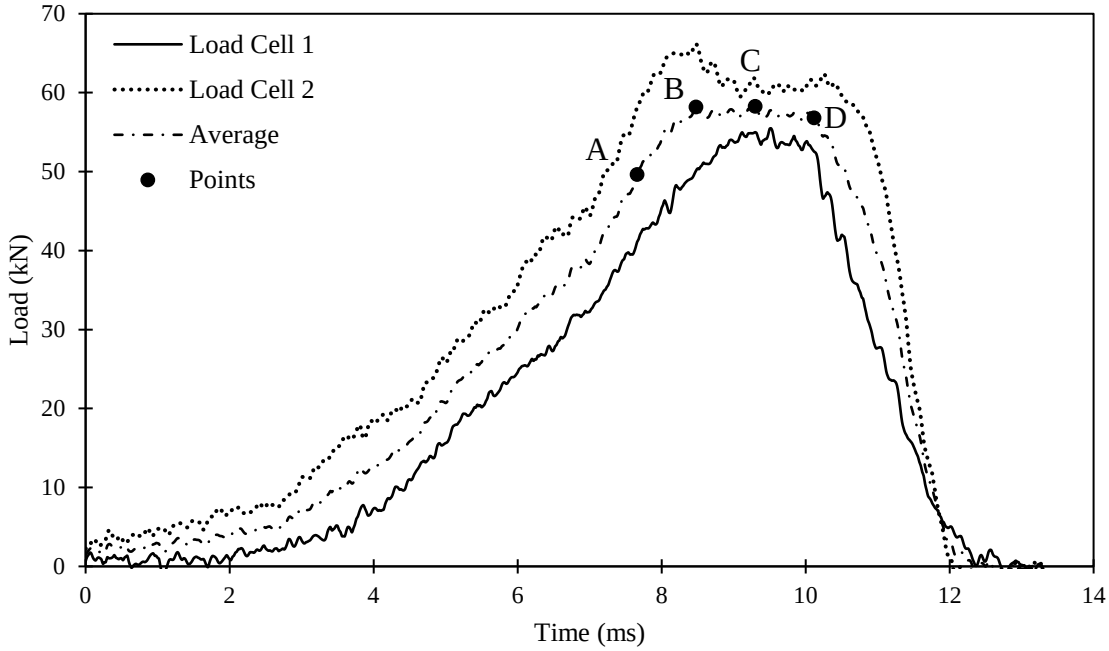

Figure B3.1: Specimen L350-1 Load Data.

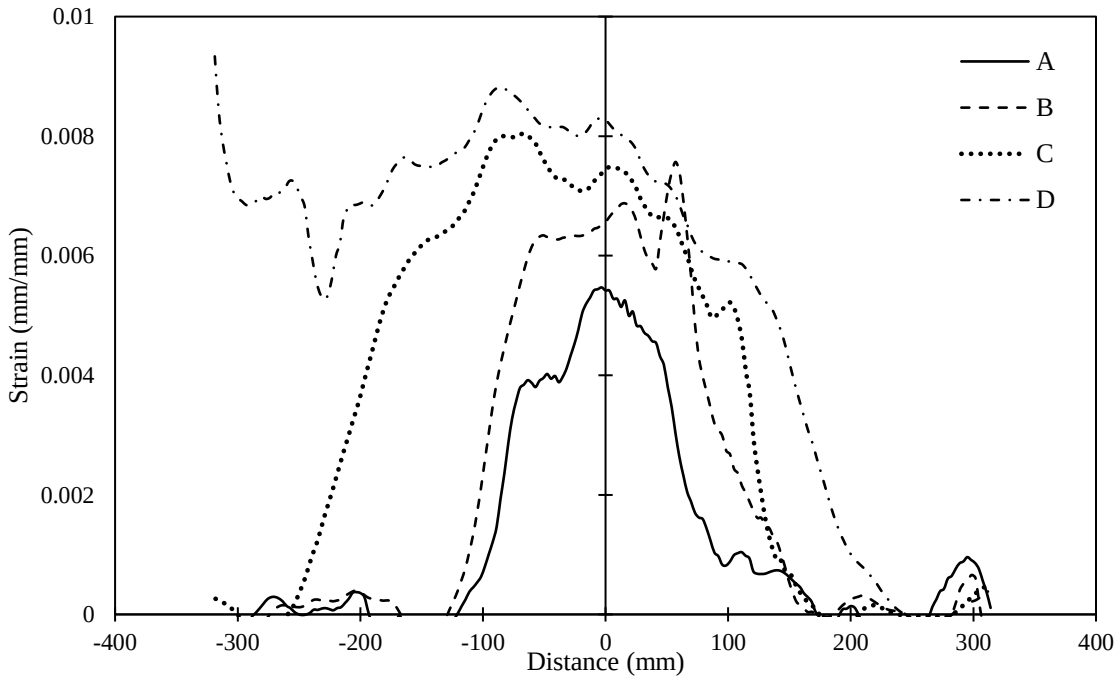

Figure B3.2: Specimen L350-1 Strain Data.

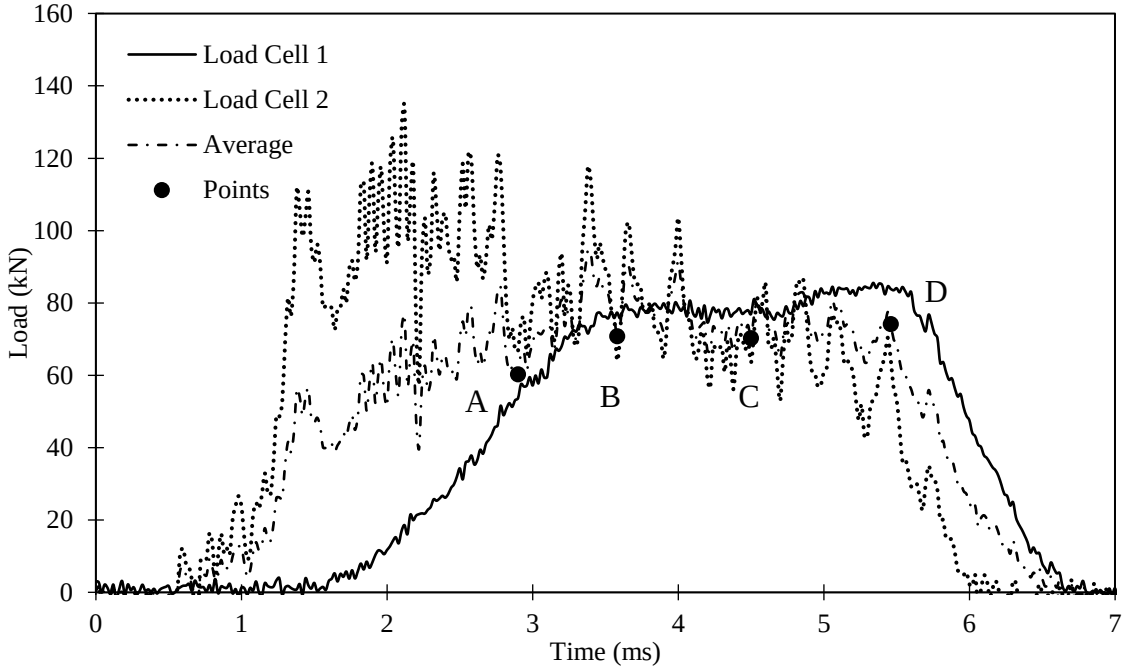

Figure B3.3: Specimen L350-2 Load Data.

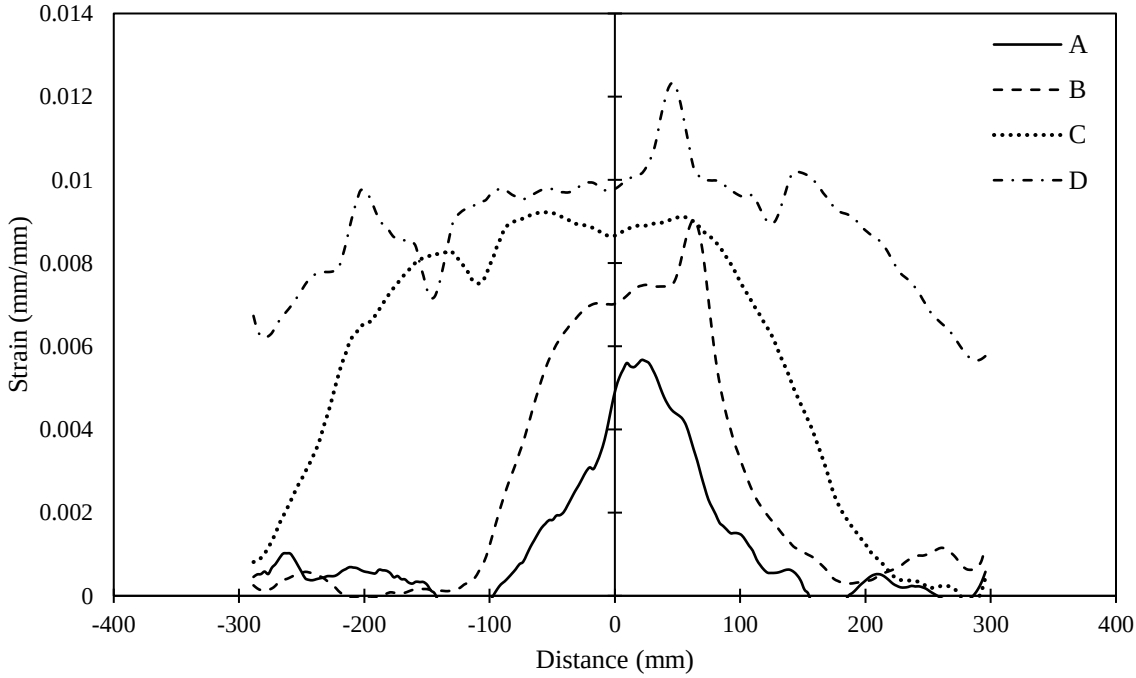

Figure B3.4: Specimen L350-2 Strain Data.

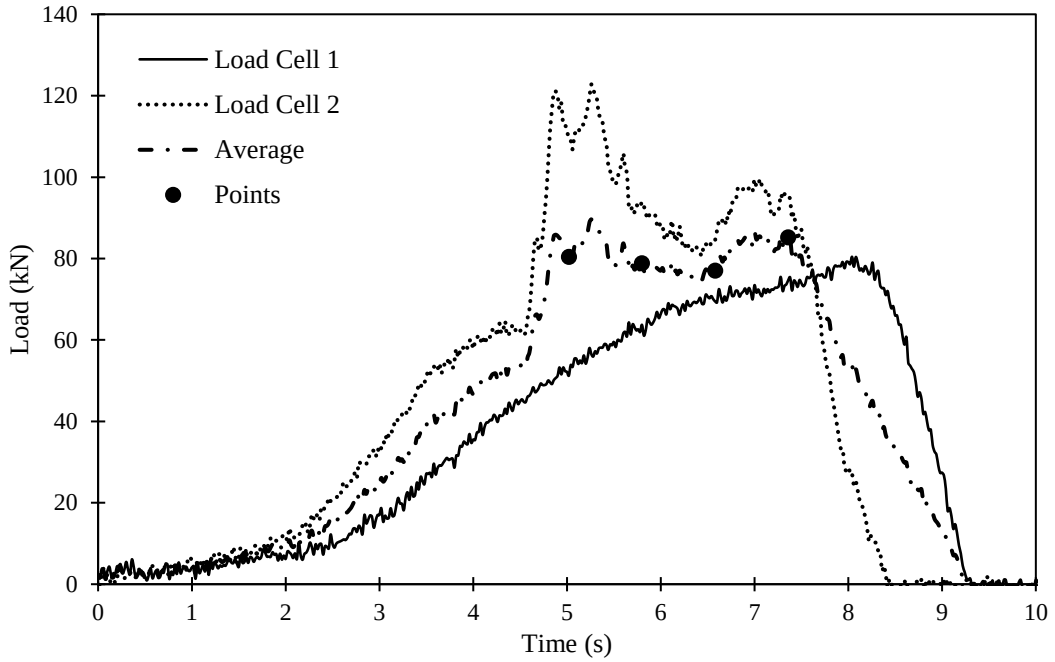

Figure B3.5: Specimen L350-3 Load Data.

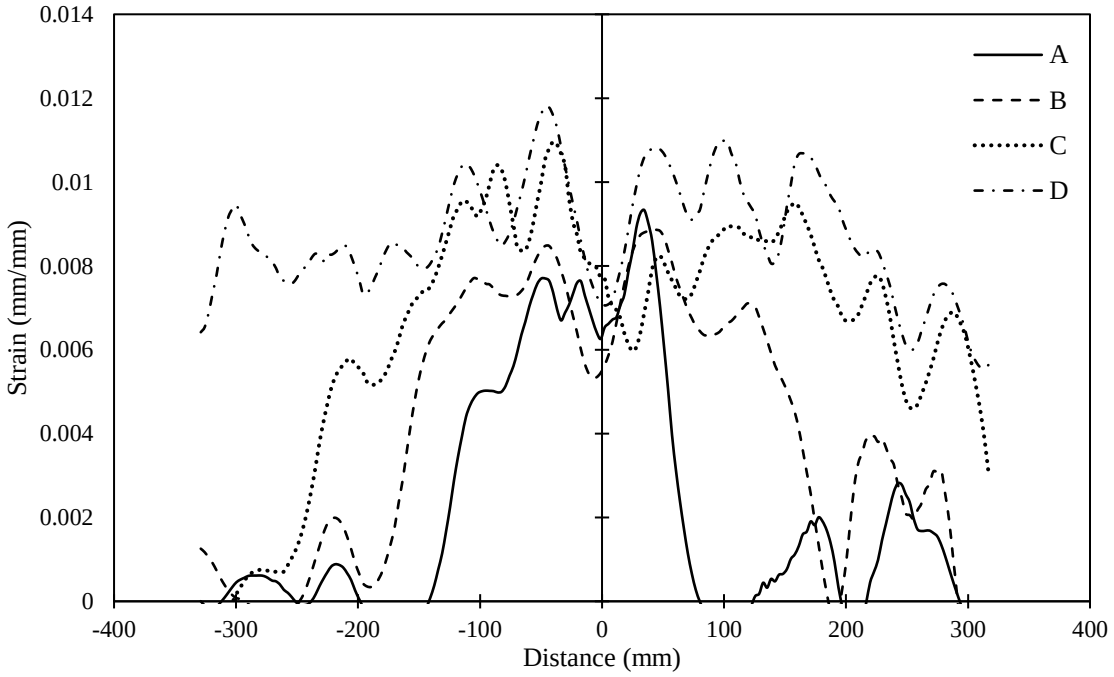

Figure B3.6: Specimen L350-3 Strain Data.

CURRICULUM VITAE

Candidate's Full Name

Jonathan Benjamin Everett Harman

Universities Attended

University of New Brunswick, B.Sc.E. (Civil Engineering), 2012-2017

Publications

Harman, J., Atunbi, E. O., & Lloyd, A. (2021). High Strain Rate Properties of CFRP Sheets Surface Bonded to Concrete. *ACI SP-347 Recent Developments in High Strain Rate Mechanics and Impact Behavior of Concrete*, 21-38.

Conference Presentations

Harman, J., Atunbi, E. O., & Lloyd, A. (2021). High Strain Rate Properties of CFRP Sheets Surface Bonded to Concrete. Presented at *ACI 370 Special Publication 347 Symposium, Recent Developments in High Strain Rate Mechanics and Impact Behavior of Concrete*, March 29.